VILNIUS UNIVERSITY

AGNĖ VAIČELIŪNAITĖ

Effects of stimulus context and behavioral context on information processing in the early visual system of the mouse

Doctoral dissertation
Biomedical sciences, biophysics (02 B)

Vilnius, 2015

Doctoral dissertation was prepared in Vilnius University, Lithuania and University of Tuebingen, Germany in 2009-2015.

Supervisor:

Prof. dr. Osvaldas Rukšėnas (Vilnius University, biomedical sciences, biophysics – 02B).

Consultant:

Dr. Laura Busse (University of Tuebingen, Werner Reichardt Centre for Integrative Neuroscience, biomedical sciences, biology – 01B).

Journal of neurophysiology and Current biology give permissions to use pieces or full text in thesis or dissertation works.

J Neurophysiol.: “Theses and dissertations. APS permits whole published articles to be reproduced without charge in dissertation and posted thesis repositories. Full citation is required.”

Curr Biol.: “Authors can use their articles, in full or in part, for a wide range of scholarly, non-commercial purposes as outlined below:

- <…>
- inclusion the article in a thesis or dissertation
- <…>

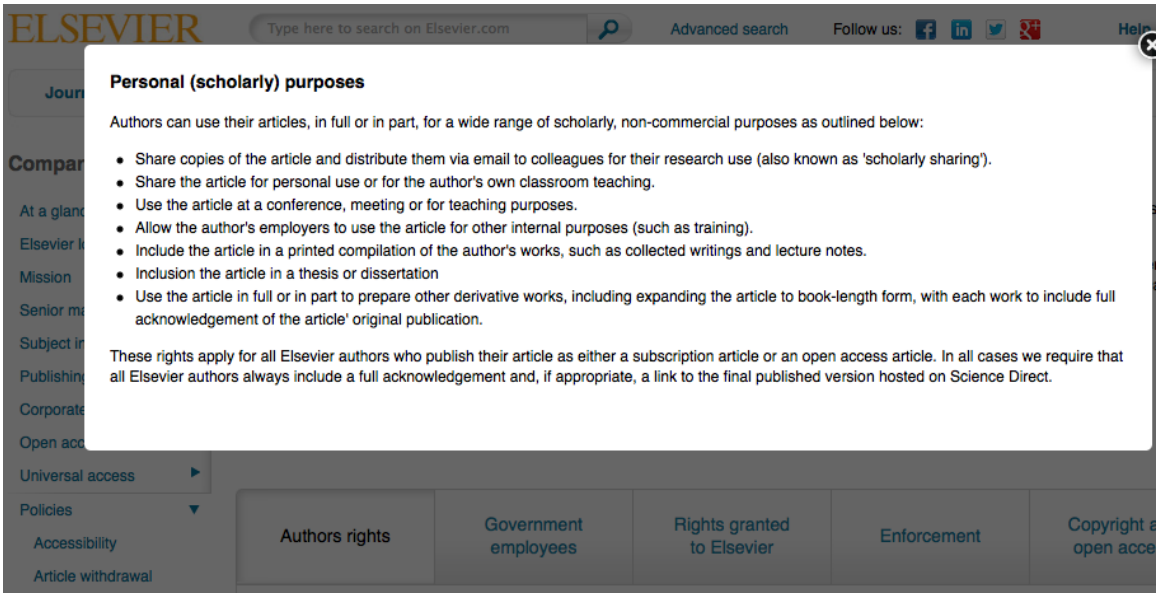

Content

Abbreviations

A – anterior visual area
AAV – adeno-associated viral vector
AL – anteriolateral visual area
AM – anatomically identified M cones
AM – anteromedial visual area
AMPA – α-Amino-3-hydroxy-5-methyl-4-isoxazolepropionic acid
AMS – anatomically identified MS cones
AS – anatomically identified S cones
AS+MS – S opsin-coexpressing MS cones.
CB – calbidin expressing inhibitory cells
CCK – cholecystokinin expressing inhibitory cells
ChAT - choline acetyltransferase expressing inhibitory cells
ChC – Chandelier cells
ChR2 – channelrhodopsin-2
CR – calretinin expressing inhibitory cells
CSD – current source density
DAPI – fluorescent stain 4',6-diamidino-2-phenylindole
DBC – double bouquet cells
DiD – fluorescent tracer 1,1'-Dioctadecyl-3,3,3',3'-Tetramethylindodicarbocyanine, 4-Chlorobenzenesulfonate Salt
dLGN – dorsal lateral geniculate nucleus
DS – selectivity to direction
EPSC – excitatory postsynaptic currents
fMRI – functional magnetic resonance imaging
G – granular layer
GABA - gamma amino butyric acid
GLT1/EAAT2 – glial glutamate transporter
hmr – half-maximum response
I – infragranular layer
i.p. – intraperitoneal
L – layer (e.g. L5)
LBC – large basket cells
LC – locus coeruleus

LED – light-emitting diode
LFP – local field potential
LI – laterointermediate visual area
LM – lateromedial visual area
MC – Martinotti cells
MT - middle temporal area
NGC – neurogliaform cells
NMDA – N-Methyl-D-aspartate
NPY – neuropeptide Y expressing inhibitory cells
OS – selectivity to orientation
P – posterior visual area
PBS – sodium phosphate buffer
PFA – paraformaldehyde solution
PM – posteriomedial visual area
POR – postrhinal visual area
PV+ - parvalbumin positive interneurons
RF – receptive field
RGCs – retina ganglion cells
RL – rostrolateral visual area
S – supragranular layer
s.c. – subcutaneous
s.e.m. – standard error of the mean
SBC – small basket cells
SC – superior colliculus
SF – spatial frequency
SI – suppression index
SOM+ - somatostatin positive interneurons
TF – temporal frequency
TRN – thalamic reticular nucleus
V1 – primary visual cortex
VIP – vasointestinal polypeptide expressing inhibitory cells
YFP – Yellow Fluorescent Protein

Introduction

In primary visual cortex (V1), many neurons exhibit selectivity for stimulus size, showing suppression of responses when stimuli extend beyond the classical receptive field (RF) into the surround (Allman et al 1985, Blakemore & Tobin 1972, DeAngelis et al 1994, Gilbert & Wiesel 1990, Knierim & van Essen 1992, Nelson & Frost 1978). Understanding the neural mechanisms of surround suppression is important, since this modulation is thought to constitute a key aspect of perception: the computation of visual saliency by integration of local information within the global context (Sachdev et al 2012).

Surround suppression is likely mediated by a combination of different neural circuits and mechanisms. In higher-order mammals, where spatial integration has been studied most extensively, surround suppression shows signatures of various components, including feedforward (e.g., (Alitto & Usrey 2008, Solomon 2002, Webb et al 2005)), feedback (e.g., (Angelucci et al 2002, Bair et al 2003)), and horizontal intracortical circuitry (e.g., (Angelucci et al 2002, Gilbert et al 1996, Reynaud et al 2012, Somers et al 1998)). The relative contributions of these circuits, however, are under debate and the cell types involved mostly unknown.

Rodents are gaining popularity in visual neuroscience because of the practical issues: the small size of mouse' nervous system gives us an opportunity to observe all visual areas (e.g. primary visual cortex and extrastriate cortex) simultaneously (Huberman & Niell 2011, Wang & Burkhalter 2007), readily available molecular and genetic tools offer unprecedented possibilities for studying how different elements of the neuronal circuit mediate key RF characteristics, such as surround suppression. Moreover, the labs prefer to use mice to investigate nervous

system because mice, comparing with primates or cats, are simpler models for brain disorders, have fast change of generations and low price (Huberman & Niell 2011).

Exploiting powerful genetic tools, recent work in mouse V1 has characterized a neural circuit for spatial integration in layers 2/3 involving somatostatin-expressing (SOM+) inhibitory interneurons (Adesnik et al 2012). SOM+ interneurons seem to have little surround suppression themselves such that they can exert inhibition onto neighboring pyramidal cells at large stimulus sizes. Moreover, optogenetic hyperpolarization of SOM+ interneurons weakens surround suppression (Adesnik et al 2012, Nienborg et al 2013).

The influence of other types of interneurons on surround suppression is an open question. Parvalbumin-expressing (PV+) interneurons constitute the major class of GABAergic interneurons in mouse V1 (Gonchar et al 2007b). Preferred size of PV+ inhibitory interneurons seems to be larger and surround suppression weaker than in the general population (Adesnik et al 2012). Furthermore, PV+ interneurons have been suggested to perform gain control and response normalization (Atallah et al 2012), computations that lie at the heart of surround suppression (reviewed in (Carandini & Heeger 2012)). Therefore, PV+ interneurons likely affect surround suppression, but the nature of their influence remains unknown.

Likewise, surround suppression beyond layers 2/3 in mouse V1 is much less explored. With the exception of a single study (Van den Bergh et al 2010), little is known about the laminar profile of surround suppression in the mouse. Yet, this study failed to observe any laminar dependence, which is a hallmark of surround suppression in higher-order mammals such as cats and primates. These recordings, however, were obtained under anesthesia, which may well have led to an underestimation of the overall impact of suppressive circuits in mouse V1 (Adesnik et al 2012, Haider et al 2013).

Neural responses not only depend on sensory inputs but also are profoundly modulated by behavioral state (Harris & Thiele 2011, Noudoost 2010). In primates, behavioral state can be elegantly controlled with a number of experimental paradigms, including those manipulating selective attention (Noudoost 2010). In rodents, where such paradigms are still lacking, behavioral state is often dichotomized into passive versus active, where the passive state is associated with slow synchronous fluctuations and the active one with desynchronized activity (Harris & Thiele 2011). Despite operating at a global scale, the active state in rodents has been suggested to share underlying processes with the attentive state in primates (Harris & Thiele 2011, Maimon 2011).

Recent studies assessing state-dependent changes of sensory processing in mouse primary visual cortex (V1) have started to characterize how locomotion modulates single neuron activity. During locomotion, V1 neurons in layers 2/3 and 4 have more depolarized membrane potentials (Bennett et al 2013, Polack et al 2013), higher firing rates (Andermann et al 2013, Bennett et al 2013, Keller et al 2012, Niell & Stryker 2010, Polack et al 2013) and increased tuning gain (Niell & Stryker 2010, Polack et al 2013). These effects may be mediated by noradrenergic inputs (Polack et al 2013). Moreover, during locomotion individual neurons respond more reliably to visual stimuli, as trial-to-trial variability of both membrane potentials and spiking responses are reduced (Bennett et al 2013, Polack et al 2013).

Although these studies show clear locomotion-related modulations of single-unit activity in upper layers of V1, the impact of locomotion on neural populations across V1 layers and on pre-cortical processing stages is not well understood. With the exception of a single two-photon calcium imaging study (Andermann et al 2013), the laminar profile of locomotion-related response modulations has not been examined. Moreover, it is a commonly accepted

notion that locomotion-related gain modulations of sensory neurons are restricted to cortex. This notion is based on the pioneering study of Niell & Stryker (Niell & Stryker 2010), who could not find locomotion-related enhancements of response magnitude in the dorsal lateral geniculate nucleus of the thalamus (dLGN). However, recently observed locomotion-related depolarizations of membrane potentials in thalamo-recipient L4 neurons (Polack et al 2013) could at least partly reflect properties of the incoming dLGN activity.

Aim

To quantify how stimulus context and behavioral context affect processing of information in the thalamus and primary visual cortex of the mouse.

Objectives

- To investigate the laminar profile of spatial integration in mouse V1;
- To explore temporal profile of the surround suppression;
- To verify the influence of parvalbumin positive interneurons to surround suppression;
- To examine an effect of anesthetic state on spatial integration;
- To investigate the effect of locomotion on neural responses at the level of the LGN;
- To check how locomotion relates to pupil dilation;

Originality of the research

Both parts of this work provide novel contributions to the visual neuroscience. We found that, analogous to what is well known from higher-order mammals, surround suppression in awake mice is strongest in superficial layers and develops over time. We demonstrate that two popular anesthetics used in acute studies of the rodent visual system profoundly

change these results: anesthesia not only reduces overall suppression strength, it also obliterates laminar specificity and slows the temporal dynamics of suppression. We also discovered that PV+ interneurons affect spatial integration by modulating overall stimulus drive. Also we found that in V1, locomotion modulates the gain of individual neurons with a distinct laminar pattern and reduces interneuronal correlations in the population response. Contrary to the current understanding, we discovered that locomotion modulates responsiveness even at the level of the dLGN. Finally, we are the first to show that locomotion in mice induces pupil dilation. Together, these results show that, in the visual system, brain state shapes activity at processing stages earlier than previously recognized.

Defensive statements

- There is laminar distribution of size tuning in mouse V1;
- Surround suppression develops over time;
- PV+ interneurons can shape surround suppression by reducing stimulus drive;
- Spatial integration is profoundly influenced by anesthetic state;
- Locomotion does increase firing rates already at the level of the thalamus;
- Effects of locomotion could also be observed at the level of the eye;

1 Literature review

1.1 Overview of the mouse early visual system

In the last decade, the mouse has strongly gained popularity as a model system for the early visual system. It has been shown that the mouse visual system is far more sophisticated than it was assumed before. This is important that the mouse contains the same, main retino-geniculate-striate pathway as higher order mammals (Figure 1) (Huang et al 2008, Huberman & Niell 2011). The mouse is very convenient model for addressing fundamental questions or targeting special cells, e.g. parvalbumin-positive or somatostatin-positive inhibitory interneurons (Adesnik & Scanziani 2010, Atallah et al 2012, Huberman & Niell 2011, Katzner & Weigelt 2013, Olsen et al 2012). In this literature review section, we discuss neural circuits for visual information processing, and anatomical, morphological, and functional properties of dorsal lateral geniculate nucleus (dLGN), thalamic reticular nucleus of the thalamus and primary visual cortex (V1). Here, we focus on surround suppression of visual receptive fields, the influence of anesthesia on visual response properties, modulations by behavioral context, such as locomotion.

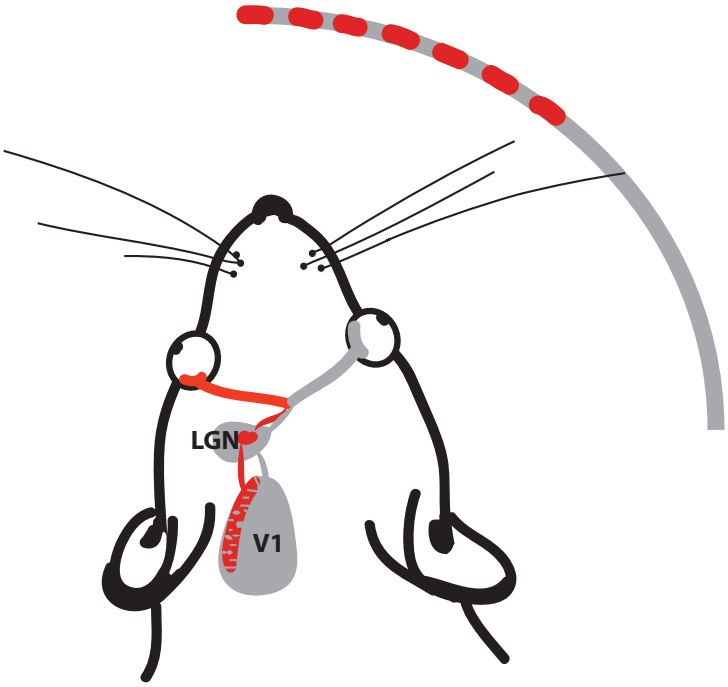

Figure 1. Schematic illustration of mouse main visual pathway. LGN – lateral geniculate nucleus, V1 – primary visual cortex. Adapted from (Huang et al 2008, Huberman & Niell 2011).

1.2 Retina of the mouse

Visual information flow starts in the light-sensitive inner side of the animal's eye, the retina (reviewed in (da Silveira & Roska 2011)). The structure of the mammalian retina is sophisticated and contains a huge diversity of neurons - more than 60 different types. These neurons interact in certain way and build approximately 20 paths from retina to brain (Masland 2012). All these types of the cells are well organized and ordered into layers and circuits (da Silveira & Roska 2011, Wässle 2004).

Despite their large diversity, mammalian retinal cells can be grouped into 6 main classes: rods, cones, bipolar cells, amacrine, horizontal cells and ganglion cells (Wässle 2004). Besides neurons, the retina also contains a glial cell population – Müller cells (Jeon et al 1998). Mice contain all these classes

of neurons (Figure 2), and their proportion does not differ substantially across different species (Figure 3). A major difference between the retina of the mouse and higher-order mammals concerns the number of types of cones (Masland 2012, Wässle 2004). Humans and primates have 3 types of cones, which are similar in terms of structure and function, but differ in the expressed opsin. Depending on the expressed opsin, cones in the primate retina are sensitive for different wavelengths of the visible light spectrum: long (L or red), middle (M or green) and short (S or blue). Other mammals, like rodents (including mice) have only S and M cones (Masland 2012, Wässle 2004). Color vision is typically based on combination of two outputs in different proportions (Masland 2012).

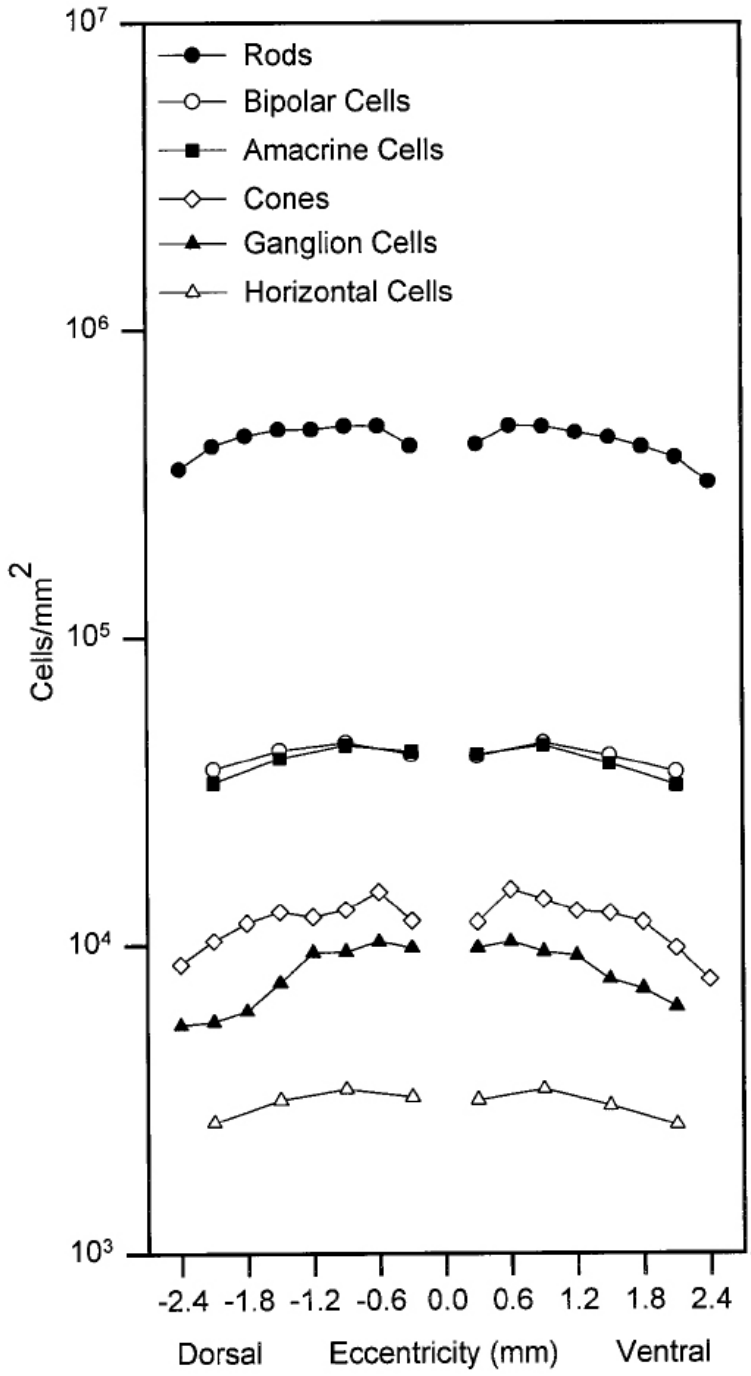

Figure 2. Distribution of the major cell classes in the retina of the C57BL/6 mouse. Adapted from (Jeon et al 1998).

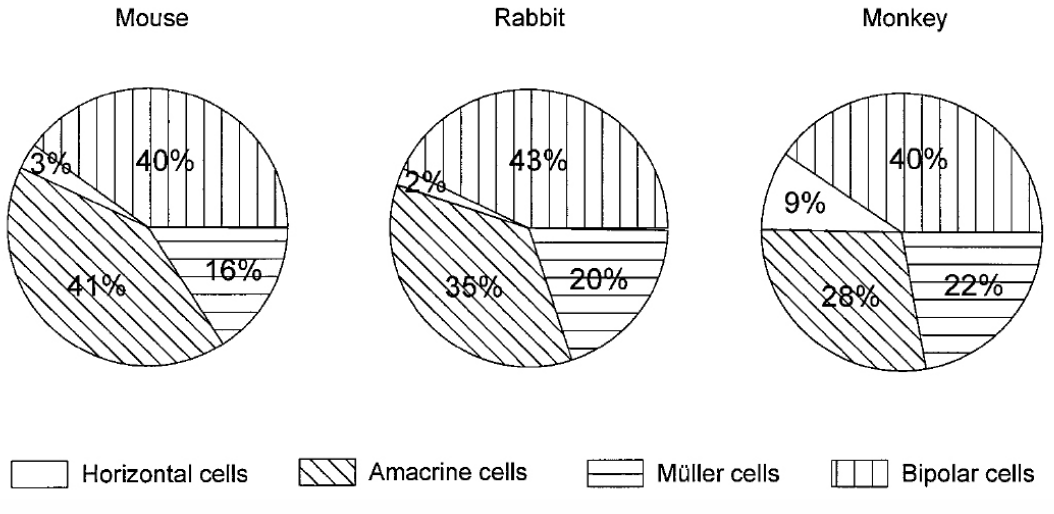

Figure 3. Distribution of some retinal cell classes (horizontal, amacrine bipolar and Müller cells) in the mouse, rabbit and monkey eye. Adapted from (Jeon et al 1998, Martin & Grünert 1992, Strettoi & Masland 1995).

The mouse is nocturnal animal, so it is not surprising that retina is rod-dominant (97% of photoreceptors). Mouse cones constitute two populations: genuine S-cones (only ~4-5% of all cones) and coexpressing cones, which also are called MS cones. Genuine S cones ("true" S cones) express only S-opsin sensitive to UV-light (360 nm) and are homogenously distributed across the retina (Baden et al 2013a, Haverkamp et al 2005, Wang et al 2011b). Moreover, S-cones make synapses exclusively with S bipolar cells (Haverkamp et al 2005). Finally, unlike in higher order mammals, S-cones are activated by very short wavelength in mice, and the big lens does not filter UV light (Corneil & Munoz 2014).

MS cones express both, M-opsin (508 nm) and S-opsin (360 nm). There is dorsal-ventral gradient of opsin coexpression of the mouse retina that results in three functional regions (Figure 4) (Baden et al 2013b, Wang et al 2011c).

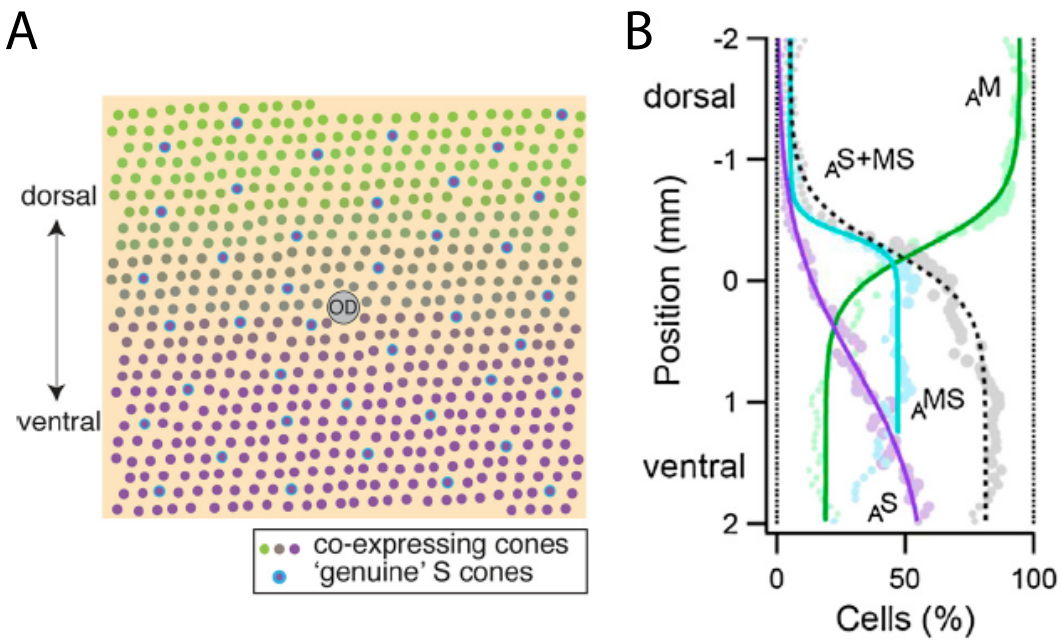

Figure 4. Anatomical coexpression of two opsins in mouse retina. A: schematic illustration of the distribution of two cone populations in the retina. Outlined in cyan circles, genuine S-cones; gradient to green, more M-opsin expression in cones; gradient to purple, more S-opsin expression in cones. B: Spatial profile of the three anatomical cone types across the retina fitted with sigmoids. Marker size contributes to the cell number per bin. AM, anatomically identified M cones; AS, anatomically identified S cones; AMS, anatomically identified MS cones; AS+MS, S opsin-coexpressing MS cones. Adapted from (Baden et al 2013b, Wang et al 2011c).

The mouse retina contains at least 22 distinct retinal ganglion cell subtypes, and this also illustrates the complexity of the mouse retina (Figure 5) (Huberman & Niell 2011, Völgyi et al 2009).

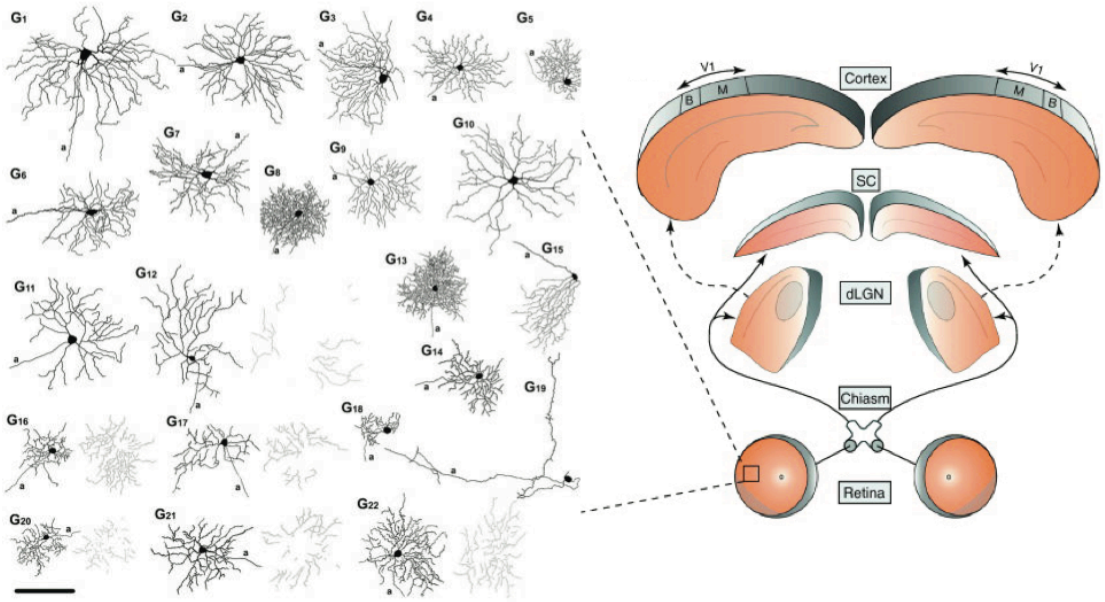

Figure 5. Mouse retinal ganglion cells (RGCs) subtypes (left) and cartoon illustrating mouse visual pathways (right; note that the majority of subcortical projections are not shown). Shaded parts in the retina denote RGCs that project ipsi-laterally into shaded parts of dLGN. In the cortex (V1) 'B' indicates the binocular and 'M' – monocular areas. Solid arrows indicate direct retinal projections to the dorsal lateral geniculate nucleus (dLGN) and superior colliculus (SC); dashed arrows indicate geniculo-cortical projections. Scale bar = 100 µm. Adapted from (Huberman & Niell 2011, Völgyi et al 2009).

All above described cell types are organized into distinct laminae (Figure 6) (Swaroop et al 2010). Photoreceptors are imbedded in the photoreceptor layer and their somas in outer nuclear layer. Rod and cone axons terminate in the outer plexiform layer, where make synapses with bipolar and amacrine cells dendrites. Inner nuclear layer contains horizontal, bipolar, amacrine and Müller glial cell bodies. Bipolar cells carry signals from photoreceptors to amacrine and ganglion cells and layer, where these cells connect is called the inner plexiform layer. In the ganglion cell layer there are localized ganglion cells which projects to the brain. Müller glial cells are the only ones that span across the all retinal layers (Helmsteadter et al 2013, Swaroop et al 2010).

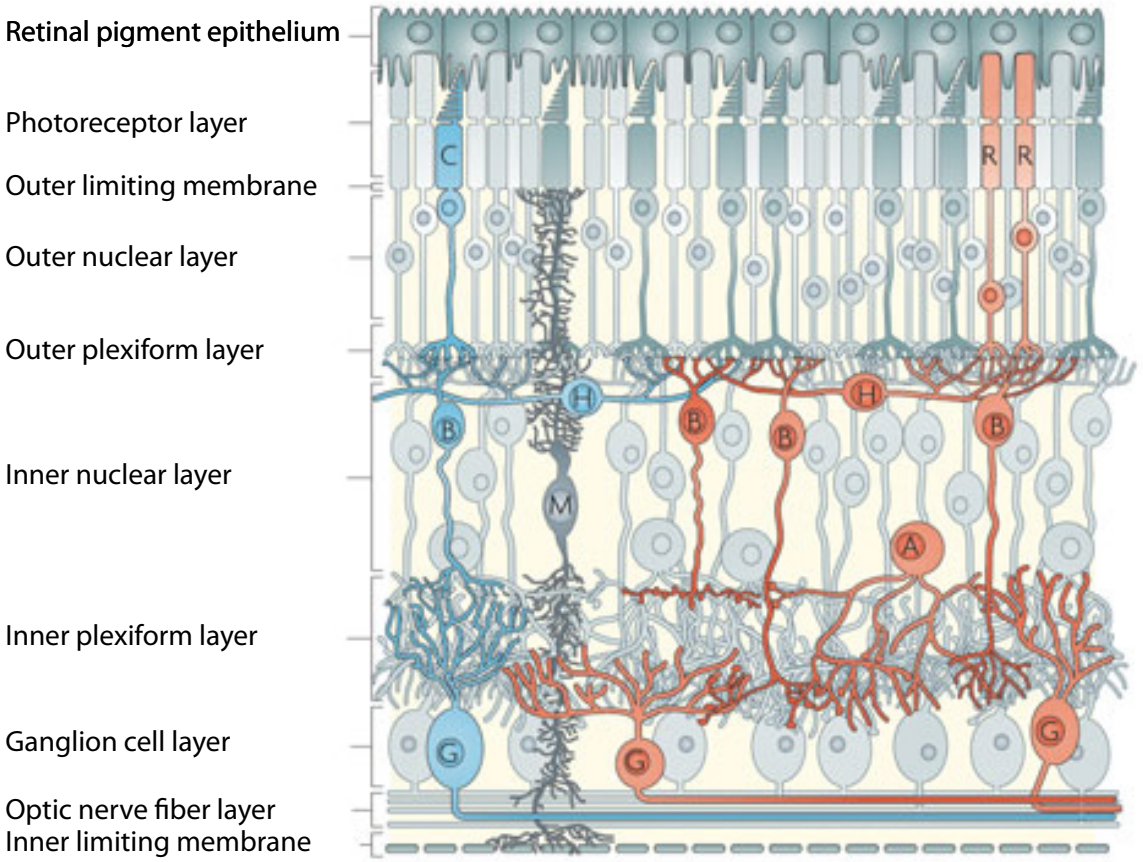

Figure 6. Laminar organization of the retina cells. Photoreceptors: R, rods and C, cones; H, horizontal cells; B, bipolar cells; A, amacrine cells; G, ganglion cells; M, Müller glial cells. In red here is shown representative path of rods and in blue – representative path of cone. Adapted from (Swaroop et al 2010).

1.3 Visual information processing in the lateral geniculate nucleus and thalamic reticular nucleus

1.3.1 Dorsal lateral geniculate nucleus (dLGN)

The dLGN is located in the thalamus and is the first center of the visual system that encodes center–surround receptive field information gained from the retina and relays it to the primary visual cortex, where new features are extracted and combined (Hirsch & Martinez 2006, Hubel & Wiesel 1962,

Piscopo et al 2013). Classical models of receptive field (RF) formation (Hubel & Wiesel 1961, Hubel & Wiesel 1962, Peterson et al 2004) support the theory, that properties are recomputed *de novo* at every visual level. Nevertheless, new studies revealed that LGN gets projection from retinal ganglion cells that carry more diverse information than was assumed previously (Cruz-Martin et al 2014, Marshel et al 2012, Masland & Martin 2007, Piscopo et al 2013).

Compared with the dLGN of higher mammals, where retinotopy is very clearly expressed in the eye-specific laminar structure established during development (Murray et al 2008, Wilson 1986), laminae in mouse dLGN are absent (Pfeiffenberger et al 2005, Piscopo et al 2013). Nevertheless, mouse dLGN still has a precise retinotopy (Figure 7) (Coleman et al 2009, Grubb & Thompson 2003, Grubb & Thompson 2004, Pfeiffenberger et al 2005). Information from the contralateral eye is represented in mouse dLGN 2-3 times more abundantly compared to the ipsilateral eye (Gordon & Stryker 1996).

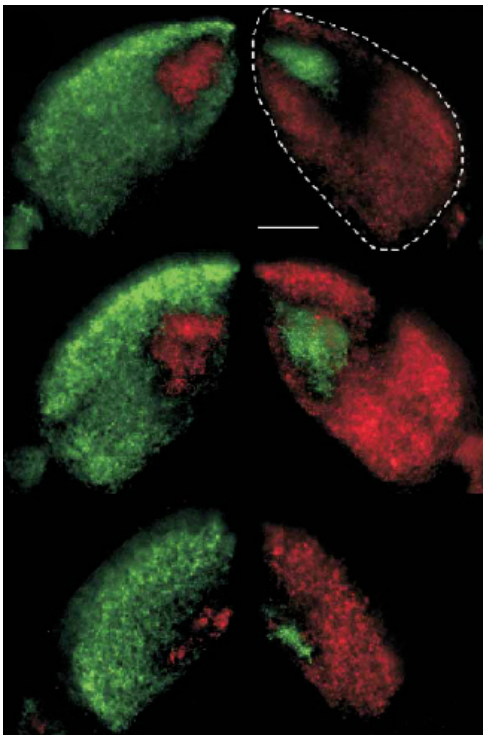

Figure 7. Coronal sections from the anterior (top) to posterior (bottom) part of the right and left dLGN of an adult wild-type mouse. Axons from right eye are shown in green, axons from left eye are shown in red. Dash line shows borders of the dLGN. Scale bar 200 mm. Adapted from (Pfeiffenberger et al 2005).

There are two main types of neurons in dLGN – interneurons and relay cells, amongst which interneurons cover 15-25% of the dLGN neuronal population. Inhibitory interneurons in rodents are distributed proportionally across all dLGN irrespective of eye dominance (Arcelli et al 1997, Sherman 2001 Feb). The remaining 75-85% of the dLGN neuronal population are thalamocortical neurons called relay cells (Halnes et al 2011). In the binocular region (dorsolateral part) of the dLGN, the ratio of contralateral vs. ipsilateral relay cells is estimated to be around 2 (Figure 8). (Coleman et al 2009).

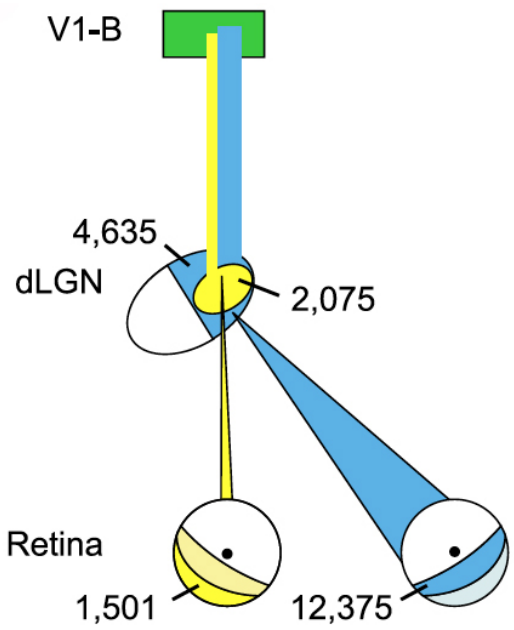

Figure 8. Schematic drawing showing binocular visual pathway in mouse. Width of lines indicates relative magnitude of contralateral (blue) and ipsilateral (yellow) projections. Adapted from (Coleman et al 2009).

As has been shown previously in cats, the relay cells in dLGN carry information from the retina to the primary visual cortex and get serotonergic and cholinergic inputs from the brainstem, GABAergic (gamma amino butyric acid) inhibitory neurons from the thalamic reticular nucleus (TRN), local inhibitory GABAergic neurons, hypothalamus and feedback connections from cortex (Figure 9) (Jurgens et al 2012, Van Horn et al 2000). The most prominent modulators are cholinergic (30% of the input) and GABAergic (Van Horn et al 2000).

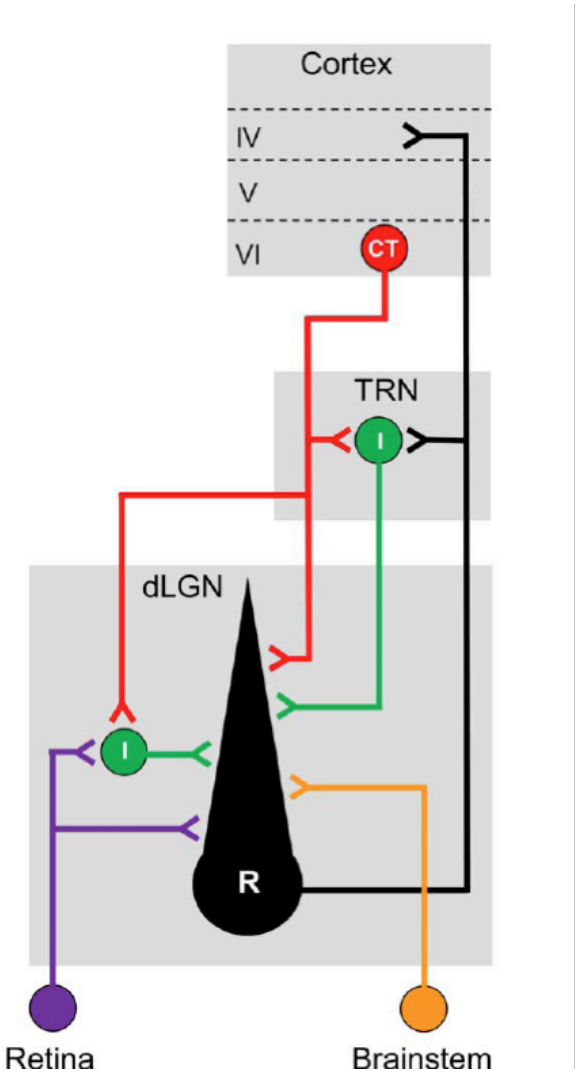

Figure 9. Schematic drawing of the circuits of the central visual pathway. Black, relay cells (R); purple, driving input from the retina; orange, modulatory input from brainstem; green, inhibitory neurons (I); red, excitatory neurons from layer 6 of visual cortex. Grey boxes indicate brain structures. TRN, thalamic reticular nucleus; dLGN, dorsal lateral geniculate nucleus. Adapted from (Jurgens et al 2012).

In higher-order mammals, relay cells are functionally and morphologically distinct, therefore segregated into Y, X and W or magnocellular, parvocellular and koniocellular cell types in cat and monkey, respectively (Friedlander 1982, Jurkus et al 2013, Saalmann & Kastner 2011, Winfield et al 1980). A similar organization has been described in rats (Gabriel et al 1996, Reese

1988). Mice seem to lack clearly separate types of relay cells (Grubb & Thompson 2003). However, in a comparable new study of Krahe et al (2011), which used *in vitro* thalamic slice recordings, according to morphology could distinguish 3 groups of relay cells that correspond to Y, X and W neurons defined in cats; these groups were present in a similar proportions (Figure 10A) (Friedlander 1982). The morphology of X-like cells is biconical shape, while Y-like cells are radially symmetric and W-like cells have a hemispheric profile (Figure 10). The majority of defined cells in mouse dLGN have a Y-like profile. X-like neurons are smaller than other types, and their population is also the smallest. In addition, the authors also claim that within dLGN, all these cells have regional preferences: X-like cells are most region-selective and occupy the ventro-posterior part of LGN and also are distributed in horizontal plane, while W-like neurons, despite being present in the whole dLGN, appear more likely than the other types in the dLGN center (Figure 10B) (Krahe et al 2011). This data is similar to findings in rats (Reese 1988). As in cats or rats, there are no clear, statistically significant, differences in resting membrane potential of these three types of relay cells (Ziburkus et al 2003).

A

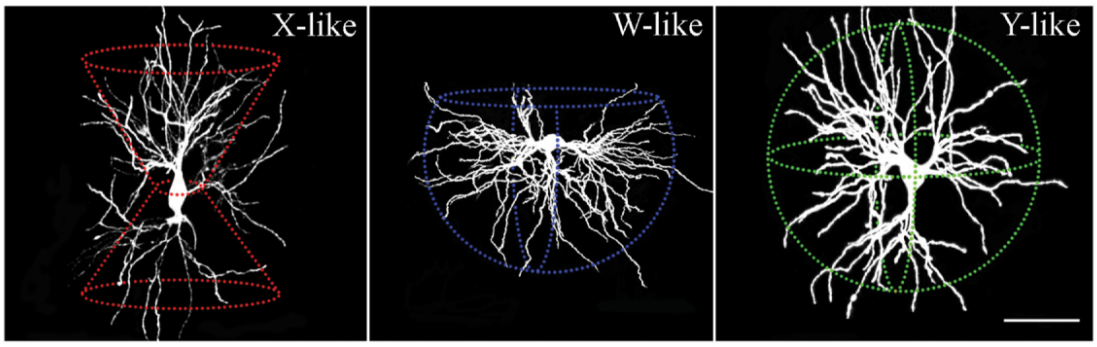

B

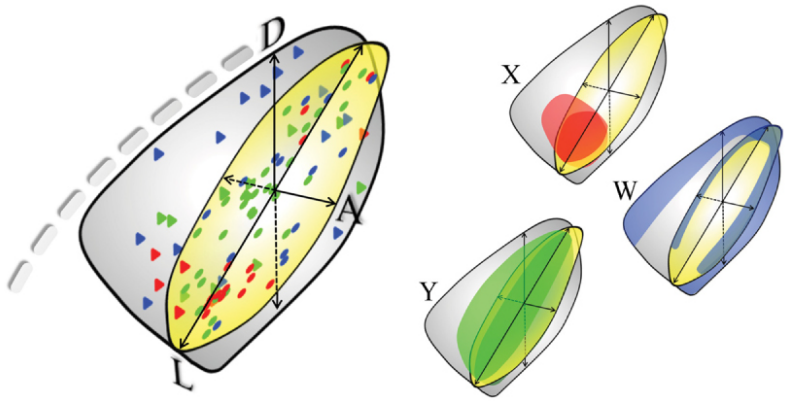

Figure 10. Morphology and distribution of mouse dLGN cells. A: Example cells of mouse dLGN depict three groups of cells: X-like, W-like and Y-like. Dashed lines indicate dendritic architecture. Scale bar 50 μ m. B: Regional preferences of Y-like (green), X-like (red) and W-like (blue) cell types in dLGN. Adapted from (Krahe et al 2011).

Grubb and Thompson (2003) used extracellular recordings in wild-type, anaesthetized mice and concluded that there are no clear functional subdivisions in the mouse dLGN. Nevertheless, they suggest that there could be Y-like relay cells. A more recent study by Piscopo et al. (2013) (Piscopo et al 2013) found only cells with of the morphological W-like class as described in Krahe et al (2011) (Krahe et al 2011), but not the other two types.

As it was mentioned previously in this work, mouse dLGN do not have clear layers as it is in higher order mammals. Nevertheless, very recent exciting study (Cruz-Martin et al 2014) divided dLGN functionally to "the shell"

(dorsal part of the structure) and “the core”. It was shown that neurons from these two parts target different layers in primary visual cortex. Cells from the dLGN core project to deeper layers of V1, whereas cells from the dLGN shell – to superficial layers of V1.

1.3.2 Thalamic reticular nucleus (TRN)

TRN is worth to mention in this work because of its direct influence on the activity of dLGN. It has been shown that when the visual cortex is optogenetically silenced, firing rate in LGN remain relatively unchanged, mainly because LGN does not only loose excitatory drive from cortex, but also inhibition from TRN (Olsen et al 2012). And as it is known, TRN, as well as LGN, is directly exited from layer 6 of the cortex (Briggs 2010, Cruikshank et al 2010, Li et al 2013, Olsen et al 2012).

TRN is the conglomeration of interneurons that surround the thalamus. Approximately one third of TRN synapses in rodents are GABAaergic. These neurons in most of the species, including rodents, inhibit relay cells in the dorsal thalamus. The TRN gets the main excitatory input (~60 %) from the cortex (Liu & Jones 1999, Steriade et al 1997, Zhang et al 2004). The GABAergic inputs in the LGN from TRN may play an important role in attention and vigilance state modulations (Jones et al 2001, McAlonan et al 2008).

Within LGN, as has been shown in higher mammals (Sherman 2004), some synapses form “triads” within the structure of a glomerulus. In these sites, 3 or more synapses are placed tightly together (Figure 11). Glomerulus is an area that is enclosed by the glial shell, but there are no astrocytes within the glomerulus. This structure permits the neurotransmitters to flow freely within the glomerulus and to affect receptors that are more far away. Triads contain two types of inhibitory sites: F1 (F stands for flattened vesicle) and F2. F1 outputs constitute axonal terminals that end on X and Y cell types

dendrites; F2 outputs constitute dendritic terminals that end mostly on presynaptic X cells or postsynaptic to both cell types, similar to the F1 type. In this way, Y cells are mostly innervated by F1 type, even though, overall, the F2 type dominates versus the F1 type. Each glomerulus contains 1 rely cell, 1 or more retinal terminal and one F2 terminal. There could be cases in which a triad is missing an F1 terminal. Interestingly, in glomeruli there are no cortical inputs (Sherman 2004, Sherman & Guillery 2006).

The presence of triads in mouse LGN has already been shown in an early study using electron microscopy (Rafols & Valverde 1973).

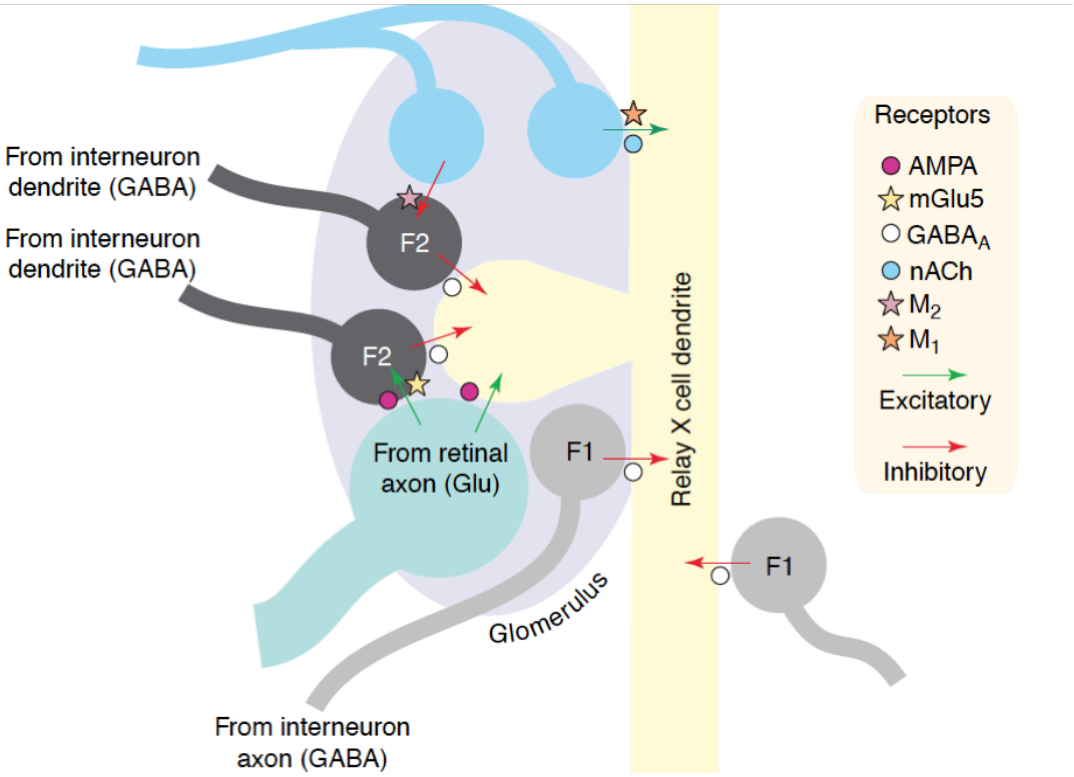

Figure 11. Schematic drawing of a glomerulus and triads in the cat LGN. Adapted from (Sherman 2004).

1.4 Visual information processing in primary visual cortex

The gross architectural and functional profile of the mouse visual cortex is similar to that of higher mammals (Vreysen et al 2012). In addition, the

laminar circuits in mouse primary visual cortex (V1) are consistent and similar with the schemes shown in cats and primates (Douglas & Martin 2004, Olivas et al 2012). In these circuits, neurons are organized in six horizontal layers. These cortical layers in mice do not have such clear cytoarchitectural boundaries as in other species and thalamic projections seem to be more extensive (Antonini et al 1999, Frost & Caviness 1980), but nevertheless, the intricate interplay between these layers seems crucial for coordination (Adesnik & Scanziani 2010) and modulation (Olsen et al 2012) of responses to sensory stimuli (Niell & Stryker 2008).

Already in the year 1987 (Bode-Greuel et al 1987), using recordings *in vitro*, the basic operating principle of simple cortical circuits has been shown. The main "gate", by which the signal from subcortical areas (such as dLGN) enters V1, is layer 4 and, albeit to lesser degree, layer 6 (Figure 12). There are numerous projections from layer 4 to layers 2/3 and 5. Between layers 2/3 and 5 there are strong reciprocal connections. In the mouse, unlike in the monkey, layer 4 has comparable weak connections to layer 6 and smaller connections from layer 6 to superficial layers (Briggs 2010). Neurons from deeper layers project to subcortical regions (Hattox & Nelson 2007, Olsen et al 2012, Thomson & Bannister 2003). Note that the proportion of connections could differ depending on the age of animals. There are data that brain and circuits of adult animals are more or less conserved across individuals, but can be distinct from juveniles (Haider et al 2013, Olivas et al 2012, Thomson & Bannister 2003).

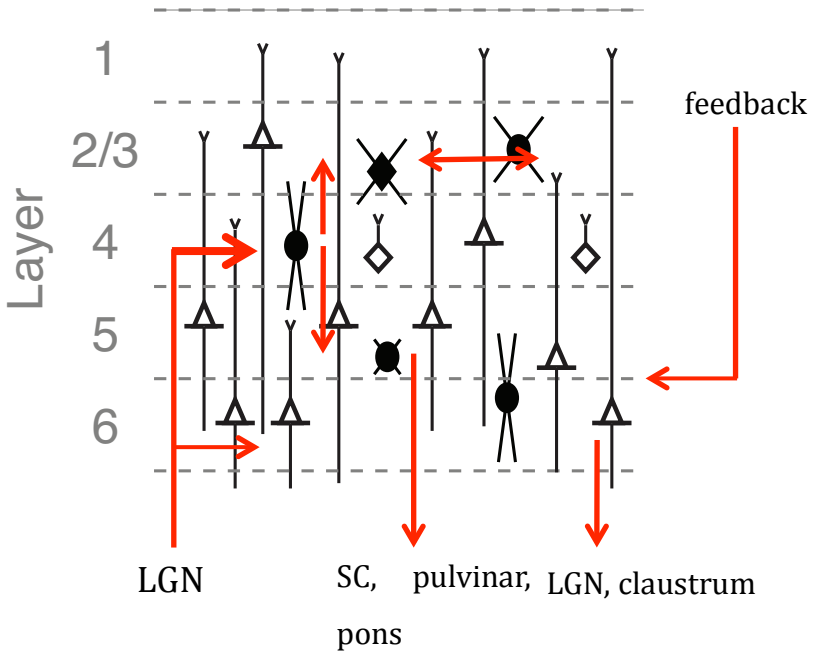

Figure 12. Interlaminar circuits in V1. Dashed lines indicates cortical layers; triangles, pyramidal cells; circles, interneurons; red lines, projections. Adapted from (Haider et al 2013, Olivas et al 2012, Thomson & Bannister 2003).

The described scheme of cortical circuits (Figure 12) is rather simple and abstract. In reality, circuits are much more complicated and contain a large diversity of cells.

It was shown, that mouse V1 is surrounded by 9 anatomically distinct visual areas – posterior (P), lateromedial (LM), anteriolateral (AL), rostrolateral (RL), anterior (A), anteromedial (AM), posteriomedial (PM), laterointermediate (LI), and postrhinal (POR) (Figure 13) (Wang & Burkhalter 2007). While these areas obviously cannot correspond in a one-to-one mapping to the > 30 higher areas of the primate (Van Essen 2004), the principles of information transfer between these areas might be similar. For instance, the responses in higher cortical areas seem to be more specialized than in V1. However, stimulus preferences have been characterized for only some of them – like LM, AL, RL, AM, PM, LI (Andermann et al 2011, Glickfeld

et al 2013, Marshel et al 2011, Tohmi et al 2009, Van den Bergh et al 2010), whereas functions of other areas remain unclear.

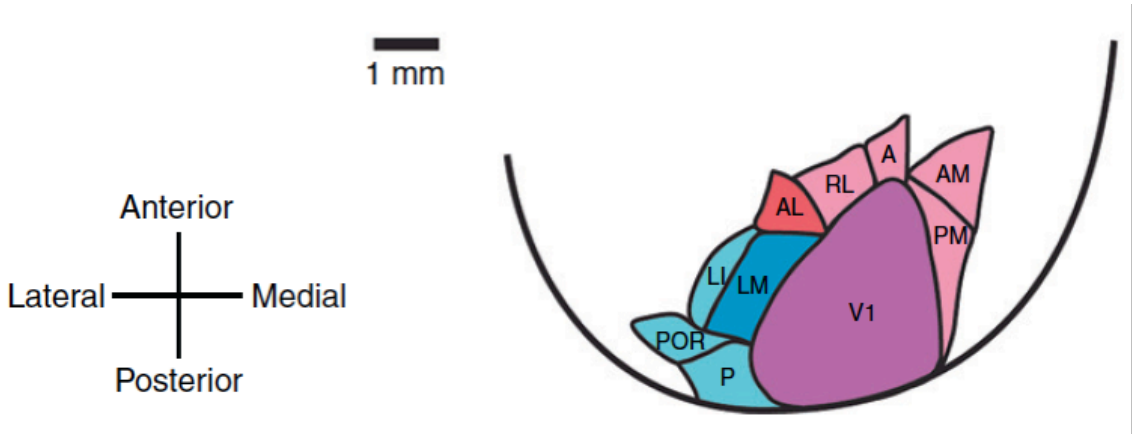

Figure 13. Visuotopically organized visual areas – primary visual cortex (V1), posterior (P), lateromedial (LM), anteriolateral (AL), rostrolateral (RL), anterior (A), anteromedial (AM), posteriomedial (PM), laterointermediate (LI), and postrhinal (POR). Adapted from (Katzner & Weigelt 2013, Niell 2011, Wang & Burkhalter 2007).

Novel, high-resolution imaging studies showed that mouse higher visual areas share similar properties with higher mammals extrastriate cortex, so scientists started to identify ventral and dorsal functional streams of visual processing (Katzner & Weigelt 2013). In primates ventral stream is specialized to recognize objects while dorsal stream is responsible for spatial perception (Kravitz et al 2011).

Strongest outputs from V1 terminate in LM and AL, and are suggested to be the main paths to ventral and dorsal streams (Katzner & Weigelt 2013, Wang et al 2011a, Wang et al 2012). Medial extrastriate visual areas of the mouse (AL, RL, A, AM an PM (Figure 13, shown in red)) are considered as homologous to the monkey dorsal stream, whereas lateral areas (LM, P, LI, POR) – ventral stream (Figure 13, shown in blue). Wang et al., (2012) also

showed that within stream connections are ~22% stronger than between streams (Wang et al 2012).

Also notable that V1 of the mouse projects to all visual areas whilst V1 of the primate projects only to V2, V3, V4 and MT (middle temporal area) (Felleman & Van Essen 1991, Wang et al 2012).

Visual information processing takes place in an intricate network composed of different cell types, which form highly specific local circuits consisting of excitatory and inhibitory neurons. These neurons in visual cortex make networks and circuits that contribute to perception and leads to behavior.

1.4.1 Inhibitory neurons

Inhibitory neurons morphologically are highly diverse (reviewed in (Markram et al 2004)) and constitute 10–30% of the neuronal population (Defelipe et al 2013, Gonchar et al 2007b, Lee et al 2012), but seem highly important for forming responses to sensory stimuli (Adesnik et al 2012, Atallah et al 2012, Haider et al 2013, Katzner et al 2011, Wilson et al 2012).

The main inhibitory neurotransmitter that is used in cortical interneurons is GABA. Despite the fact that neurons use the same neurotransmitter, there is big diversity in different types of GABAergic neurons according to their features such as connectivity, firing pattern or morphology (Figure 14) (Gonchar et al 2007b, Kawaguchi & Kondo 2002, Markram et al 2004).

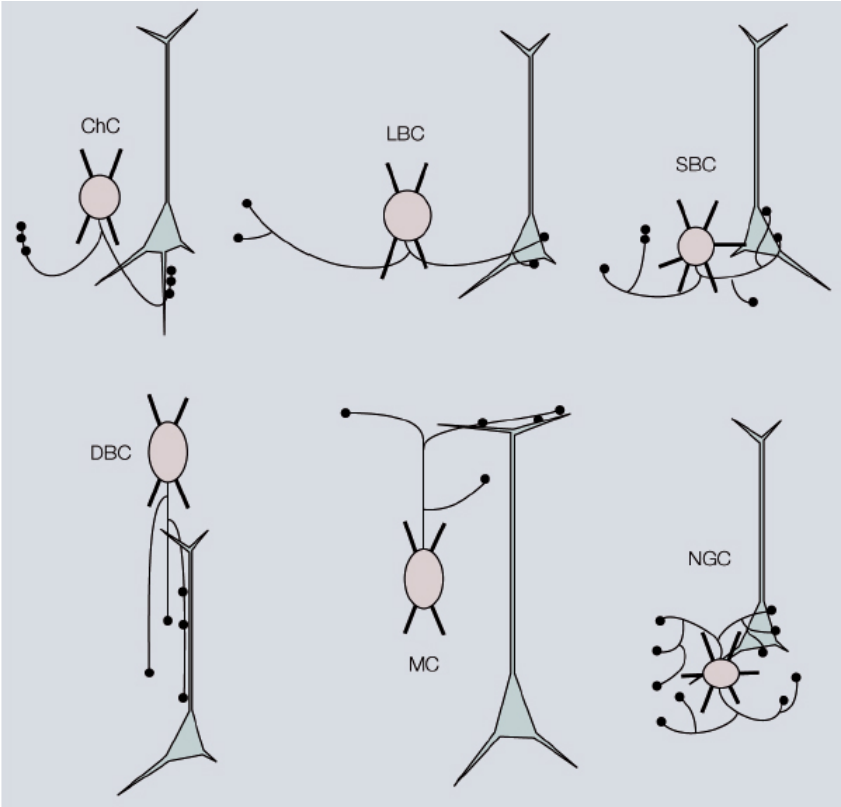

Figure 14. Morphological diversity of interneurons found in neocortex. Interneurons are distinguished mainly according to their axonal arborization and their target cells. Chandelier cells (ChC), small basket cells (SBC), large basket cells (LBC), neurogliaform cells (NGC), double bouquet cells (DBC) and Martinotti cells (MC). Adapted from (Burkhalter 2008).

Moreover, inhibitory cells can be classified according to expressed calcium-binding proteins and peptides: calbidin (CB), parvalbumin (PV), somatostatin (SOM), calretinin (CR), vasointestinal polypeptide (VIP), neuropeptide Y (NPY), cholecystokinin (CCK) and choline acetyltransferase (ChAT) (Figure 15) (Defelipe et al 2013, Gonchar et al 2007b, Lee et al 2010, Markram et al 2004).

Using triple immunostaining (PV, SOM and CR), it was shown that PV interneurons never coexist with other chemical profiles in the mouse primary visual cortex (Gonchar et al 2007b). Controversially to that, in earlier studies it was shown that they might coexist (Markram et al 2004). Other markers

have shown different combinations and overlaps between groups. In this way, at least 13 different groups of interneurons have been counted (Gonchar et al 2007b).

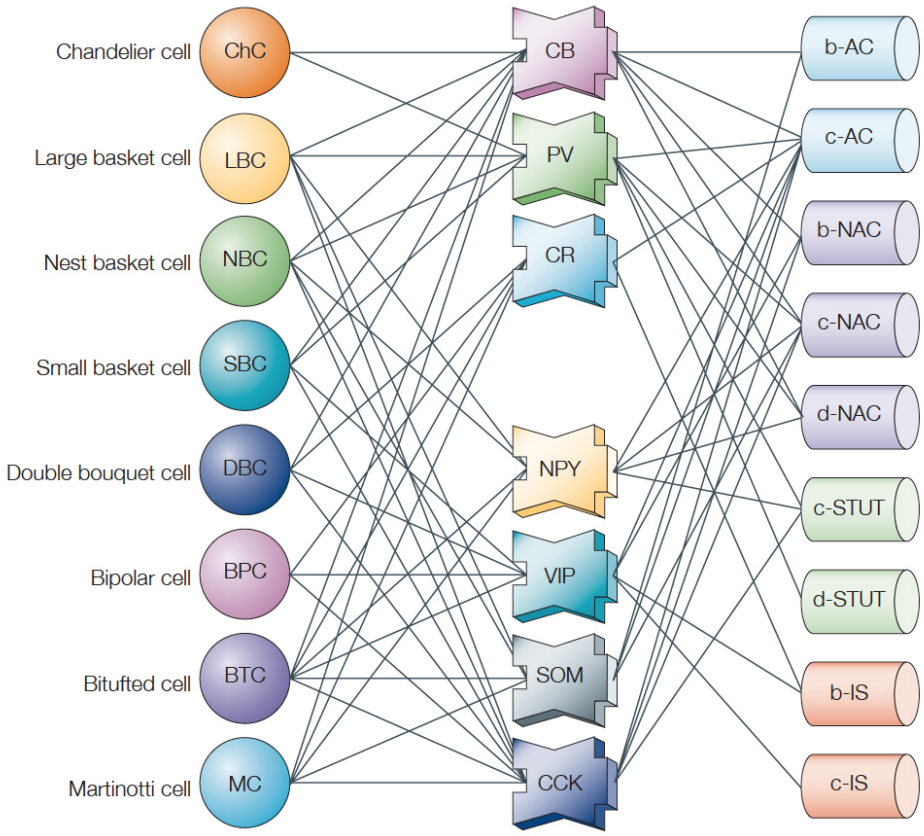

Figure 15. Expression of calcium-binding proteins and peptides in different electrophysiological and morphological neuron types. Calbidin (CB), parvalbumin (PV), somatostatin (SOM), calretinin (CR), vasointestinal polypeptide (VIP), neuropeptide Y (NPY), cholecystokinin (CCK). AC, accommodating; b, burst subtype; c, classic subtype; d, delay subtype; IS, irregular spiking; NAC, non-accomodating; STUT, stuttering. Adapted from (Markram et al 2004).

After the different types of interneurons were first described in terms of their morphology, the following was inquired: what are the firing properties and more important, what is the function of each type of interneuron group? After a pioneering study of McCormick (1985), in which he separated interneurons

and pyramidal cells, all inhibitory interneurons were described as fast-spiking cells (Connors & Gutnick 1990, McCormick et al 1985). Later recordings revealed that inhibitory cells could have a diversity of firing patterns. Hence, inhibitory interneurons can be classified into different electrophysiological types according to their action potential waveform (Figure 16) (Ascoli et al 2008, Burkhalter 2008, Connors & Gutnick 1990, Kawaguchi 1993, Markram et al 2004). Krimer et al. (2005) in his study with monkeys pointed out that sometimes electrophysiological and morphological properties match (Krimer et al 2005). The authors assigned fast spiking properties to cells with BSs and ChCs morphological properties, intermediate spiking (that Makram et al. (2004) has not described) to DBs or MCs, which have vertically orientated axons, and non-fast spiking properties to NGCs (Krimer et al 2005). Extracellular recording studies in mice, rats or cats sometimes still classify neurons into 2 main groups: narrow–spiking cells as interneurons and broad–spiking as excitatory neurons (Atencio & Schreiner 2008, Bartho et al 2004, Niell & Stryker 2008).

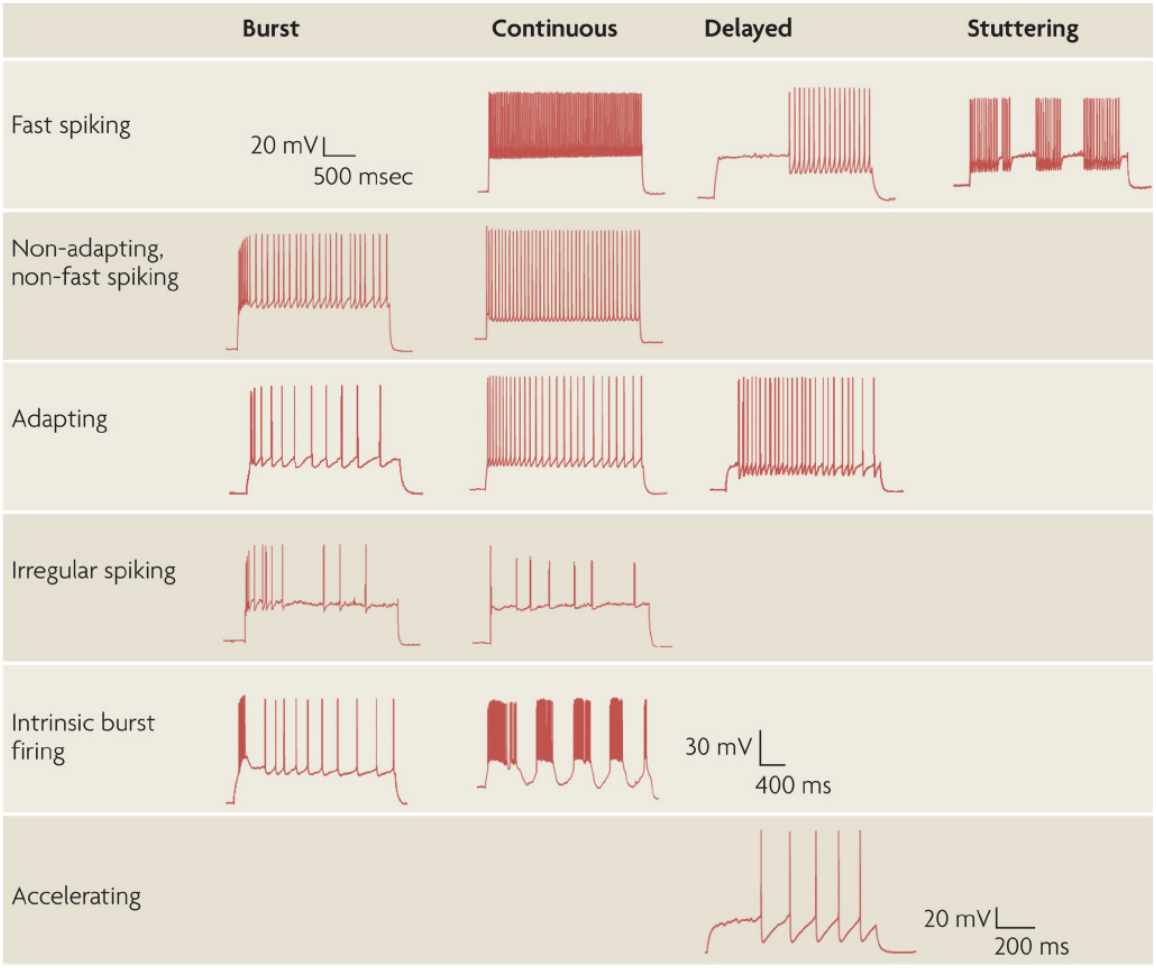

Figure 16. Electrophysiological types of inhibitory interneurons as described in the Petilla terminology. Adapted from (Ascoli et al 2008).

Different groups of inhibitory neurons in mouse visual cortex have a distinct laminar distribution (Figure 17) (Butt et al 2005, Gonchar et al 2007b, Xu et al 2004). Moreover, during postnatal development, the number of different interneuron classes is not constant. During the first postnatal week, GABAergic neurons still contain very little CR, SOM or PV; but a laminar distribution is already observable – CR immunoreactive cells (Figure 17, cells labeled in green) are most numerous in layer 2/3, while SOM cells (Figure 17, cells labeled in blue) are found in deepest layers. At P13, SOM-positive cells are already found in layers 2/3 and 4. At P0 PV immunoreactivity is absent

and appears only after two weeks, right before eye opening. In adult mice, PV-positive interneurons (Figure 17, cells labeled in red) are founded in all layers except layer 1. It has been shown that the highest proportion of PV-positive interneurons is found in layer 5, where they constitute more than half of all GABAergic neurons. It is interesting to note that CR- and SOM-positive interneurons develop from different embryonic structures; in newborns they are expressed in different neurons separately and only after approximately one week they start to coexist together. In the beginning of postnatal development, the largest proportion of inhibitory interneurons expresses CR and is found mostly in layer 1 and the cortical plate, but surprisingly, the majority of these neurons are not GABA immunoreactive. In the second postnatal week, appear such combinations as SOM + CR in upper layers. After eye opening (around P16), more types of interneurons (CR, SOM and PV) can be found in primary visual cortex of mice (Butt et al 2005, Gonchar et al 2007b, Xu et al 2004).

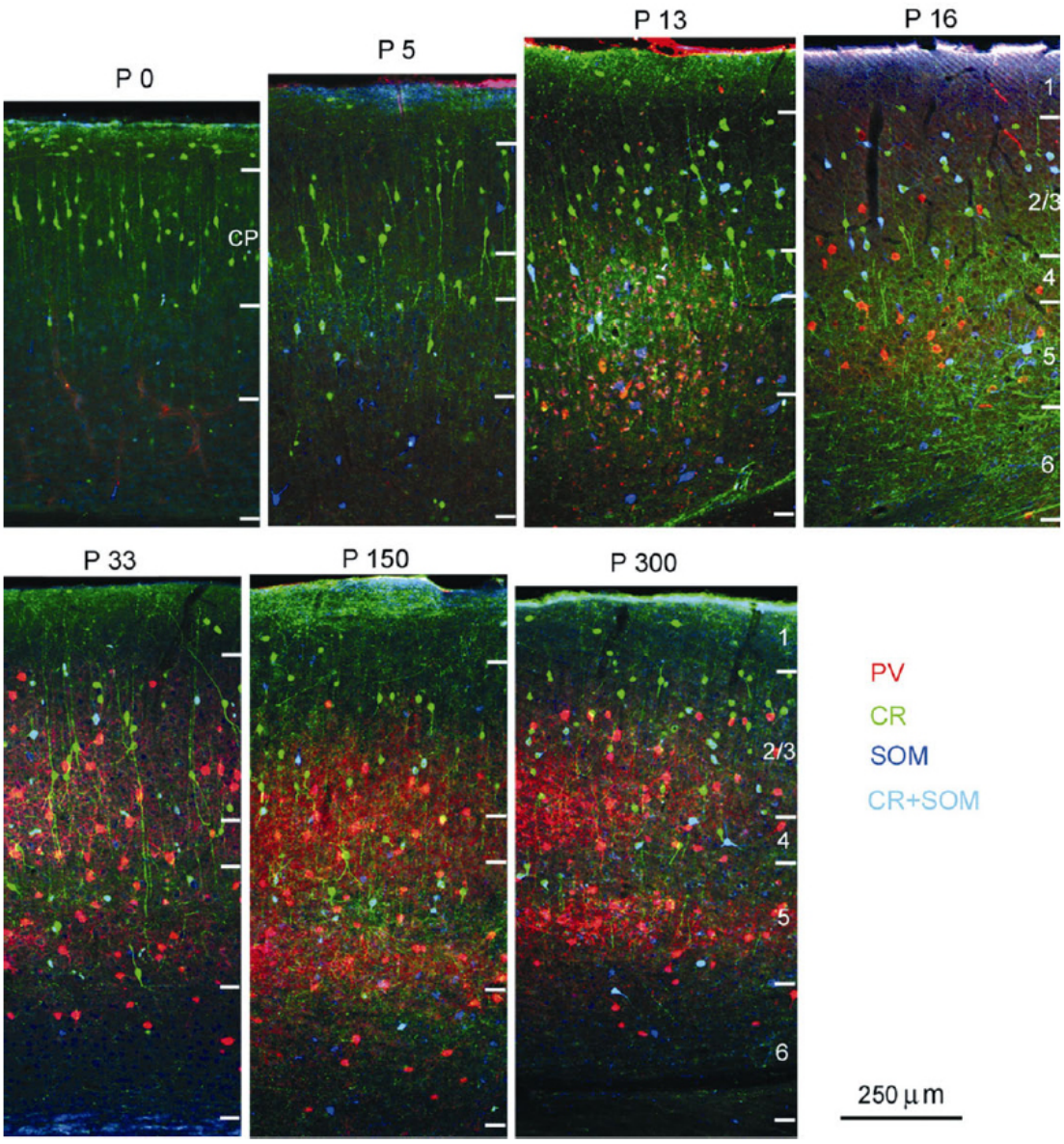

Figure 17. Immunolabeling with antibodies against PV, CR and SOM during different periods of development. P13 – one day before eye opening which coincides with presence of PV expression. Adapted from (Gonchar et al 2007b).

Since the most abundant interneurons in the primary visual cortex of the mouse are soma-targeting PV-positive (PV+), here we will discuss more closely only PV+ interneurons and will compare PV+ vs. SOM+ interneurons

(as the second largest class of interneurons). Later in this thesis, we will describe optogenetical experiments targeting in particular PV+ cells.

1.4.1.1 PV interneurons:

As it was mentioned previously, parvalbumin (PV) interneurons are the largest class of inhibitory neurons in visual cortex. It has been shown that PV immunoreactive cells constitute a smaller proportion (40-50%) of GABAergic neurons in rodent V1 compared to macaques (74% of GABAergic population) (Burkhalter 2008, DeFelipe 1999, Gonchar et al 2007a). It is known that this group of interneurons contributes to gain control (Atallah et al 2012, Helm et al 2013), sharpens selectivity of neighboring neurons to particular stimulus features such as direction or orientation, enhances perceptual discrimination (Lee et al 2012) and induces gamma rhythm (Cardin et al 2009). As it is reviewed in Markram et al (2004), not all fast spiking cells are PV^+ neurons or inhibitory interneurons and moreover, not all PV^+ cells are fast spiking cells. In the border between layer 1 and 2, there are PV neurons that act as multipolar bursting (MB) cells (Blatow et al 2003). MB cells were described in neocortex and supposedly by recruiting cholinergic activity create theta oscillations and in this way regulate the output of pyramidal cells (Blatow et al 2003).

There are two main morphological groups of fast-spiking PV+ interneurons: chandelier and basket cells (Figure 18) (Helm et al 2013, Karube et al 2004, Patz et al 2004).

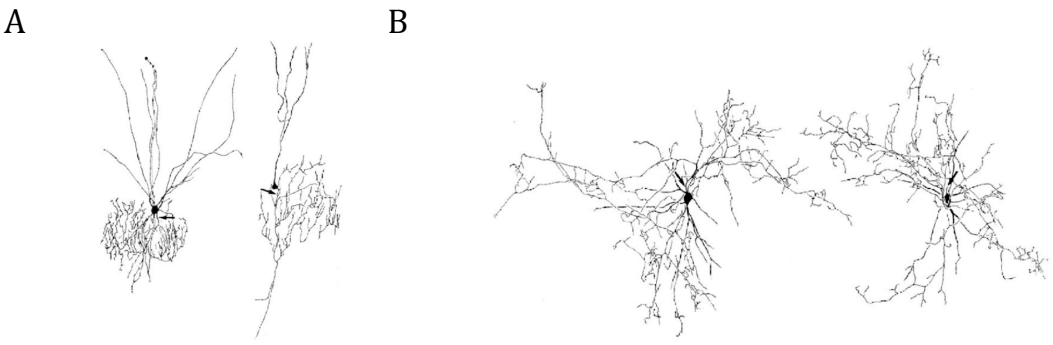

Figure 18. Morphological types of PV-interneurons. A: Chandelier cells. B: Basket cells. Adapted from (Patz et al 2004).

Chandelier cells terminate on the initial segment of the axon, while basket cells target soma and proximal dendrites (Karube et al 2004, Markram et al 2004). There is little known about firing rates of basket cells due to the diversity of receptive field and electrophysiological signal properties (Helm et al 2013, Runyan et al 2010). Chandelier cells are more homogenous and show short delay to action potential (AP) onset (Helm et al 2013).

In recent study (Helm et al 2013), authors described 4 different types of PV^+ basket cells in layer 2/3 of mouse visual cortex according to their firing properties (Figure 19). They found that with strong stimulation, all PV interneurons develop continuous firing. Subgroups differ in resting membrane potential, action potential shape and excitatory inputs. PV1a subtypes start fire at much higher rates compared to PV1b when current is close to rheobase, PV2 shows the same stuttering effect, just in a higher range and subtype PV3 loses its stuttering pattern.

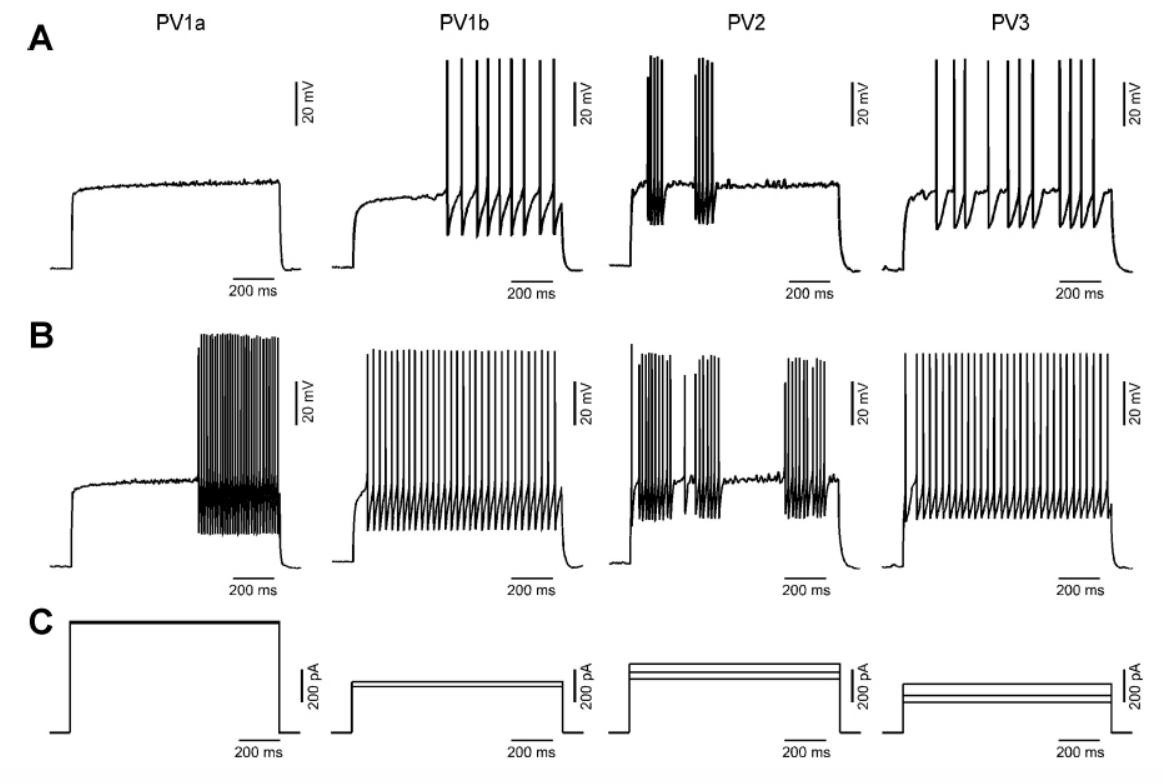

Figure 19. Membrane properties of PV interneuron subgroups. Action potential (AP) firing patters from example cells from all (PV1a, PV1b, PV2 and PV3) subgroups. A: near-rheobase voltage traces contain ~10 APs. B: the same cells as in A, but voltage traces contain ~30 APs. C. depolarizing currents injected into current-clamped PV interneurons (for cells shown in A and B). Adapted from (Helm et al 2013).

The cortical circuits formed by PV^+ interneurons have already been investigated broadly by many scientists and it has been revealed that fast-spiking PV+ interneurons are involved in feedforward inhibition in thalamocortical, interlaminar and interareal circuits (Burkhalter 2008, Nienborg et al 2013, Porter et al 2001, Thomson et al 2002). In feedforward inhibitory circuit, thalamocortical axons projects and excites both, spiny neurons in layer 4 and PV+ interneurons. Responses of spiny cells are very short because of the simultaneously incoming inhibitory signal from PV+ cells.

Parvalbumin cells inhibit the somatic and perisomatic compartments of pyramidal cells (Kawaguchi & Kubota 1997). In this way PV cells modify the responses of principal cells (Atallah et al 2012).

Whereas PV^+ cells include several morphological subtypes of interneurons, the properties of PV^+ interneurons are heterogeneous (Lee et al 2012, Runyan et al 2010). Nevertheless, RF size and spatial tuning is similar to the rest population of neurons in V1. Some PV^+ interneurons have sharp orientation tuning, but some cells have broad range of orientation tuning. It is not clear yet why there is this diversity of results (Runyan et al 2010). There are suggestions that broadly tuned PV^+ cells are important for "contrast-invariant orientation tuning" (Nienborg et al 2013, Runyan et al 2010).

Sharply tuned PV^+ cells can be explained by feedforward push-pull model. According to this model, stimulus selectivity is sharpened when the excitation, arising from the thalamocortical projections, ("push") is supplemented by an opposing polarity inhibition ("pull") (Runyan et al 2010).

Some groups (Atallah et al 2012, Li et al 2014) manipulated PV cell activity in visual cortex and revealed that parvalbumin interneurons strongly modulate spiking activity of pyramid cells in layer 2/3. Tuning properties to visual stimuli are affected only mildly.

PV interneuron activation in V1 also increases the preferred stimulus size of neighboring neurons and independently from the layer (Figure 20D-F), similar to effects of reducing overall stimulus contrast (Figure 20A-C); SOM-driven inhibition, on the contrary, leads to a decrease of preferred size (Figure 20G-I), but only in superficial layers (Nienborg et al 2013).

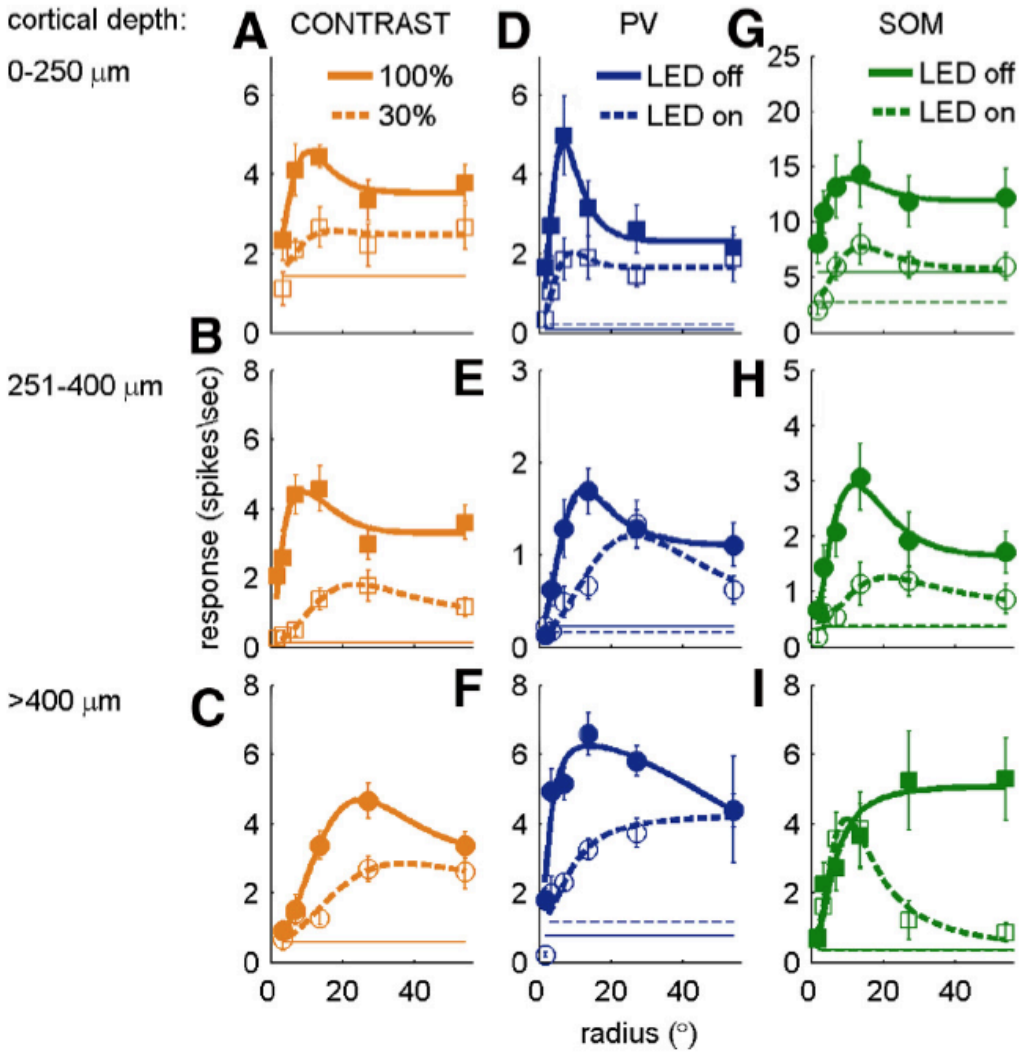

Figure 20. Contrast, PV- or SOM- driven responses in laminar profile. A-C: Size tuning properties to 100% contrast (solid line) and to 30% contast (dashed line). D-F: Size tuning properties to 100% visual stimuli during PV-driven visual cortex inhibition. G-I: Same as D-F, during SOM-driven inhibition. Squares – data from single units, circles – data from multiunits. Adapted from (Nienborg et al 2013).

1.4.2 Excitatory neurons

The major excitatory cells constituting 70 – 85% of neuronal population in the cortex are pyramidal (principal) neurons. The classical pyramidal neuron is described as a cell, in which from the apex of the soma a single axon

emerges and which has spiny dendrites, separated in several short basal dendrites and one long apical dendrite (Figure 21). These cells are also known as the major cortico-subcortical projected neurons (Romand et al 2011).

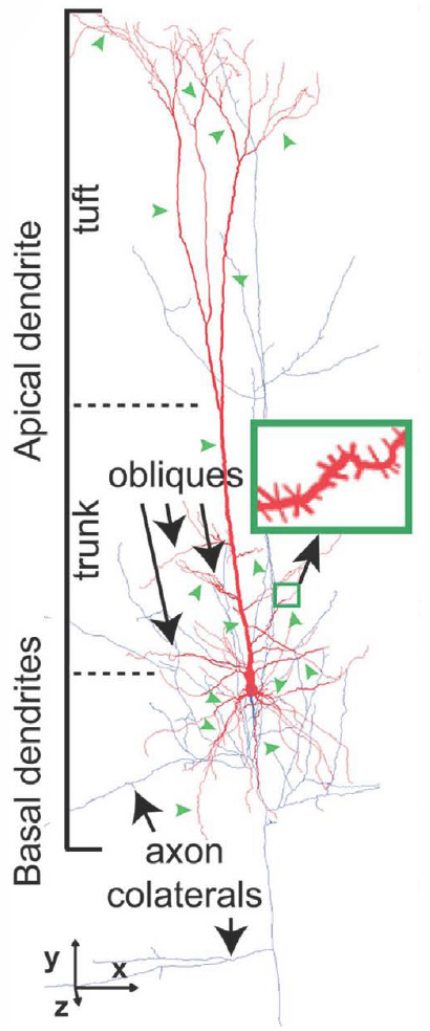

Figure 21. Morphometric analysis of a pyramidal cell. As an example given thick-tufted layer V pyramidal (TTL5) cell. Red, dendrites; blue, axon; green arrowheads, randomly selected sites with spines. Adapted from (Romand et al 2011).

Excitatory pyramidal cells are an anatomically inhomogenous group. Often, pyramidal cells from the same layer can target different regions. In layer 5, the largest, burst-firing pyramidal neurons are found, which have long apical

dendrites that terminate in layers 1 and 2 (Wang & McCormick 1993). The same cells can project to superior colliculus (SC) and pons (Wang & McCormick 1993). Regular spiking pyramidal neurons, that are also found in layer 5, are smaller and usually do not reach further than layer 3; however, regular spiking pyramids can project to striatum (from upper layer 5) or terminate in non-specific regions of the thalamus (from lower layer 5) (Thomson & Bannister 2003, White & Hersch 1982). From there, the signal is carried on via other pyramidal cells to the pulvinar and SC. These cells do not project to dLGN or TRN (Jones et al 2001). Pyramidal cells from layer 6 are morphologically diverse and can be 1) small, short pyramids; 2) modified pyramids; 3) inverted pyramids and 4) spiny bipolar cells. Upper layer 6 contains more vertically oriented cells that project to layers 4, 5, V2, MT, SC and thalamus while the lower part contains more horizontally oriented cells that project locally to layer 6 (Briggs 2010, Zhang & Deschenes 1997). In cats it has been shown that simple cells from layer 6 project to layer 4 and complex cells to layer 2/3. Layer 4 contains spiny excitatory cells with various axonal arbors that target layers 2, 3 and deeper layers. Pyramidal cells in layer 3 have long axon collaterals and spiny dendrites. Axons of these cells furcate in layers 2/3, 5 and 6. Pyramidal axons of layer 5 ramifying mostly in the same layer and can have long horizontally distributed brunches. These cells can project to all other layers, but layer 2/3 receives weak, although prominent projections (reviewed in: (Thomson & Bannister 2003)). Rodents and cats layer 6 of sensory cortices have less morphologically heterogeneous, nevertheless bigger proportion of corticothalamic neurons compared to primates (Briggs 2010).

1.4.3 Mouse line B6;129P2-Pvalb$^{tm1(cre)Arbr}$/J

Circuit disruption methods are useful to investigate the precise function of the certain brain structure or even specific type of the neurons. To inactivate

cortex various methods can be used, such as cooling (Webb et al 2002), pharmacology (Jones et al 2000) or optogenetics (Adesnik et al 2012, Nienborg et al 2013, Olsen et al 2012). In this work we will use PV-Cre mouse line to inactivate cortex optogenetically by activating PV+ interneurons.

B6;129P2-Pvalb$^{tm1(cre)Arbr}$/J is a transgenic mouse line model that has recombination with loxP sites in more than 90% of PV+ cells. Cre recombinase is expressed from the endogenous Pvalb gene locus (http://jaxmice.jax.org/strain/008069.html).

To express channelrhodopsin-2 (ChR2) in the area of interest, CRE-dependent adeno-associated virus (AAV) is used. Within a few weeks after injection, ChR2 is expressed selectively in PV+ interneurons that can be activated by blue light (Adesnik et al 2012).

1.5 Receptive fields of RGCs, LGN and V1 neurons

Since different stages of the visual processing hierarchy contain different cells with various response properties, here we describe receptive filed (RFs) properties of mouse retina' ganglion cells (RGCs), lateral geniculate nucleus (LGN) and primary visual cortex (V1), mainly focusing on LGN and V1.

In classical Hubel and Wiesel (Hubel & Wiesel 1962) model, LGN simply relay concentric and unturned retinal RFs to the V1, where they get selective for the visual stimulus properties (Figure 22) (Scholl et al 2013). Recent studies in mice revealed, that in mouse even in retina RF' already has orientation or/and direction selectivity (Niell 2013, Scholl et al 2013).

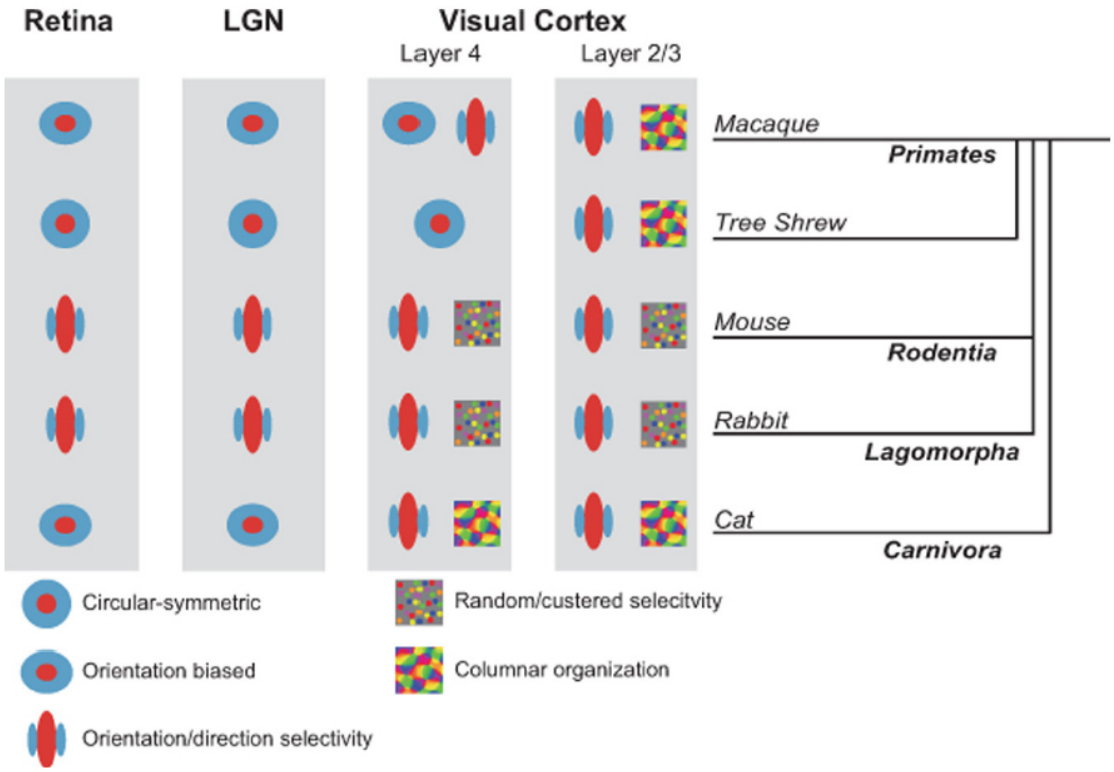

Figure 22. RF properties of the early visual system in different species. Adapted from (Scholl et al 2013).

In mouse RGCs the range of RF sizes is 4-20 degrees, but the mean diameters of RFs center of ON-center and OFF-center cells are similar (11.9±0.86 and 11.3±0.51 respectively) (Figure 23) (Nirenberg & Meister 1997, Porciatti et al 1999, Sagdullaev & McCall 2005, Sinclair et al 2004). Despite the fact that the overall distributions of the optimal spot diameter of ON- and OFF-center cells in mouse retina overlap and there is no difference in means, RGC show spatial summation within their RF (Sagdullaev & McCall 2005).

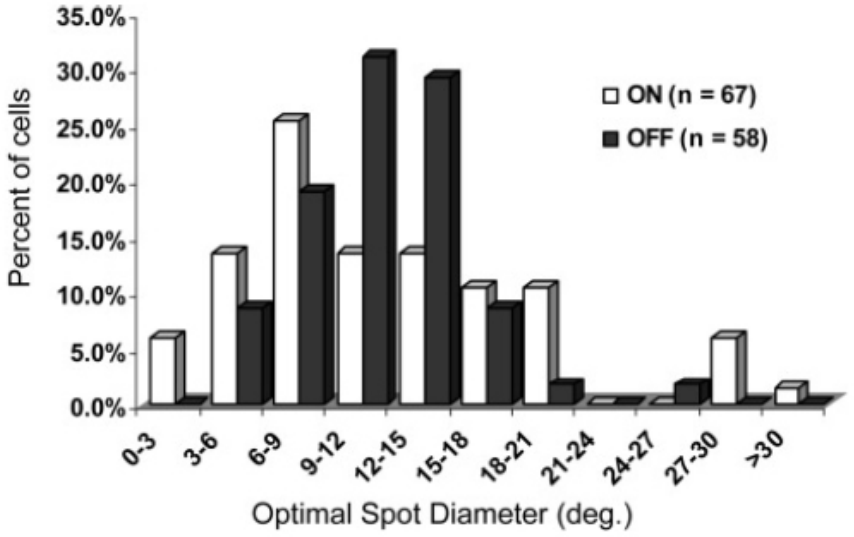

Figure 23. The distributions of optimal spot diameter between ON- and OFF-center cells in mouse RGC. Black are OFF-center units, white are ON-center units. Adapted from (Sagdullaev & McCall 2005).

In a recent paper, Piscopo et al (2013) described typical receptive field characteristic of several classes of dLGN neurons. According to their results, receptive fields (RFs) in mouse dLGN are organized, as in RGCs (Sagdullaev & McCall 2005), in a center – surround manner (sustained ON, sustained OFF and transient OFF (Figure 24A)) and have linear spatial summation (Krahe et al 2011, Piscopo et al 2013). Similar findings have been shown in monkeys' M-cells, which correspond to mouse Y-like cells (Krahe et al 2011, Usrey & Reid 2000). Moreover, almost all these center–surround cells have strong surround suppression (Figure 24E). Cells respond to all orientations equally, but fire in a characteristic periodic pattern (F1 response component) at the temporal frequency of the grating (Figure 24B,C). Moreover, dLGN prefer higher speed than cortical neurons (Figure 24F) (Piscopo et al 2013).

It is noteworthy that some authors failed to find direction selective cells in dLGN. One reason could be that direction selective cells (which at least partly seems to be inherited from retina (Cruz-Martin et al 2014)) are imbedded

only in dorsolateral part of dLGN (Huberman et al 2009, Kim et al 2010, Kim et al 2008, Krahe et al 2011, Marshel et al 2012, Rivlin-Etzion et al 2011).

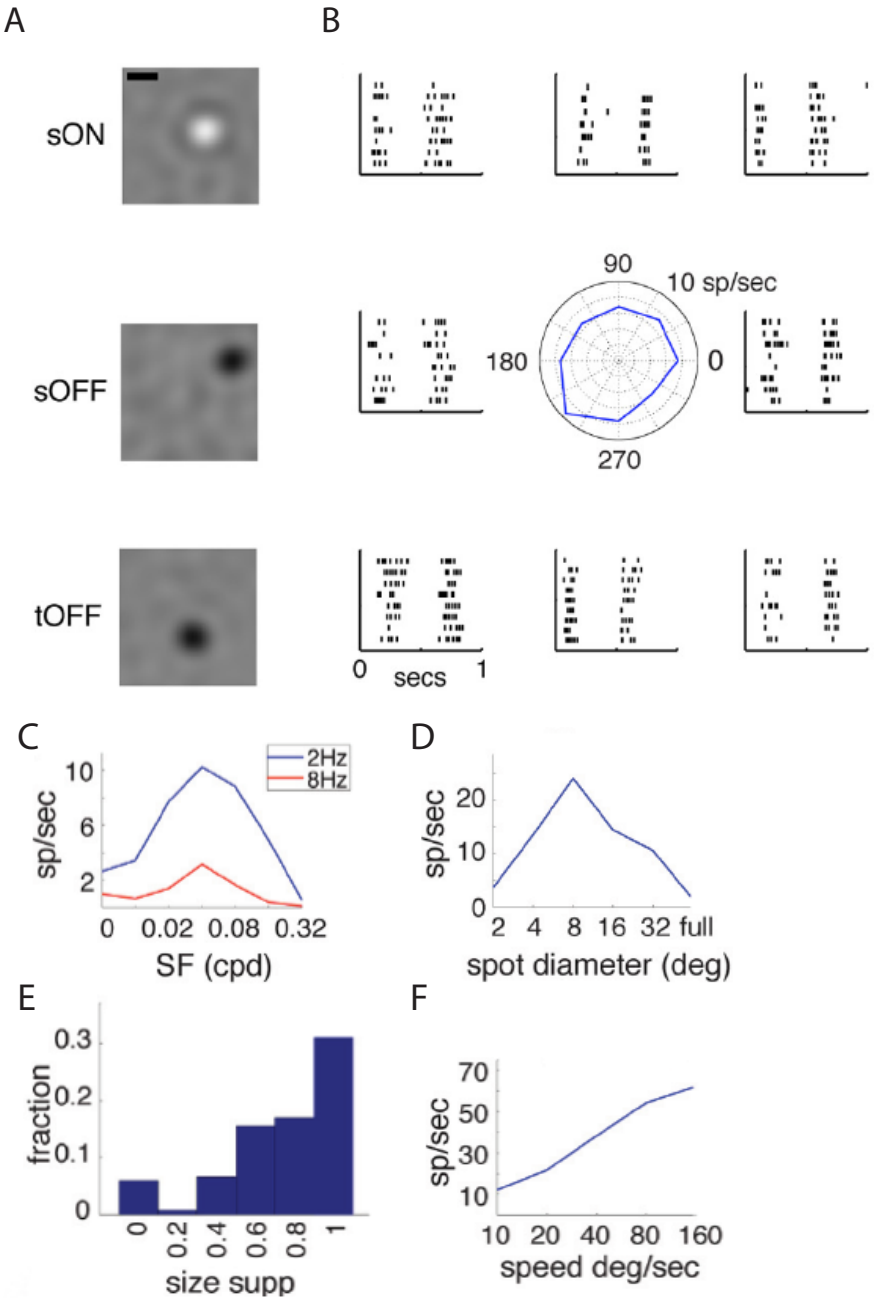

Figure 24. RF properties of mouse dLGN. A: Representative example RFs from sON, sOFF and tOFF groups. Scale bar, 10°. B: Raster plots for sON RF shown in A **part with strong F1 response component. Responses to drifting gratings to 8 directions at 2Hz temporal frequency and 0.04 cpd spatial frequency. C: Spatial-frequency tuning curve for unit demonstrated in** B**. D: Size-tuning**

curve examined with flashing spots. E: Size suppression in all 3 center-surround groups. F: Speed-tuning curve measured with moving spots for unit demonstrated in B**. Adapted from (Piscopo et al 2013).**

The mean size of RFs in the mouse dLGN is approximately 10 degrees (example cell in Figure 24D), but depending on source of literature varies from 6 to 14 degrees; no significant difference in RF size between anaesthetized and awake state has been found (Gordon & Stryker 1996, Grubb & Thompson 2003, Metin et al 1988, Piscopo et al 2013). These results show that the diameters of RFs are comparable to those found for mouse RGC (Sagdullaev & McCall 2005).

Niell and Stryker (2008) reported that majority of the neurons in V1 strongly respond at least to one feature (a temporal or a spatial frequency, an orientation or a direction) of the presented visual stimuli.

Receptive fields in V1 are wider than in LGN and constitute 10-30 degrees. Excitatory cells have smaller receptive fields compared to inhibitory cells, and the overall smallest RFs are found in superficial layers (10-14 degrees) (Figure 25) (Niell & Stryker 2008).

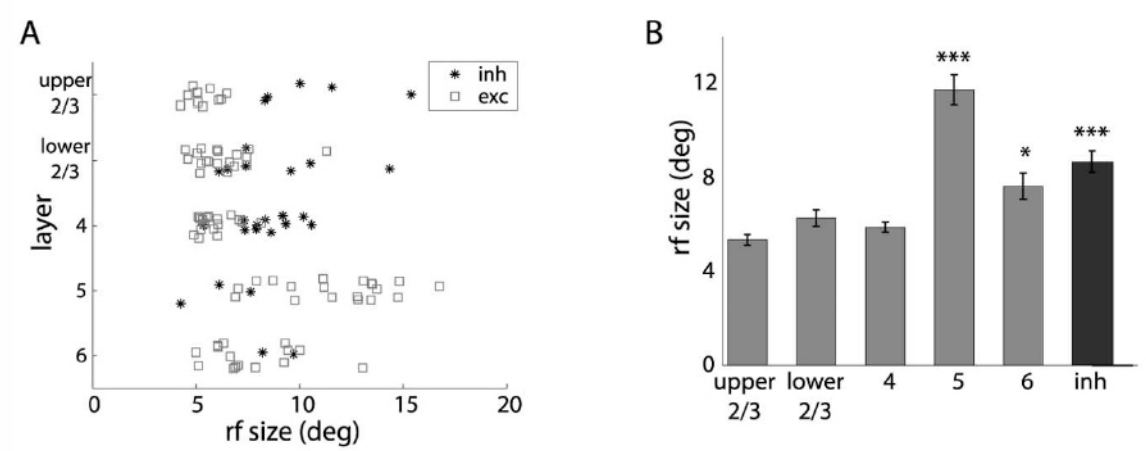

Figure 25. Receptive field size and laminar distribution. A: RF size distribution of 108 units by layer and cell type: inhibitory, stars; excitatory, squares). B: Mean RF sizes. Stars show significance between groups. Excitatory neurons, grey columns; inhibitory neurons, black column. Adapted from (Niell & Stryker 2008).

Mice, similar to rats or squirrels, do not have a columnar organization and orientation map in V1 as it is shown in higher mammals, but nevertheless, cells show selectivity to orientation (OS) (Figure 26) (Gur et al 2005, Jin et al 2011, Maier et al 2011, Niell & Stryker 2008, Ohki et al 2005, Sirotin & Das 2010, Van Hooser et al 2005). Cortical inhibition can sharpen OS, and most pieces of evidence come from electrophysiological studies with monkeys (Ringach et al 2003, Xing et al 2011). In mouse V1, neurons are well tuned for orientation; orientation tuning is sharpest in superficial layers (Metin et al 1988, Niell & Stryker 2008). It is a currently debated whether RFs in mouse dLGN are already selective to orientation and direction (DS) or not. In two recently published *in vivo* studies of mouse dLGN (Marshel et al 2012, Piscopo et al 2013), the authors claim that dLGN RFs encodes much more diverse information than previously thought and are selective to both orientation and direction. Piscopo et al. (2013), using extracellular recordings, revealed that 11% of LGN neurons are OS/DS selective and these units are nonlinear cells – they respond to drifting gratings in a continuous

way. Moreover, the majority of OS/DS neurons in dLGN are driven by stimuli moving along the cardinal axis and the remaining OS/DS cells are driven by intermediate directions. Since the retinal DSGCs which projects to LGN already contain similar OS/DS properties (Huberman et al 2009, Weng et al 2005), the authors concluded that majority of OS/DS LGN neurons could already get motion inputs from RGC. Marshell et al (2012), using two-photon calcium imaging, found that OS/DS cells are more selective for horizontal – axis motion. But in this study they where imaging only upper 75 µm of dLGN. It is worth to mention that natural scenes also contain more vertical and horizontal patterns compared with diagonals (Girshick et al 2011).

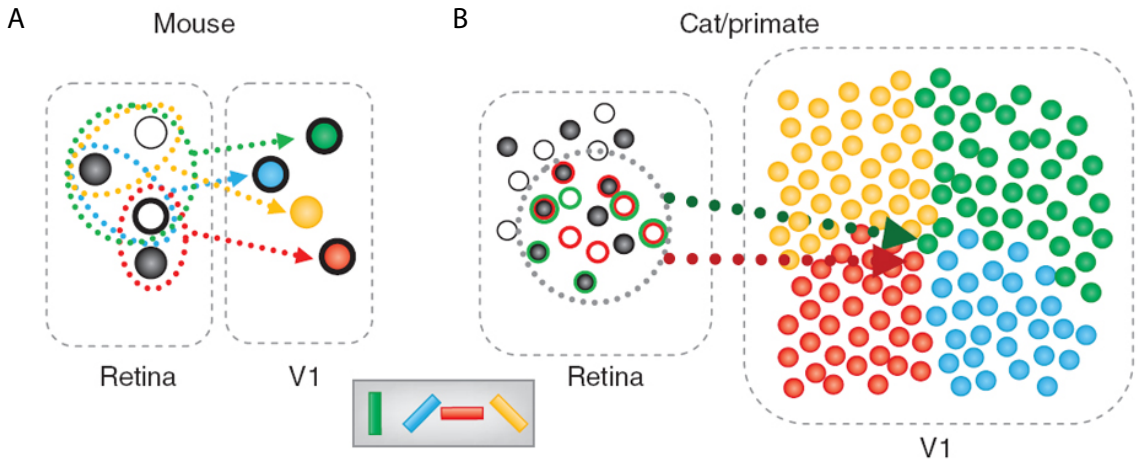

Figure 26. Comparison of receptive field tuning properties in visual cortexes of rodents and cats/macaques. A: Schematic illustration of orientation map in rodent retina and primary visual cortex. Mouse retina contains ~1 RGC per input neuron in V1. Horizontal (red) and vertical (green) tuned cells share subfields in retina, nevertheless being far away from each other in cortex. B: Schematic illustration of orientation map in cat and macaque retina and primary visual cortex. One RGC cell have connections with ~ 100 cortical neurons, which are precisely arranged. Different colors correspond to different orientations. Dotted circle, the net receptive field position. Adapted from (Sirotin & Das 2010).

In LGN there are more OS than DS cells and these findings are opposite to those obtained in ganglion cells of the retina, where DS tuned neurons

constitute a bigger population than OS tuned (Jaubert-Miazza et al 2005, Piscopo et al 2013).

There is number of papers where authors reported direction selective cells in the earliest stage of visual processing – retina (Huberman et al 2009, Kay et al 2011, Rivlin-Etzion et al 2011, Weng et al 2005).

Temporal frequency (TF) responses in different processing levels of visual system also differ. In mouse LGN TF values are relatively high – 4 – 16 Hz (Grubb & Thompson 2003). Similar to results in higher-order mammals, neurons in primary visual cortex of the mouse significantly loose temporal resolution, but still remain broadly tuned, i.e. approximately 0.5 - 2 Hz (Niell & Stryker 2008, Roth et al 2012). This loss of temporal resolution is comparable to previous findings in macaques (Hawken et al 1996). Preferred TF significantly increases in layer 4 (Figure 27A,B). Interneurons seem to have higher TF preferences as well (Niell & Stryker 2008).

The spatial frequency (SF) in V1 and LGN is similar. In mouse LGN SF response depends on cell type and vary from 0.02 to 0.1 cpd. Only direction selective cells, which constitute the minority of the population, prefer high values of SF. All other cells (Figure 24C) have similar SF preference as in excitatory cells of V1 – approximately 0.03 cpd (Figure 27) (Grubb & Thompson 2003, Niell & Stryker 2008, Piscopo et al 2013). As a matter of fact, in V1 cells, SF can also vary from 0.02 to 0.08 cpd (Figure 27C). It is noteworthy that preferred SF does not change across layers, but in layer 6, preferred SF values are smaller and are comparable with SF of inhibitory interneurons (Figure 27D). Moreover, SF preference in mouse V1 changes to higher values over duration of the response (Vreysen et al 2012).

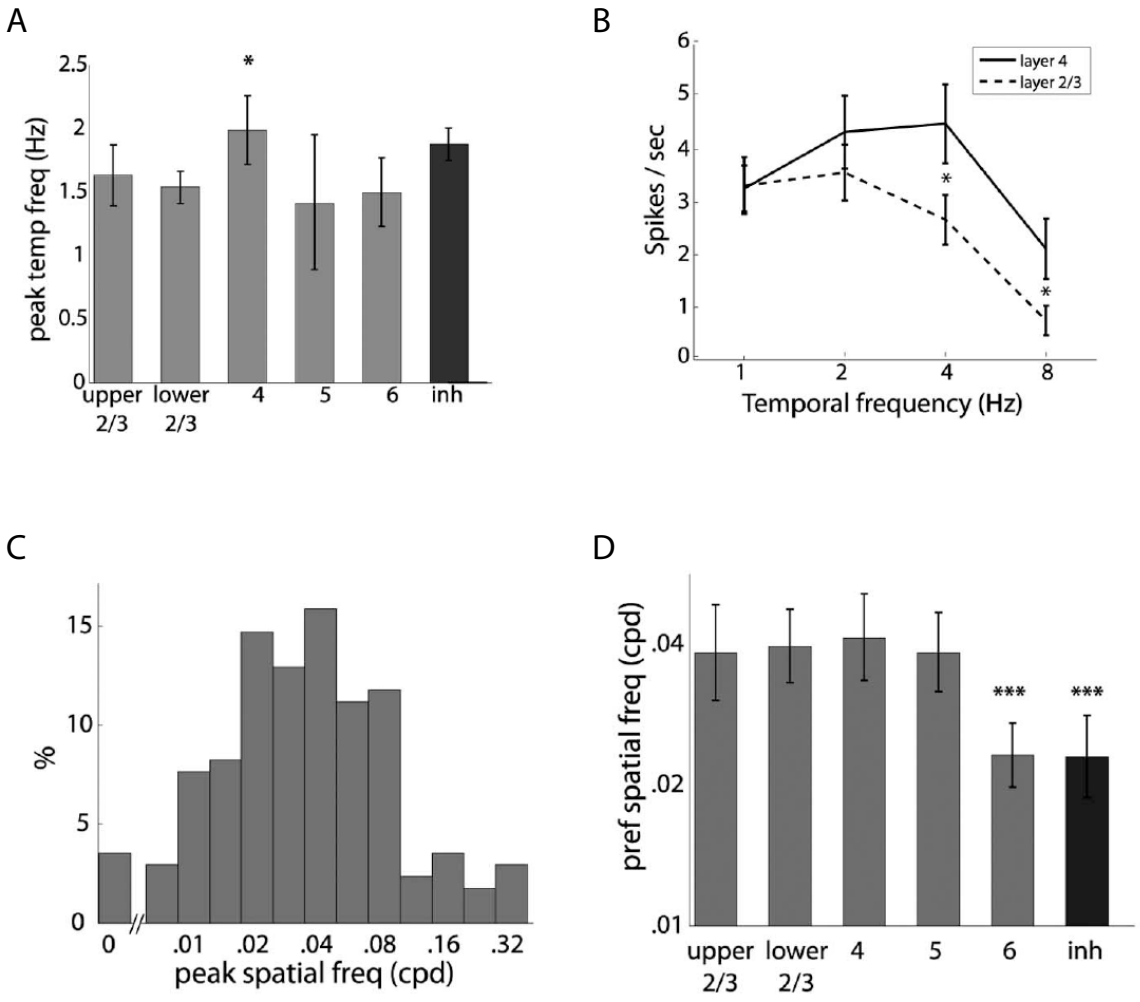

Figure 27. Receptive fields properties in the primary visual cortex of the mouse. A: Averaged median peak temporal frequency for excitatory and inhibitory cells and cortical layers. B: Mean temporal frequency tuning in layers 2/3 and layer 4. C: Spatial frequency preference. D: Median spatial frequency preferences across layers. Adapted from (Niell & Stryker 2008).

There are some studies that explored the role of contrast in the visual system (Busse et al 2011, Li et al 2012, Niell & Stryker 2010, Nienborg et al 2013, Piscopo et al 2013, Prusky & Douglas 2004). Already in Hubel and Wiesel's model (1962) it has been shown that OS does not broaden with increasing contrast. I*n vivo* intracellular recordings in mice revealed that in layer 4, increase in contrast sharpens OS of excitatory neurons (Li et al 2012).

Authors noticed that response was enhanced along with increased contrast for the preferred orientation, but to orthogonal orientation contrast made no difference. Also recent study (Nienborg et al 2013) revealed that lower contrast of stimulus increased the size of preferred stimulus and decreased surround suppression. Although this phenomenon is observed in all layers, in deeper layers the effect is stronger. Interestingly, increased contrast flattered orientation tuning of PV inhibitory neurons (Li et al 2012).

LGN also contains suppressed-by-contrast mechanism (Piscopo et al 2013). There is not known yet a clear function of these, suppressed-by-contrast cells, but some speculations are given by Troy and Enroth-Cugell (1989) suggesting that it could serve as control mechanism for contrast gain.

Surround suppression - when neurons exhibit selectivity for stimulus size, showing suppression of responses when stimuli extend beyond the classical RF into the surround (Adesnik et al 2012, Angelucci & Bressloff 2006, Vreysen et al 2012). In mice, comparable with cats, surround suppression strength is enhanced and higher in dLGN than in RGCs (Grubb & Thompson 2003, Usrey & Reid 1999). It is worth to notice that the strong surround suppression which has been observed in almost all *in vivo* studies, could not be seen exploring in vitro preparations (Stone & Pinto 1993) but see (Adesnik et al 2012). It suggests that a bigger cell pool is required in order to develop surround suppression.

There still remains unclear what is the laminar distribution of size tuning in mouse V1 and how this tuning changes across the layers depending of wakefulness state. Also there is open question how the temporal response profile develops over time and whereas anesthesia changes it. Finally, it is interesting how the spatial integration in V1 can be shaped by PV+ interneurons.

1.6 The influence of locomotion on neural responses of visual cortex

There are suggestions that neuronal responses in mouse visual cortex can be modulated by behavior such as locomotion (Andermann et al 2011, Ayaz et al 2013, Keller et al 2012, Niell & Stryker 2010, Szuts et al 2011). Locomotion leads to more depolarized and less variable membrane potential of all cell types (Polack et al 2013).

One pharmacological study has examined the role of neuromodulators during locomotion in V1 (Polack et al 2013) and found that cholinergic and noradrenergic inputs are both important and act in different ways. Noradrenalin assures the tonic depolarization during locomotion and choline acts during immobility and seems to be responsible for maintaining a unimodal distribution of membrane potential (Polack et al 2013). One of the main sources of noradrenalin is locus coeruleus (LC), which has been noticed activated during mouse walking on the ball (Carter et al 2010). Also there are findings that electrical stimulation of the rat LC (Holdefer & Jacobs 1994) and pharmacological application of noradrenaline agonists in the cat LGN (Funke et al 1993) reduce thalamic burst mode firing.

Increase in neural response can shape spatial integration (Ayaz et al 2013). Lately studies in mouse suggest that locomotion has two main impacts: increases overall spontaneous activity almost double in V1 all layers equally and weakens suppression (Ayaz et al 2013). Suppression index during stationary state decreases by 15% comparing to locomotion. V1 (Andermann et al 2011, Niell & Stryker 2010) and AL (Andermann et al 2011) neurons also show significant increase in peak response. Moreover, locomotion tends to increase responses to larger stimuli versus small (Ayaz et al 2013).

Interestingly, Niell and Stryker (2010) did not observe change in selectivity for stimulus orientation during locomotion (Niell & Stryker 2010).

Another study revealed that temporal frequency tuning and speed tuning are enhanced when animal moves, but apparently it has no effect on spatial frequency tuning (Andermann et al 2011). These findings are specific not only to V1, but also in some other, higher visual areas. Andermann et al. (2011) observed speed peak differences between behavioral states in areas AL and PM, and found similar increase of firing rate in both areas (Figure 28), the increase in PM was just not significant. Finally, it has been reported that in mouse LGN modulation of responses by locomotion is absent (Niell & Stryker 2010).

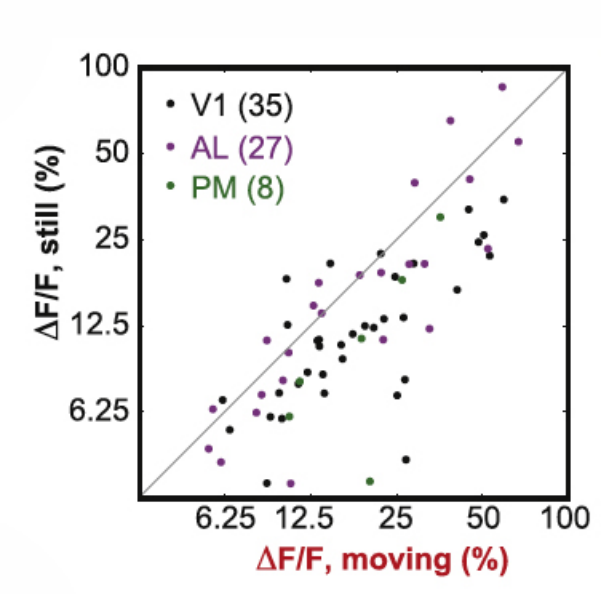

Figure 28. Neural responses in different visual areas during locomotion and still states. Black, V1; purple, AL; green, PM. Adapted from (Andermann et al 2011).

Where does this motor-related input come from? One possibility is that V1 gets inputs directly from motor cortex, as it is shown in mouse barrel cortex (Mao et al 2012). Another possibility is that motor-related connections come via indirect inputs from secondary visual areas (Wang et al 2011a). Keller et

al. (2012) using two-photon imaging found in visual area of behaving mice three components: motor-related signals, sensory signals and mismatch signals. Following their findings, they suggested, that already V1 plays a significant role in sensorimotor integration (Keller et al 2012).

Intriguingly, responses in visually unrelated areas such as somatosensory or auditory cortex appear to be reduced during motor activity (Ferezou et al 2007, Otazu et al 2009).

There is still not clear how locomotion affects neural responses in the level of LGN and across the layers in V1. Moreover, there are no studies that would show how locomotion relates to the pupil dilation, which is known as an important behavioral marker of arousal and cognitive processes (Bradley et al 2008, Goldinger & Papesh 2012, Hoeks & Levelt 1993).

1.7 Effect of anesthesia on neuronal activity

Cortical state refers to patterns of spontaneous activity in neural populations and sensory-evoked responses. The majority of electrophysiological recordings are made with anaesthetized animals, so the results could differ from sensory processing in the awake state. A classical model describes anesthesia as a change in balance between excitation and inhibition in brain circuits. As it is has been shown, visually evoked conductance is dominated by inhibition in awake V1 rather than excitation. Also Haider et al. (2013) demonstrated that neural responses of awake animals to visual stimuli are more spatially selective and much shorter (Ferron et al 2009, Haider et al 2013, Harris & Thiele 2011).

Interestingly, the largest spontaneous fluctuations in the cortical population activity are seen not only during sleep and anaesthesia, but also during quiet wakefulness. In the cortex of awake animal spontaneous activity of neuronal population contains various fluctuations, changing between periods of

synchronized and desynchronized states and correlating with behavior such as grooming, whisking or locomotion. In the synchronized state, fluctuations generate up (network is active) and down (network is quiet) phases. In the desynchronized state fluctuations of spontaneous activity are much smaller (Figure 29). These two states are seen not only during wakefulness, but also during sleep or certain anesthetics (Harris & Thiele 2011).

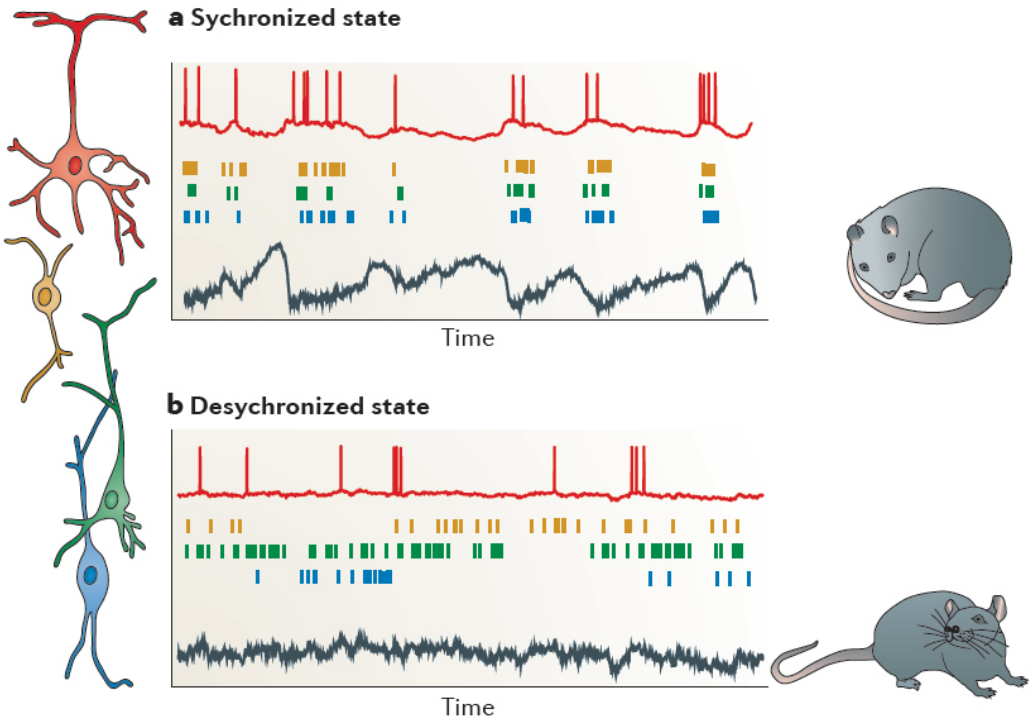

Figure 29. Cortical states in awake rodents. Adapted from (Harris & Thiele 2011).

Under urethane anesthesia, cortical state is synchronized even more than during slow-wave sleep, but also shortly desynchronized, as it is typically observed during REM sleep or waking (Clement et al 2008, Harris & Thiele 2011). Also cortical spontaneous activity was noticed to be different during different cortical states. In the synchronized state, the population activity as measured by the LFP contained more lower frequencies; population responses also exhibited higher spontaneous and noise correlations. Such

kinds of response properties also resemble responses to unattended stimuli. Based on this observation, Harris and Thiele (2011) propose two hypotheses: 1) neural activity during synchronized state acts in "power safe mode" 2) fluctuations show non-sensory information processing, that can be not related to external stimuli, but just a memory recall.

Spontaneous up-phases do not depend on cortical layer. Suppression in spontaneous fluctuations can be due to attention (Harris & Thiele 2011).

Several things can cause changes in cortical state. $GABA_A$ receptors are the main targets of anesthetic agents (Garcia et al 2010). But as a huge body of research has revealed, not only the GABAergic system is influenced by anesthesia (Harris & Thiele 2011).

1.7.1 Isoflurane

Isoflurane is an inhaled anesthetic with quick onset and recovery (Altholtz et al 2006, Szczesny et al 2004), making it a popular choice for small animals such as mice, because administration is easily controlled. Unfortunately, isoflurane also has severe affects on the neural circuitry.

Isoflurane reduces excitatory postsynaptic currents (EPSC) at synapses. Deep anesthesia level suppresses bursts and causes unstable cortical excitability. Anesthetic acts through several membrane receptors such as $GABA_A$, glycine and K^+ channels. In addition to that, it stimulates GLT1/EAAT2 glial glutamate transporter. *In vitro* studies in hippocampus and amygdala revealed that this particular anesthetic reduces synaptic transmission (Ferron et al 2009, Garcia et al 2010, Kroeger & Amzica 2007). It has been shown in mice (Whittington & Virag 2006) that isoflurane decrease significantly hippocampal serotonin (5-hydroxytryptamine) level. Furthermore, isoflurane can violate the regulation of serotonergic neurotransmission by effecting presynaptic activity (Martin et al 1990). Moreover, the influence of isoflurane on $GABA_A$ inhibitory currents is not

unanimous. Some results show that anesthetic by binding postsynaptically, decreases current amplitude of $GABA_A$ IPSCs in hippocampal and cortical neural cells (Banks & Pearce 1999, Ferron et al 2009, Pearce 1996). Controversially, there is demonstrated that the same amount of agent does not change the $GABA_A$ inhibitory synaptic current amplitude, but just increases the duration (Ranft et al 2004, Westphalen & Hemmings 2003). Even low concentrations of isoflurane can prolong GABA induced synaptic inhibition. Wu et al. (2004) propose in their work in rat brainstem that isoflurane reduces glutamate release and the presynaptic action potential amplitude and that, as a result, cause EPSP inhibition. Investigating γ oscillations in the frontal cortex, visual cortex and hippocampus in freely moving rats, Hudetz et al. (2011) concluded that administration of isoflurane reduces the power of high-frequency, but not low-frequency, γ oscillations. Cortical γ oscillations are known to participate in conscious cognitive functions (Hudetz et al 2011).

1.7.2 Urethane

Urethane (ethyl carbamate) is ethyl ester of carbamic acid. This injectable anesthetic contains advantages: it can produce long lasting, stable anesthesia with relatively small amount of administration and has analgesic effects. Biggest disadvantages are that the anesthetic is mutagenic, carcinogenic and can not be used in recovery surgeries (Field & Lang 1988, Flecknell 1996, Ghanayem 2007).

Urethane is thought to cause minimal signal disruption in the neocortex. Nevertheless, the anaesthetic agent depresses depolarizing current in cortical neurons and decrease membrane resistance. Urethane, unlike isoflurane, does not alter excitatory or inhibitory synaptic transmission (Sceniak & Maciver 2006).

Hara and Harris (2002) in their work using Xenopus oocytes concluded that even small changes in various different receptors can produce reliable anesthesia. Authors suggest that urethane inhibit 10% of NR1a/NR2A NMDA and 18% of GluR1/GluR2 AMPA receptors and enhance 23% of $GABA_A$, 33% of α1 glycine and 15% of nAch receptors. Intriguingly, other anesthetics have opposite effect on nAch receptors and inhibit function (Hara & Harris 2002).

Also as shown by Devonshire et al (2010) who combined optical imaging and electrophysiology in rat barrel cortex, under urethane anesthesia, evoked cortical response amplitude decreases, early components are protracted and the activated area of the cortex is diminished. The observed drop in the evoked response amplitude is most significant when the sensory stimulation is of high-frequency (Devonshire et al 2010).

How anesthesia influence spatial and temporal response profiles it is still an open question.

2 Methods

2.1 Methods for part I: "Surround suppression in mouse primary visual cortex: laminar dependence and effects of anesthesia"

Experiments were performed on adult C57BL/6J and PV-IRES-cre male mice (P60-120). Procedures were in accordance with the standards of the Society for Neuroscience, the German Law for Protection of Animals and approved by the local authorities. License numbers: CIN1/10, CIN3/11, CIN1/13 and CIN4/12. Recordings from V1 were obtained through a craniotomy (<1mm^2) located 3 mm lateral to the midline and 1.1 mm in front of the anterior margin of the transverse sinus (Wang et al 2011a). Extracellular recordings in V1 were performed with 16-channel silicon probes (Neuronexus, model A1x16-3mm50-177, 50 µm inter-contact spacing) (Figure 30). Online estimates of RF position, orientation preference, and contrast sensitivity relied on high-pass filtered signals crossing a fixed threshold (typically 4.5-6.5 SDs). For offline data analysis, spikes were extracted for each electrode contact separately from the unfiltered signal sampled at 30 kHz using the NDManager software suite (Hazan et al 2006). Here, spike detection threshold was automatically determined (Quiroga et al 2004) and multiplied by a factor of two to avoid spurious threshold crossings by noise. This procedure typically resulted in high-quality multi-unit activity (Figure 30B). Since only suboptimal spike sorting strategies were available for high-density multi-electrode arrays (Einevoll et al 2012), we did not attempt to perform systematic spike sorting.

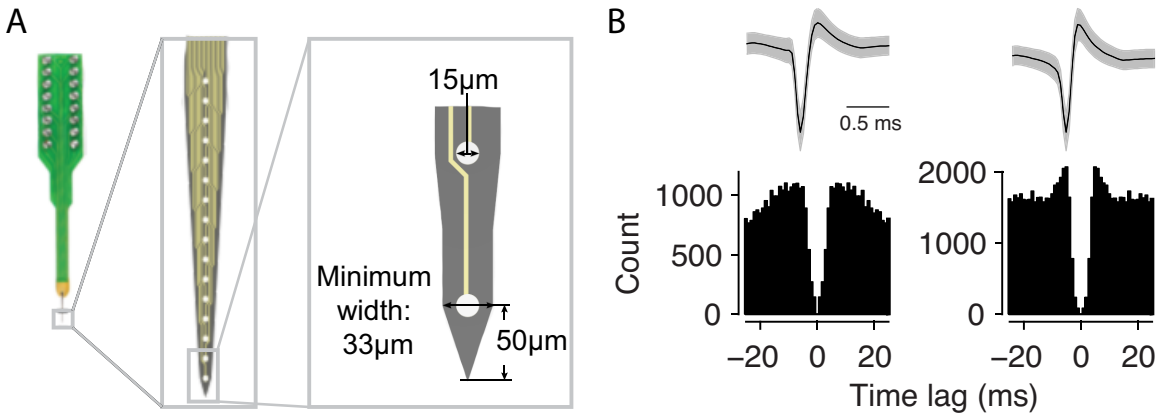

Figure 30. A: 16-channel linear silicon probe (Adapted from NeuroNexus catalog). B: Example spike waveforms and autocorrelograms.

2.1.1 Anesthetized animals recordings

In 6 C57BL/6J mice, anesthesia was induced by 3% isoflurane, and maintained during surgery by a combination of urethane (750 mg/kg, i.p.) and isoflurane (1-2%). Buprenorphine (0.1 mg/kg, s.c.) was used for analgesia, Atropine (0.3 mg/kg, s.c.) to reduce bronchial secretions. Animal temperature was kept at 37°C by a feedback-controlled heating pad (WPI, ATC-1000 DC Temperature Controller). A custom-designed headpost was mounted to the skull using dental cement (Tetrik EvoFlow, Ivoclar Vivadent). A reference wire was placed into the cerebellum, a ground wire under the skin. During recording, isoflurane was reduced to ~0.5%.

2.1.2 Awake animals recordings

Under isoflurane anesthesia (3% induction, 1–2% maintenance), 6 C57BL/6J mice were implanted with a headpost and miniature screws over the cerebellum for ground and reference wires. Atropine (0.3 mg/kg, s.c.), antibiotics (Baytril, 5 mg/kg, s.c.) and analgesics (Buprenorphine, 0.1 mg/kg, s.c.) were given during surgery, and the following 3 days the same antibiotics and longer lasting analgesics (Carprofen, 5 mg/kg, s.c.) were injected. The

animals were habituated to being head-fixed and placed on an air-suspended Styrofoam ball (Figure 31) (Dombeck et al 2007). Following habituation, a craniotomy over V1 or LGN was performed under isoflurane anesthesia, which was sealed with Kwik-Cast (WPI) after each recording session, lasting about 3-4 hours. To avoid residual effects of anesthesia, recordings were never performed on the day of the craniotomy. Ball movements were registered at 90 Hz by two optical mice connected to a microcontroller (Arduino Duemilanove).

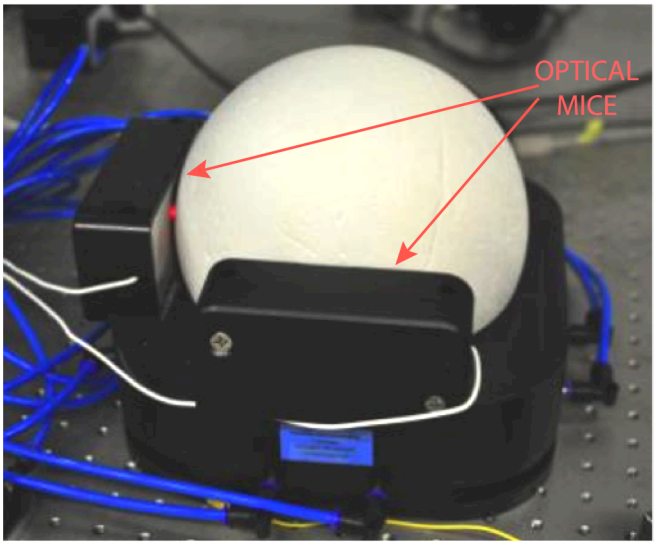

Figure 31. An air-suspended Styrofoam ball.

Eye position was monitored under infrared illumination using a camera (Guppy AVT, frame rate 50 Hz) coupled to a zoom-lens (Navitar Zoom 6000). Although eye movements were occasionally observed, their amplitude was small (within a trial 1-2 degrees) and less of a concern, as we were able to consistently evoke visual responses even with the smallest stimulus size (Figure 32). In addition, removing trials with eye movements does not substantially alter size tuning curves in mouse area V1 (Adesnik et al 2012). During recordings, the setup was enclosed with a dark curtain and there was no ambient light other than that of the stimulus monitor.

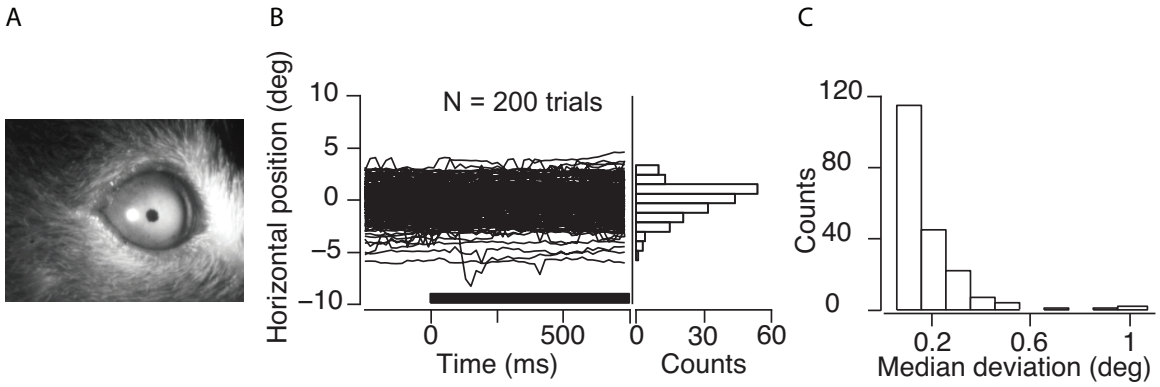

Figure 32. Analysis of eye movements. A: Screen shot of the mouse eye recorded during an experiment. B: Right: Horizontal position of the eye in degrees for 200 trials, black bar denotes stimulus duration; left: distribution of eye position across trials and C: Median deviation of eye position within trials.

2.1.3 Awake recordings with optogenetics

7 PV-IRES-cre mice (B6;129P2-Pvalb$^{tm1(cre)Arbr}$/J, The Jackson Laboratory) underwent headpost surgery as described above. They were additionally injected with AAV2/1.EF1a.DIO.hChR2(H134R)-EYFP.WPRE.hGH or AAV2/9.EF1a.DIO.hChR2(H134R)-EYFP.WPRE.hGH (UPenn Vector Core) through a small craniotomy 3 mm lateral to the midline and 1.5 mm in front of the anterior margin of the transverse sinus. A glass pipette connected to a Picospritzer III (Parker) was slowly lowered to ~750 µm below the brain surface and a total of 100-150 nl of virus was injected every 100 µm while gradually retracting the pipette. The pipette was left in place for an additional 5 minutes to allow viral diffusion, and the craniotomy was covered with Kwik-Cast (WPI). Neurophysiological recordings with photostimulation were performed at least 3-4 weeks after virus injection. For these recordings, a second craniotomy was performed over V1 as described above.

2.1.4 Photostimulation

Photostimulation was carried out using a fiber-coupled light-emitting diode (LEDs; Doric lenses) with a center wavelength of 473 nm driven by a LED driver (LEDD1B, Thorlabs). The fibers were mounted on a manual manipulator and positioned less than 1 mm from the cortical surface. LED light was delivered in the middle of the visual stimulus presentation for the 250 ms with a light intensity of 22 mW/mm^2 measured at the tip of a 200 µm diameter core.

2.1.5 Histology

For histological analyses, mice were transcardially perfused under pentobarbital anesthesia (200 mg/kg) with 0.2M sodium phosphate buffer (PBS) followed by 4% paraformaldehyde (PFA) in PBS. Brains were post-fixed for 24 h at 4 °C in PFA and then rinsed 3 times with 1 x PBS. Free-floating sections (60 µm) were cut using a vibratome (Microm HM 650 V-Thermo Scientific) and incubated at room temperature for 1 h with blocking solution (10% Roche blocking reagent for Elisa in PBS with 0.3% Triton-X 100 detergent) and then for 24 h with anti-PV primary antibody (Sigma; 1:2000 in blocking solution with PBS and 0.3% Triton-X 100 detergent). After rinsing 3 x 10 min in 1 x PBS, sections were incubated in Alexa-Fluor 647 conjugated secondary antibodies (Invitrogen, 1:1000 in blocking solution with PBS and 0.3% Triton-X 100 detergent). Sections were rinsed 3 x 10 min in 1 x PBS, mounted on glass slides with Vectashield (Vector Laboratories) and coverslipped. Slides were inspected for the presence of YFP and Alexa-647 using a Zeiss Imager.Z1m fluorescent microscope (Figure 33).

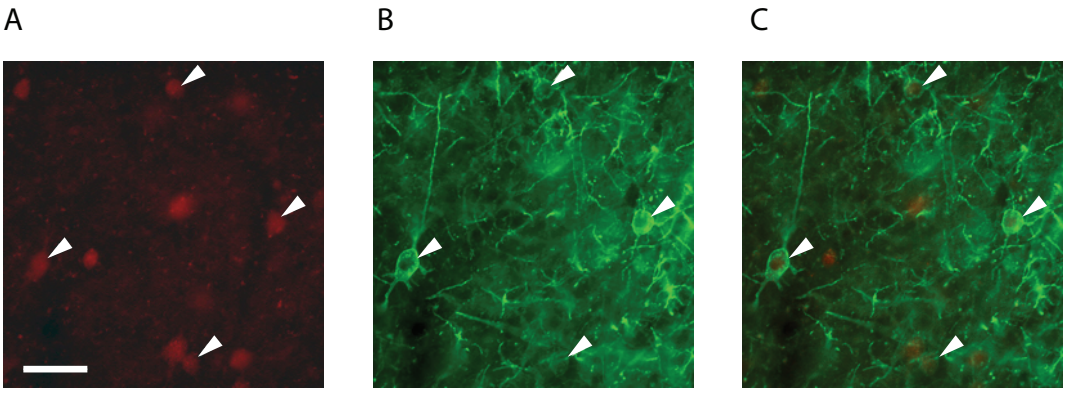

Figure 33. Transfection of PV+ interneurons by channelrhodopsin 2 (ChR2-eYFP). *A*: PV immunostaining B: ChR2-eYFP expression C: overlay of PV immunostaining and ChR2-EYFP expression. White arrowheads indicate cells with overlay. Scale bar, 50 μm.

We excluded from the analysis one animal, in which there was no effect of optogenetic photostimulation on firing rates. In this animal, post-mortem histological analysis confirmed insufficient viral expression. We also excluded recordings from PV+ interneurons, which we identified by transient and strong increases in firing rate time-locked to blue light stimulation.

2.1.6 Visual stimulation

Stimuli were presented using custom software (EXPO; https://sites.google.com/a/nyu.edu/expo/home) on a calibrated LCD monitor (Samsung 2233RZ, mean luminance 50 cd/m^2).

To estimate RF position before measuring size tuning curves, ON and OFF subfields of RFs were mapped using a sparse noise stimulus (Liu et al 2009). This stimulus consisted of white or black squares (4 deg diameter) flashed for 180 ms on a 40 deg square grid (Figure 34A). Subsequent stimuli were presented at the average RF center across recording sites.

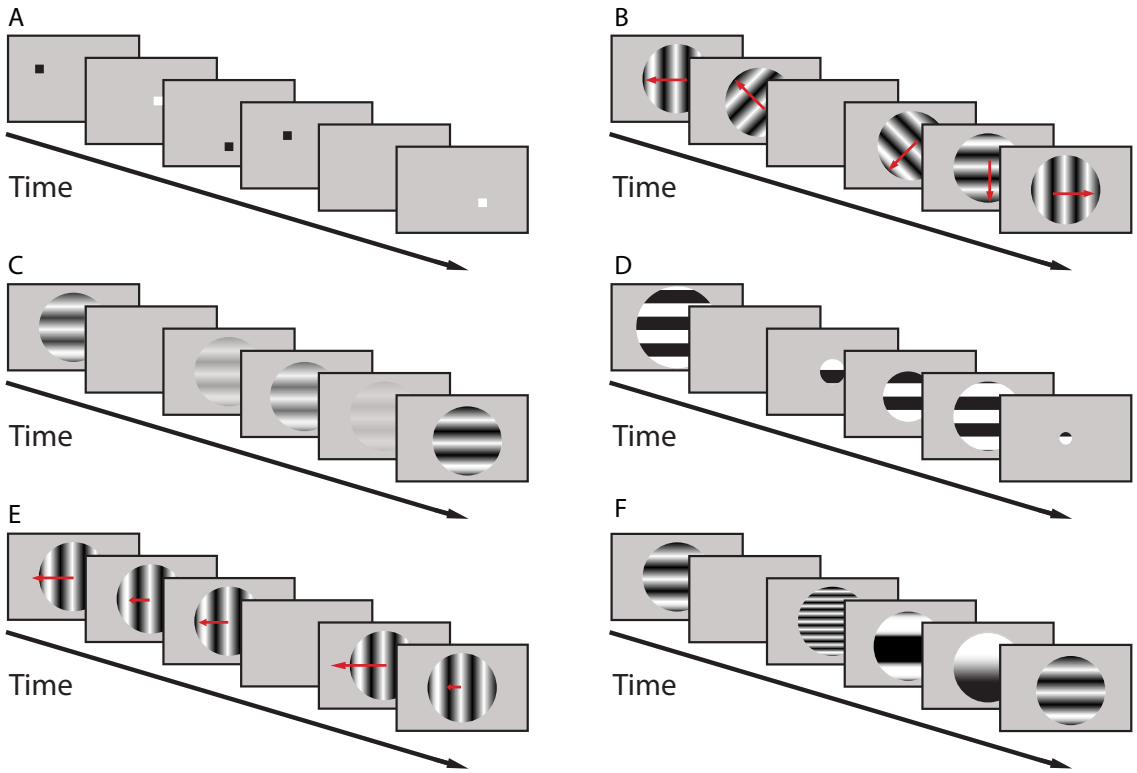

Figure 34. Stimulus set used in experiments. A: sparse noise stimulus. B: orientation tuning stimulus. C: contrast tuning stimulus. D: size tuning stimulus. E: temporal frequency tuning stimulus. F: spatial frequency tuning stimulus.

To guide the choice of stimulus orientation (Figure 34B) for the size tuning experiment (Figure 34D), we assessed online orientation biases in threshold crossings using 2 s sinusoidal gratings moving in 8 different directions (spatial frequency 0.02 cycles/deg, temporal frequency 1.5 cycles/s). These spatial and temporal frequencies represent average optimal values for mouse V1 (Marshel et al 2011). The salt-and-pepper organization of orientation preference in rodent V1 (Ohki et al 2005) excludes the possibility to determine preferred orientation from multiunit activity. However, we tried to optimize stimulus orientation as much as possible by choosing the orientation that elicited the strongest activity in the cleanest spike waveforms.

For size tuning experiments, we presented 750 ms sinusoidal gratings at a single orientation centered over the previously determined average RF center. Grating diameter ranged from 4 to 67 deg. The interstimulus interval was 0.5 s.

For size tuning during optogenetic depolarization of PV+ interneurons, we delivered, in half of the trials, a blue light pulse 250 ms after stimulus onset for a duration of 250 ms. Trials with and without photostimulation were interleaved in pseudo-random order. Size tuning experiments with optogenetics were performed in awake mice only.

A blank screen condition (mean luminance) was included to estimate the spontaneous firing rate. To determine the laminar location of our recording sites, we presented full-field, contrast-reversing checkerboards at 100% contrast, with a check size of 25 deg and a temporal frequency of 1.5 cyc/s.

2.1.7 Data analysis

Size tuning curves were fit with a Ratio-of-Gaussians model (Cavanaugh et al 2002):

$$R(x) = K_c L_c(x)/(1 + K_s L_s(x)),$$

where $L_c(x) = (w_c * \mathrm{erf}\left(\frac{x}{w_c}\right))^2$ and $L_s(x) = \left(w_s * \mathrm{erf}\left(\frac{x}{w_s}\right)\right)^2$

Here, R is response, L_C is summed squared activity of the center mechanism, L_S - for surround mechanism, x is stimulus diameter, $K_c, K_s, w_c,$ and w_s are parameters for the gain and width of the center and surround mechanisms. For fitting, we imposed $w_c < w_s$. We defined RF center size as the stimulus diameter eliciting the maximal response, and surround size as the diameter for which the response reached asymptote (i.e., where a 1 deg increment in size failed to alter firing rate by 0.5%). We determined suppression strength

with a suppression index: $SI = (R_{opt} - R_{supp)}/R_{opt}$, where R_{opt} is the peak response and R_{supp} the asymptotic response. Following Van den Bergh et al (2010), units with SI > 0.1 were considered suppressed. We excluded multiunits if maximal firing rate was < 1 spike/s or if the percentage of variance explained by the model was < 85%.

We computed the current source density (CSD) from the second spatial derivative of the local field potentials (Mitzdorf 1985) evoked by a full-field checkerboard reversing in contrast. We determined layer 4 as the center of the initial current sink (Maier et al 2011), and assigned recording sites to supragranular, granular or infragranular laminae. In addition to classifying the location of recording sites into the three categories, we also evaluated our results as a function of relative cortical depth, where 0 represents the middle of layer 4 as determined by CSD analysis. We then used a local robust regression to estimate a smoothed average (MATLAB function *smooth*, method *rlowess*).

To analyze the temporal dynamics of spatial integration we aligned normalized responses for all multiunits to stimulus onset. We defined response latency (response onset) as the first of 20 consecutive time points (1 ms interval), where activity exceeded 2.58 times the standard deviation of the baseline response (0-200 ms before stimulus onset).

2.2 Methods for part II: Attention-like signatures of locomotion in the early visual system of the mouse

2.2.1 Electrophysiological recordings

As described in the methods for part I, 'Awake recordings', mice were implanted with headpost and miniature screws over the cerebellum for ground and reference wires. After habituation and training mice were placed

on the air-cushioned ball, head-fixed and allowed to move freely. Eye and ball movements were monitored as well.

Extracellular recordings were performed with 16 or 32 channel linear silicon probes (Neuronexus, A1x16-3mm-50-177 (Figure 35D), A1x32-3mm-25-177 (Figure 35B), A1x32Edge-5mm-20-177-A32 (Figure 35C)) or tetrodes (Neuronexus, A2x2-tet-3mm-150-150-121 (Figure 35E)). All electrodes were inserted perpendicular to the brain surface. For V1 recordings, linear probes were lowered to ~900 μm and tetrodes to ~600 μm below the brain surface. For dLGN recordings (stereotaxical coordinates: 2.5 mm posterior of bregma and 2 mm of midline (Franklin & Paxinos 2008, Grubb & Thompson 2003)), linear probes were lowered to 3 mm, and neurons were determined to be from dLGN based on the characteristic RF progression along the electrode shank, the high temporal frequency preference, and the prevalence of F1 responses to drifting gratings (Grubb & Thompson 2003, Piscopo et al 2013).

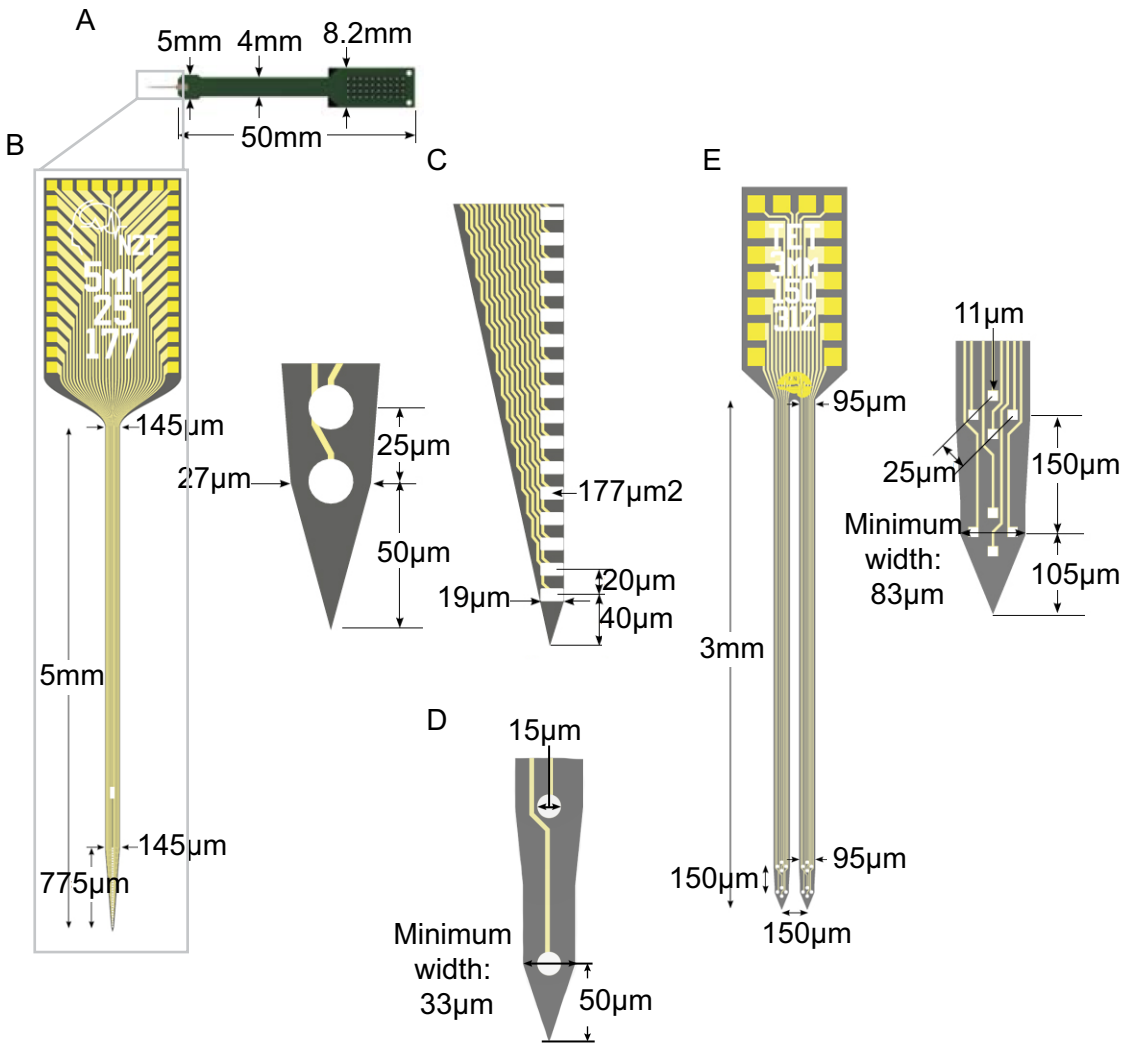

Figure 35. Probe configurations. A: 32-channel silicon probe. B: Magnified tip of probe with linear configuration. C: Same as B, for edge configuration. C: Same as B, for 16-channel configuration. D: Magnified tip of probe with tetrode configuration. (Adapted from NeuroNexus catalog).

2.2.2 Visual stimulation

Visual stimulation was performed as described in the methods for part I, 'Visual stimulation'.

2.2.3 Data analysis

Error bars represented mean +/- s.e.m. unless otherwise noted. We used paired t-tests to assess statistical significance unless otherwise noted. None of the reported results change qualitatively if equivalent, non-parametric tests were used instead.

2.2.4 Locomotion

Locomotion speed was computed as the Euclidean norm of three perpendicular components of ball velocity (Figure 36) (Dombeck et al 2007). We considered the animal to be moving when locomotion speed exceeded 1 cm/s (Niell & Stryker 2010) and stationary when speed was below 0.25 cm/s for at least 0.4 s. We used this additional cutoff to ensure that the stationary condition did not contain periods with small ball movements, such as those occasionally triggered by whisking. For locomotion-triggered neural responses, we considered only those events for which speed was consistently below movement threshold for at least 0.5 s prior to crossing and above threshold for at least 0.5 s after crossing. To determine modulations of tuning properties by locomotion we considered stimulus presentations as locomotion trials if speed was above the movement threshold for at least 80% and as stationary trials if speed was below the threshold for at least 80% of the trial.

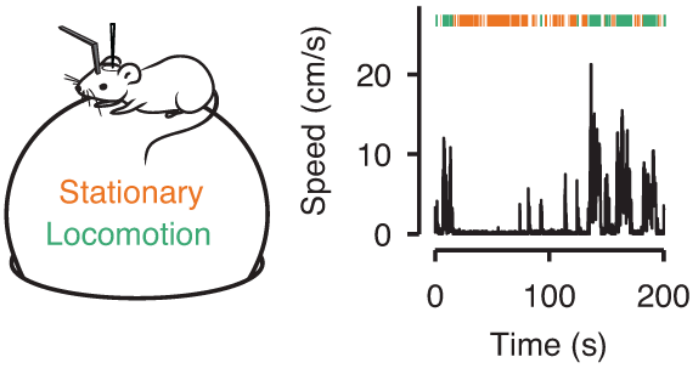

Figure 36. Experimental setup and segmentation of speed trace into stationary periods (orange) and locomotion (green).

2.2.5 Unit extraction and spike sorting

Wideband extracellular signals were digitized at 30 kHz (Blackrock microsystems) and analyzed using the NDManager software suite (Hazan et al 2006). The LFP was computed by downsampling to 1250 Hz. For linear probe recordings, we triggered the LFP to contrast reversals of the checkerboard stimulus and calculated the current source density (CSD) as it is explained in the methods for part I, 'Data analysis' (Figure 37A) (Mitzdorf 1985).

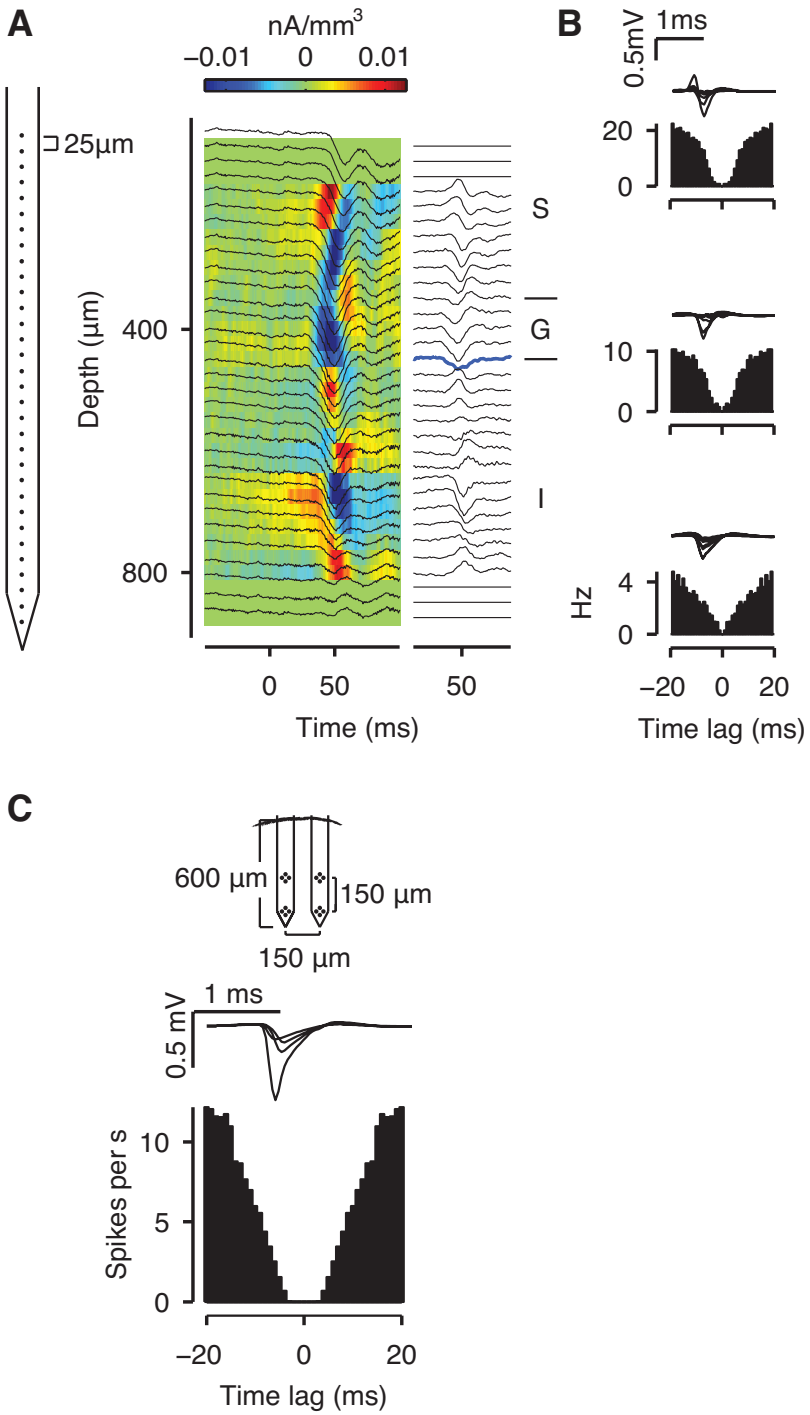

Figure 37. Example responses isolated from a linear and tetrode recordings in V1. A: Left: shematic drawing of linear 32-channel probe. Middle: CSD image (color) and superimposed LFP traces (black). Right: CSD traces. Thick blue line marks the polarity inversion of the CSD used to determine the base of putative layer 4. S – supragranular; G – granular; I – infragranular. B: Spike waveforms and autocorrelograms of representative neurons for each putative

laminar location. C: Waveforms and autocorrelogram of an example neuron isolated from a tetrode recording.

In order to isolate single neurons from linear arrays, we grouped neighboring channels into 5 equally sized "virtual tetrodes/octrodes" (4 channels per group with 1 channel overlap for 16 channel probes and 8 channels per group with 2 channel overlap for 32 channel probes). Using an automatic spike detection threshold (Quiroga et al 2004) multiplied by a factor of 1.5, spikes were extracted from the high-pass filtered continuous signal for each group separately. The first 3 principal components of each channel were used for semi-automatic isolation of single neurons with KlustaKwik (Henze et al 2000). Clusters were manually refined with Klusters (Hazan et al 2006). We assigned each unit to the contact with the largest waveform, and gave a single score based on the subjective rating of the manual sorter, the firing rate, the cleanness of the refractory period, and the stability over time. In order to avoid duplication of neurons extracted from linear probe recordings, we computed cross-correlograms (CCHs, 1 ms bins) between pairs of neurons from neighboring groups. Pairs for which the CCH's zero-bin was 3 times larger than the mean of non-zero-bins were considered to be in conflict. For each conflicting pair, the cell with the best score was kept. Conflicts across pairs (e.g. cell A in group 1 conflicts with both cell B and cell C in group 2, and cell A is better than cell B but worse than cell C) were resolved by collecting all possible sets of cells and keeping the set with the best total score. For recordings involving the LGN, we determined the highest and lowest electrode contacts with visually responsive units. Units assigned to contacts outside of this range were discarded from further analysis (Figure 37B,C).

2.2.6 Locomotion-triggered responses

For the analysis of locomotion-triggered responses we considered neurons with at least 10 locomotion onsets and a mean firing rate greater than 1.5 spikes/s during the total 1s time window centered on each locomotion onset.

2.2.7 Tuning

Orientation tuning curves were fit with a sum of two Gaussians with peaks 180 deg apart, which could have different amplitudes but equal width and a constant baseline (Katzner et al 2011). For the analysis of locomotion-based modulations of orientation tuning (Figure 44C), we fit curves separately for locomotion and stationary trials. For the population orientation tuning curves (Figure 44D), we averaged fitted parameters after aligning the orientation preference of individual tuning curves.

Contrast response functions were fit with a hyperbolic ratio function (Albrecht & Hamilton 1982): $R_c = R_0 + R_{\max} * c^n/(c_{50}^n + c^n)$ where c is stimulus contrast. The function has four parameters: baseline response R_0, responsiveness $R_{\max}$, semisaturation contrast c_{50}, and exponent n. In the analysis of contrast-dependence of correlations, we only included neurons with average firing rates across orientations > 1 spike/s and for which the proportion of explained variance was at least 70%.

2.2.8 Pairwise correlations

We determined pairwise correlations by segmenting each locomotion and stationary period into non-overlapping 100 ms bins, which we used for spike counting. For both conditions, we then concatenated all spike counts of each simultaneously recorded pair and computed a Pearson correlation coefficient. The results do not change qualitatively if a bin size of 300 ms was used, or if correlation coefficients were computed separately for each period and averaged across periods, weighted by period length. For mean-matching,

we randomly removed for each neuron excess spikes across all locomotion and stationary periods before binning and computing correlations. This process was repeated 20 times.

2.2.9 Fano factor

For each neuron, the Fano factor was computed as the variance over the mean of the spike counts obtained in the bins for the computation of correlations. To compute the Fano factor in the population, we simply averaged the individual neurons' Fano factor. The results do not change if the population Fano factor was computed using a type II regression based on the log-log scatter plots of the variance against the mean spike count (Gu et al 2011).

2.2.10 Linear models

For the comparison of locomotion-triggered response modulations in V1 between spontaneous and visually driven activity (Figure 44B) we used an analysis of covariance (ANCOVA) with the average firing rate 0.5 s before locomotion onset (stationary) as continuous variable and visual stimulation (spontaneous vs. visually driven) as a categorical factor to model the average firing rate 0.5 s after locomotion onset (locomotion).

For the comparison of the relationship between r_{signal} and r_{sc} between stationary and locomotion periods, we used an ANCOVA with r_{signal} as continuous variable and animal's state (locomotion vs. stationary) as a categorical factor to model r_{sc}.

To analyze the ratio of responses before and after locomotion onset across layers (Figure 46C,D) we performed a Kruskal-Wallis ANOVA with the factor layer (supragranular, granular, infragranular).

2.2.11 Analysis of dLGN recordings

Analysis of locomotion-triggered responses was the same as for V1 recordings. For dLGN response modulations during stimulus presentations (Figure 47D-G), we considered neurons responding with a mean firing rate greater than 1 spike/s and at least 5 locomotion and 5 stationary trials of each full-contrast drifting grating condition. F1 and F0 response components were calculated by Fourier analysis, separately for each trial and then averaged across trials. Burst were defined as groups of spikes with inter-spike intervals of <4 ms following a period of at least 100 ms without spikes (Grubb & Thompson 2005, Niell & Stryker 2010).

2.2.12 Analysis of pupil position and size

To analyze eye position we first defined the 15 x 15 pixel symmetric Gaussian filter G with a sigma of 5 pixels (imgaussian, MATLAB). For pupil detection, we first calculated a binary image B with nonzero pixels wherever $G \bullet I_{eye} < \lambda$, a user-adjustable threshold. We then applied a morphological opening operation of 50 pixels (bwareaopen, MATLAB), and extracted object boundaries (bwboundaries, MATLAB). In case multiple objects were found we used the one with the most circle-like shape. To quantify pupil position and size we fitted an ellipse to the detected pupil. To detect and compensate for translations of the eye parallel to the image plane, we also determined the position of a landmark, which could be either the 1st Purkinje image of the infrared light, or a point near the tear duct in the medial corner of the eye (Wallace et al 2013). The 1st Purkinje image was found by applying radial feature extraction (fastradial, MATLAB), followed by thresholding (graythreshold, MATLAB) and extraction of object boundaries (bwboundaries, MATLAB). In case the 1st Purkinje image could not be used, the user manually marked in the first frame a point in the medial corner of the eye, around which we extracted a 50 x 50 pixel region. For all subsequent

frames, we then found the same point by minimizing the difference between each 50 x 50 pixel region and the landmark image, following published procedures (Wallace et al 2013). We computed relative pupil displacements by subtracting, for each frame the landmark position from the pupil position. To convert pupil displacements to angular displacements, we assumed that the center of eye rotation was 1.041 mm behind the pupil (Stahl et al 2000). Eye velocity was computed as $\dot{E}(i) = (E(i+1) - E(i-1)) / 2dt$ where as $\dot{E}(i)$ is the eye velocity at time i , $E(i)$ is the position at time i, and dt is the sampling interval (Sakatani & Isa 2007). We defined saccades as changes in eye position greater than 2 degrees (Saleem et al 2013). Taking into account that the average mouse saccade lasts a little over 50 ms (Sakatani & Isa 2007), we detected saccades at each time point i by taking the difference of the mean eye position 60 ms before and after, centered on i.

3 Results

3.1 Results part I: "Surround suppression in mouse primary visual cortex: laminar dependence and effects of anesthesia"

We were interested in surround suppression in the different layers and at different brain states in the mouse primary visual cortex. We performed extracellular multi-electrode recordings in area V1 of anesthetized and awake mice. We extracted spikes from continuously recorded data and typically obtained high-quality multiunit activity (Figure 38A). For both anesthetized and awake animals, we first used a sparse noise stimulus consisting of briefly flashed black and white squares (Liu et al 2009) (see Methods) to estimate RF positions for all recording sites (Figure 38B). As expected for vertical penetrations, RF center locations were generally overlapping, but also exhibited some scatter (6.7 ± 0.7 deg). This amount of scatter was about one-third the diameter of a typical receptive field recorded during wakefulness (awake 19.8 ± 1.9 deg, n = 44, vs. anesthetized 32.7 ± 1.5 deg, n = 76, ANOVA, $F(1,114) = 9.9$, $p = 0.002$), and is similar to what has previously been reported for mouse visual cortex (Bonin et al 2011, Smith & Hausser 2010). We then measured size tuning by increasing the diameter of a grating centered over the average location of the cells' RFs (Figure 38C). For some multiunits, responses increased asymptotically with increasing stimulus size (open circles); for other multiunits responses reached a peak, after which further increases in stimulus size led to a suppression of responses (closed circles). We estimated center and surround sizes by fitting a Ratio-of-Gaussians model (Cavanaugh et al 2002), and, for multiunits

showing surround suppression, we quantified suppression strength using a suppression index (SI).

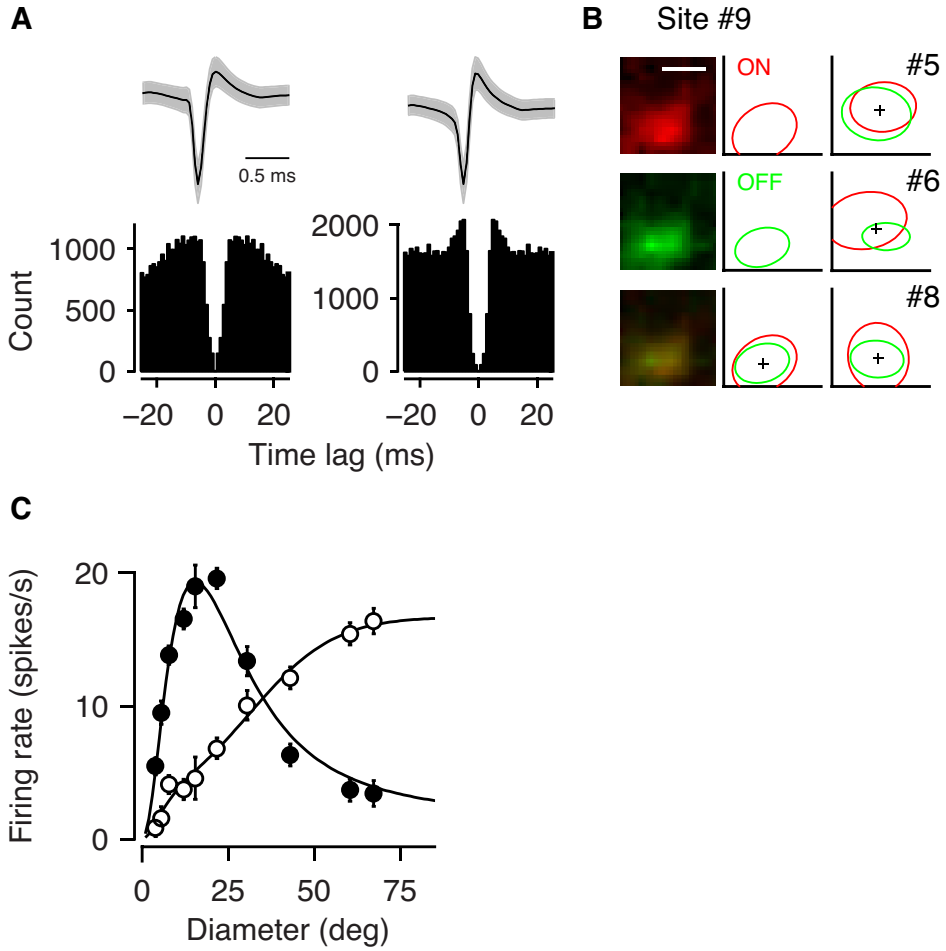

Figure 38. Recording and analysis methods. A: Example waveforms and autocorrelograms. B: Left: Color maps of ON (red) and OFF (green) subfields and their superposition along with ellipses depicting the fitted outline of the spike subfields for a single recording site. Right: RF outlines of another three, simultaneously recorded sites. White scale bar: 10 deg. Same scale applies to the fitted RF outlines. Black cross: average RF position. C: Example multiunits without (open symbols) and with surround suppression (closed symbols), recorded in two different experiments. Solid lines are fits of a Ratio-of-Gaussians model. All example data in this figure come from recordings during wakefulness. Here and in all subsequent figures, shaded regions and error bars indicate +/- sem.

3.1.1 Size tuning across cortical layers

We compared key measures of size tuning across cortical layers during anesthesia and wakefulness (Figure 39). We report data for 68 multiunits from 6 awake mice collected in a total of 17 penetrations, and 163 multiunits from 6 anesthetized mice collected in a total of 22 penetrations. Using current source density analysis (Mitzdorf 1985), we classified the laminar location of each recording site as supragranular, granular, or infragranular (Figure 39A,B). We took responses with SI > 0.1 as suppressed (Van den Bergh et al 2010), and found that the percentage of suppressed multiunits depended on both brain state (awake vs. anesthetized) and laminar position (supragranular vs. granular vs. infragranular) (Log-linear analysis, AIC = 19.21) (Figure 39C). The overall prevalence of suppression was higher in awake vs. anesthetized animals (65% vs. 47%, $p = 0.012$, chi-square test) and higher in supragranular than infragranular layers (75% vs. 37%, $p < 0.0001$, chi-square test). Focus on size tuning curves with surround suppression (Figure 39D) revealed that key features of spatial integration depend on both brain state and laminar position (Figure 39E,F). RF center size was smaller for awake than for anesthetized mice (19.8 ± 1.9 deg, $n = 44$, vs. 32.7 ± 1.5 deg, $n = 76$, ANOVA, $F(1,114) = 9.9$, $p = 0.002$) and increased with laminar position (ANOVA, $F(2,114) = 13.8$ $p < 0.0001$) (Figure 39E). Likewise, suppression strength was higher, overall, for awake than for anesthetized mice (SI = 0.70 ± 0.03, $n = 44$, vs. 0.45 ± 0.02, $n = 76$, ANOVA, $F(1,114)=30.8$, $p < 0.0001$). The laminar pattern of suppression strength depended on brain state (ANOVA, $F(2,114) = 6.3$, $p = 0.003$): in awake animals, surround suppression was stronger in supragranular than infragranular layers (SI = 0.80 ± 0.03, $n = 23$, vs. 0.54 ± 0.07, $n = 14$, t-test, $p = < 0.0001$), while under anesthesia, the strength of suppression did not differ across laminar positions (ANOVA, $F(2,73) = 0.8$, $p = 0.5$) (Figure 39F). A similar pattern was

observed when RF center size and surround suppression were plotted as a function of cortical depth relative to layer 4 (Figure 39G,H). There were no significant differences in suppression strength and RF center size between granular and other layers ($p > 0.1$).

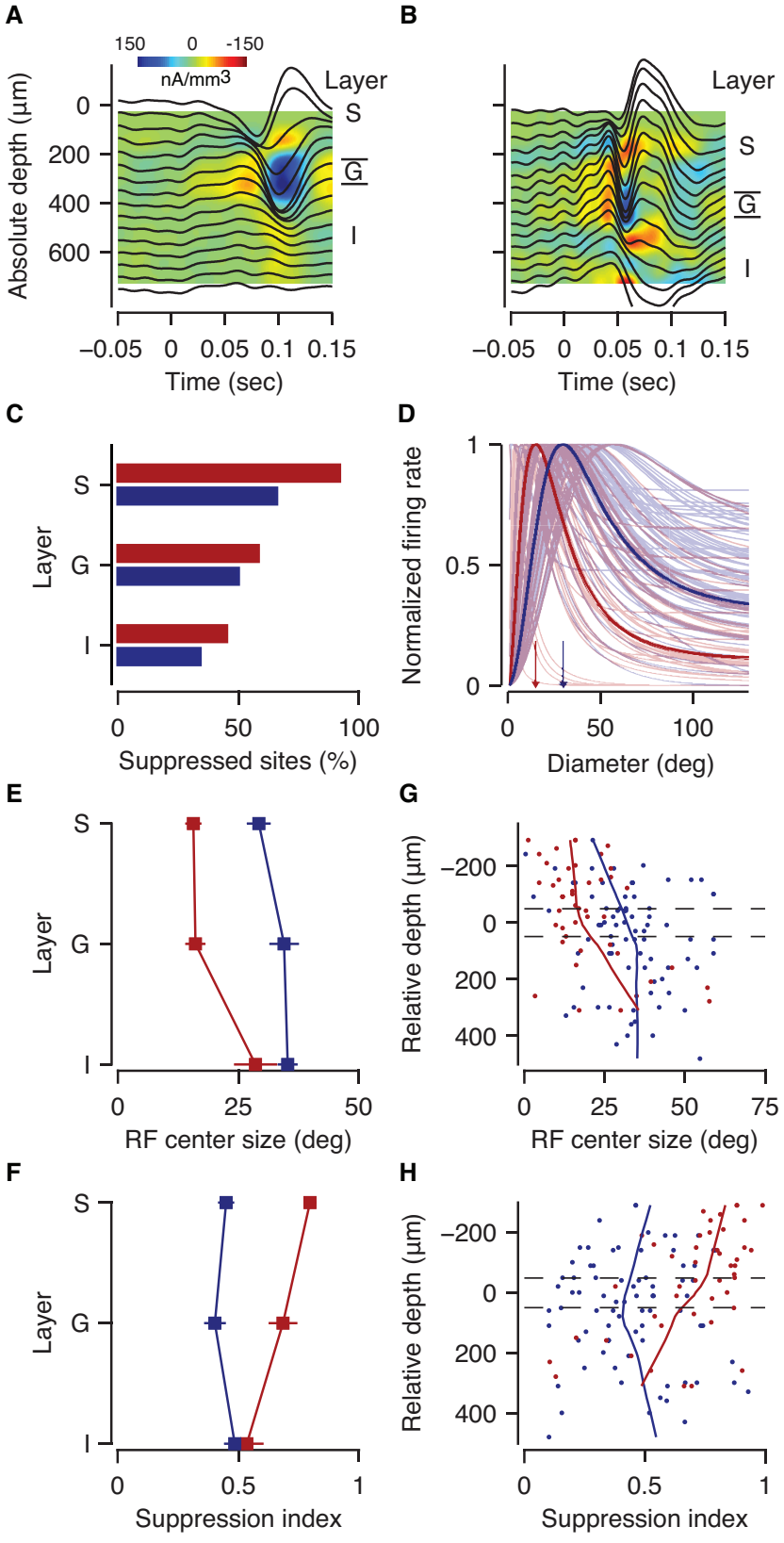
A
150
0
-150
nA/mm3
Layer
S
G
I
Absolute depth (µm)
0
200
400
600
−0.05
0
0.05
0.1
0.15
Time (sec)
B
Layer
S
G
I
−0.05
0
0.05
0.1
0.15
Time (sec)
C
Layer
S
G
I
0
50
100
Suppressed sites (%)
D
Normalized firing rate
1
0.5
0
0
50
100
Diameter (deg)
E
Layer
S
G
I
0
25
50
RF center size (deg)
G
Relative depth (µm)
−200
0
200
400
0
25
50
75
RF center size (deg)
F
Layer
S
G
I
0
0.5
1
Suppression index
H
Relative depth (µm)
−200
0
200
400
0
0.5
1
Suppression index

Figure 39. Spatial integration varies with brain state and laminar location. A, B: Current source density profile examples, obtained during anesthesia (A) and wakefulness (B). C: Proportion of suppressed multiunits (SI > 0.1) as a function of laminar location (red: awake, blue: anesthetized). D: Fitted size tuning curves for all recorded multiunits and the mean obtained by averaging parameters (solid traces). Arrows depict average RF center sizes. E, F: RF center size (E) and suppression index (F) as a function of cortical layer. G, H: Same, for cortical depth relative to the granular layer identified by CSD analysis, along with the local-robust-regression line. Dashed lines indicate estimated upper and lower boundaries of layer 4. S – supragranular, G – granular, I – infragranular.

3.1.2 Differences in spatial integration between brain states

We next asked whether these marked differences in spatial integration between brain states could simply be explained by differences in firing rates. We first compared average firing rates between the two brain states, and found that stimulus-evoked peak firing rates were indeed higher during wakefulness compared to anesthesia (18.7 ± 2.2, n = 68, vs. 11.9 ± 1.2 spikes/s, n = 163, t-test, $p < 0.01$, Figure 40A). We then considered a random subset of the data, in which firing rates approximately matched. Even with matched firing rates, the effects of brain state on spatial integration persisted, both in terms of RF center size and suppression strength (Figure 40B). Thus, differences in firing rates between brain states cannot explain the observed differences in spatial integration.

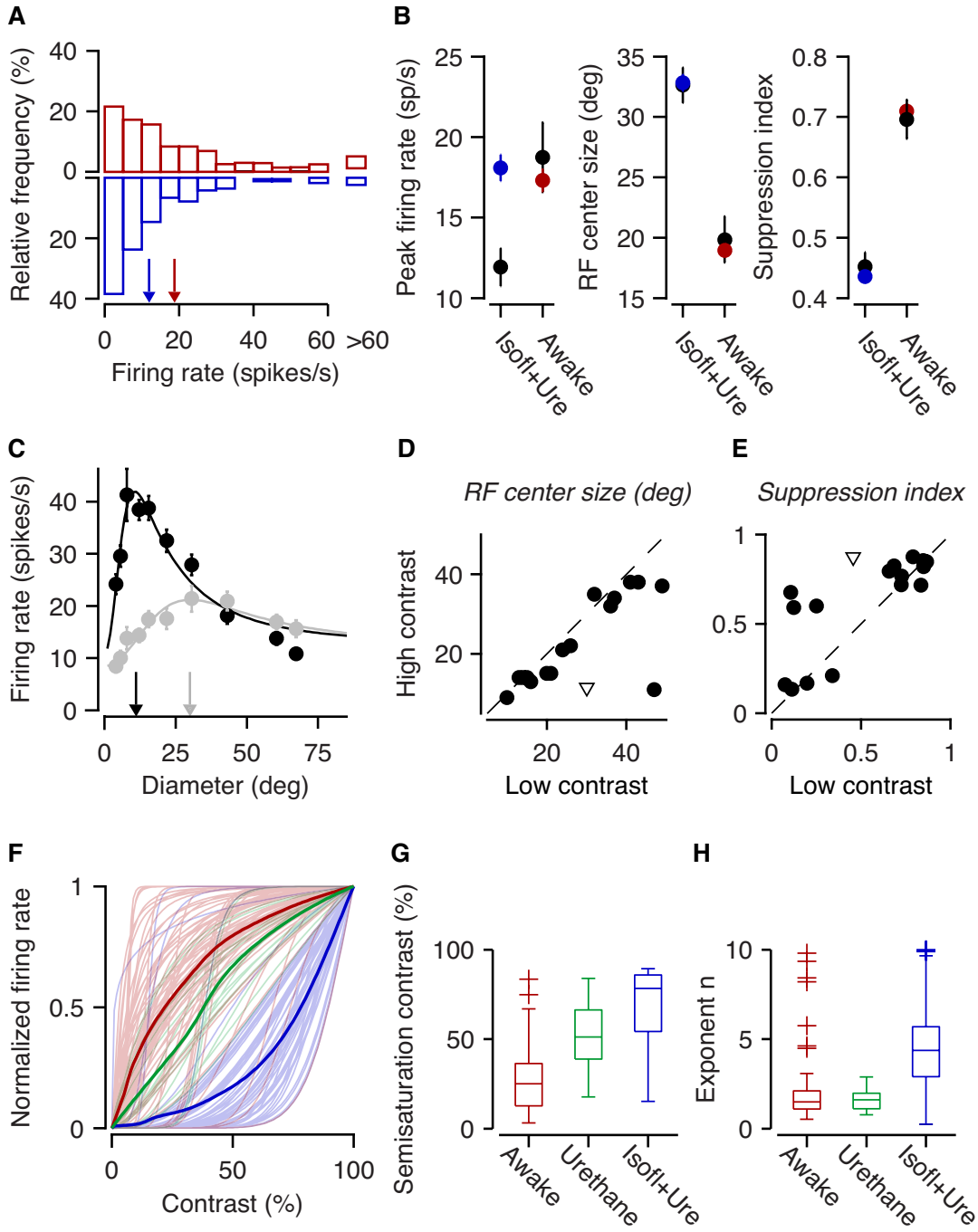

Figure 40. Anesthesia modulates surround suppression by affecting contrast normalization. A: Distributions of stimulus-evoked peak firing rates under wakefulness (red) and anesthesia (blue). Arrows represent population means. B: Differences in spatial integration between awake and anesthetized animals persist after matching firing rates. Black: original data set; colors: rate-matched data set. Left: peak firing rate. Middle: RF center size. Right: suppression strength. C: Example multiunit with size tuning curves recorded at 100% (black) and 18% contrast (gray). Arrows indicate RF center sizes. D: Scatter plot of RF center size at high vs. low contrast. E: Same, for suppression

strength (SI). Triangles in (D-E) depict example multiunit from (C). F: Contrast response functions under wakefulness (red), anesthesia with isoflurane and urethane (blue), and anesthesia with urethane only (green). Bold lines represent averages. G, H: Distributions of parameters of the hyperbolic ratio function fitted to the contrast response data by brain state (G) Semisaturation contrast c_{50} (H) Exponent n.

As the responses under anesthesia were reminiscent of responses typically obtained at low levels of stimulus contrast (Figure 39D and Figure 40C), we hypothesized that anesthesia modulates surround suppression by affecting contrast normalization. We therefore hypothesized that anesthesia reduces sensitivity for stimulus contrast, making a high-contrast stimulus appear as having lower contrast.

To test this hypothesis, we studied surround suppression at different levels of contrast, and measured the effects of anesthesia on contrast responses; the results provide support for our hypothesis. First, we confirmed that, just as in cat and monkey (Albrecht et al 2002, Cavanaugh et al 2002, Sceniak et al 1999), spatial integration in mouse V1 depends on stimulus contrast (Figure 40C). At high stimulus contrast (black), RF size of this example multiunit is small, and large stimuli cause full suppression, bringing responses almost back to baseline level. At low stimulus contrast, however, RF size is larger and suppression weaker (gray). These effects of stimulus contrast were consistent across the population of recorded multiunits (Figure 40D,E): with higher contrast, RF center size was smaller (21.9 ± 3.2 vs. 27.9 ± 2.7 deg diameter, n = 17, p = 0.02, paired t-test) and suppression was stronger (SI 0.63 ± 0.07 vs. 0.51 ± 0.08, p = 0.03, paired t-test). Second, we found that anesthesia indeed reduces contrast sensitivity (Figure 40F). Throughout the sample of recorded multiunits with contrast saturation, the semisaturation contrast c_{50} was lower (27.3 ± 2.3, n = 58 vs. $67.5 \pm 7.5\%$, n = 13, $p < 0.0001$, t-test) in awake (red) than in animals anesthetized with isoflurane and

urethane (blue), which is reflected in a rightward shift of the contrast response functions under anesthesia.

Likewise, the slope n was steeper during wakefulness than under anesthesia (2.1 ± 0.3 vs. 4.4 ± 0.3, $p < 0.0001$, t-test). Indeed, a substantial number of multiunits recorded in anesthetized animals did not even show saturation of responses (25.8%), which was clearly present for almost all multiunits recorded during wakefulness (97.9%). Note that contrast response functions obtained in additional experiments with urethane as the sole anesthetic (green), were more similar to those obtained during wakefulness but still not as sensitive (c_{50} = 52.6 $\pm$ 5.2%, n = 15, t-test, $p < 0.001$, Figure 40G; exponent n = 1.6, not significant; Figure 40H). Together, these findings are consistent with the idea that anesthesia with isoflurane/urethane influences surround suppression by affecting contrast normalization. Third, anesthesia had an effect on response dynamics (Figure 41). During wakefulness, stimulus onset evoked vigorous transient responses, while under anesthesia responses lacked the onset transient and were sluggish. This effect of brain state on response dynamics was present in individual multiunits (Figure 41A,B) as well as in the population (Figure 41C,D). Also, responses to both optimal and largest stimuli had faster onset latencies during wakefulness (40.0 ± 1.2 ms, n = 44) compared to under anesthesia (54.7 ± 2.7 ms, n = 51, $p < 0.0001$, Figure 41E-G).

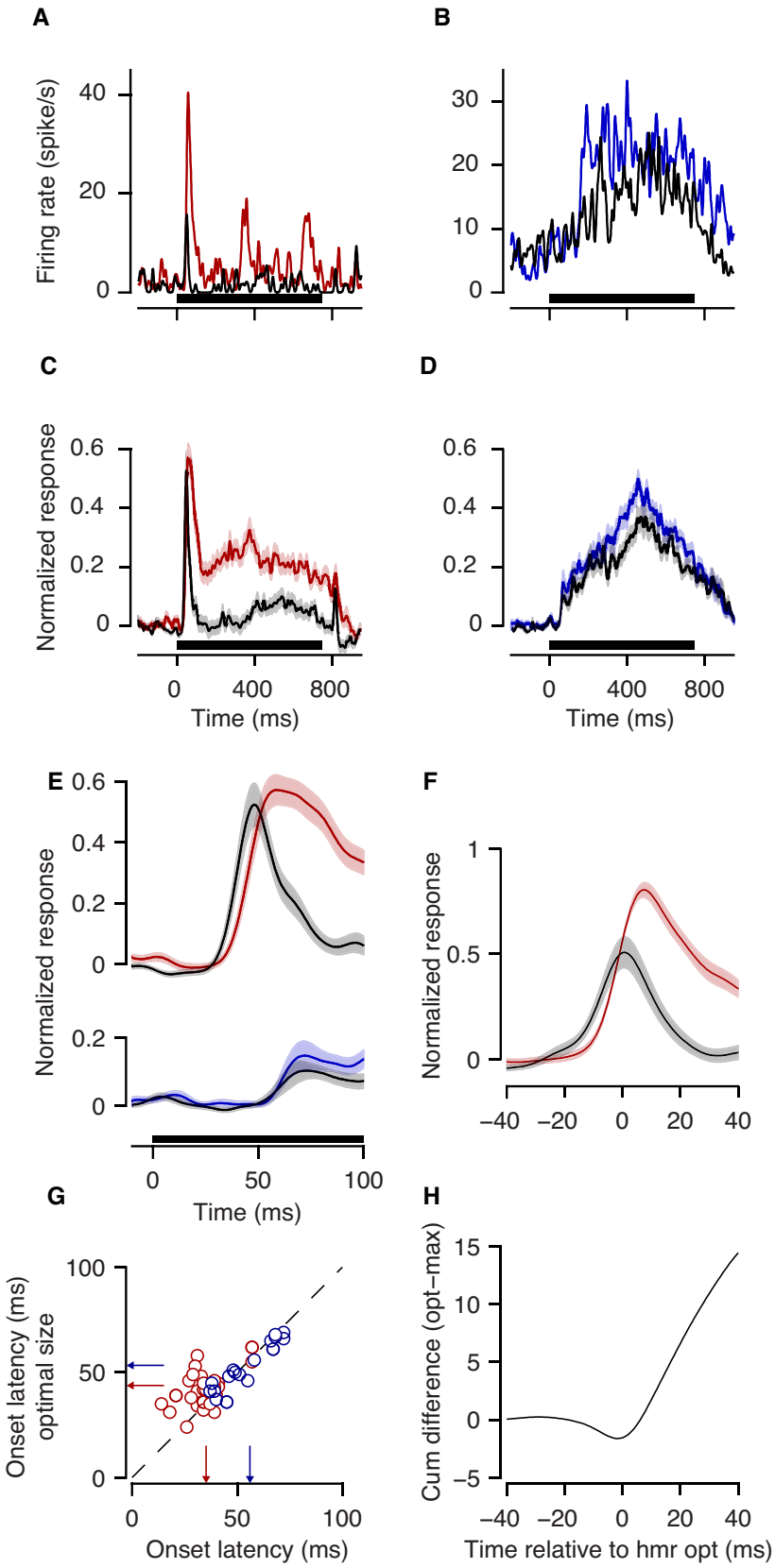
A
B
Firing rate (spike/s)
40
20
0
30
20
10
0
C
D
Normalized response
0.6
0.4
0.2
0
0
400
800
Time (ms)
E
F
Normalized response
0.6
0.4
0.2
0
0.2
0
0
50
100
Time (ms)
1
0.5
0
−40
−20
0
20
40
G
H
Onset latency (ms)
optimal size
100
50
0
0
50
100
Onset latency (ms)
Cum difference (opt−max)
15
10
5
0
−5
−40
−20
0
20
40
Time relative to hmr opt (ms)

Figure 41. Dynamics of responses to the optimal (colors) and maximal size stimulus (black in A-F). Horizontal bar indicates stimulus presentation. A: Example multiunit recorded during wakefulness. B: Example multiunit recorded under anesthesia. C: Averaged response across the population during wakefulness. D: Averaged response across the population under anesthesia. E: Initial 100 ms of the average response; data are replotted from C and D. F: Average responses during wakefulness aligned to the half-maximal response to the optimal-size stimulus (hmr opt). Color conventions as in (E). G: Distribution of onset latencies under wakefulness (red) and anesthesia (blue). Arrows depict population means. H: Cumulative difference between responses to the optimal-size and maximal-size stimulus.

3.1.3 Temporal dynamics of spatial integration

Next, we assessed the temporal dynamics of spatial integration. We noticed that during wakefulness (Figure 41E, top), but not during anesthesia (Figure 41E, bottom), responses to large stimuli (black trace) were faster than responses to stimuli of preferred size (colored trace). These effects of stimulus size on latency were consistent across the population of recorded multiunits (Figure 41G). During wakefulness, average latencies in response to the maximal and optimal stimulus were 35.1 ± 1.5 ms and 43.7 ± 1.5 ms ($p < 0.0001$, t-test). Under anesthesia, latencies increased to 53.3 ± 3.6 ms and 56.0 ± 3.9 ms ($p = 0.6$, t-test). These observations indicate that, under wakefulness, the preferred stimulus size progressively decreases during the initial portion of the response. This temporal advantage of large stimuli was also evident when, prior to averaging, normalized responses of each site were aligned at half-maximal response to the optimal size (Figure 41F), and in the cumulative difference of responses to optimal and large size stimuli (Figure 41H). We next analyzed the time course of responses to all stimulus sizes, and found that the preferred-size stimulus quickly (in less than 50 ms) changes from large to progressively smaller diameters (Figure 42A, top). In this analysis, we found dissociation between the changes of preferred stimulus

size and firing rate, ruling out a simple “iceberg effect” in time, in which stronger responses could yield earlier latencies (see also (Ruksenas et al 2007) (Figure 42A, bottom; Figure 42B). Even after peak firing rate is reached, preferred stimulus size continues to decrease (t-test, $p < 0.0001$) (Figure 42B). To quantify the temporal progression of preferred stimulus size, we determined the preferred stimulus size at response onset (see Methods) and 40 ms later, when the peak response is expected. Across the population, the preferred-size stimulus decreased from 48.3 ± 2.9 to 26.7 ± 2.6 deg diameter ($p < 0.0001$, t-test) between these time points (Figure 42C).

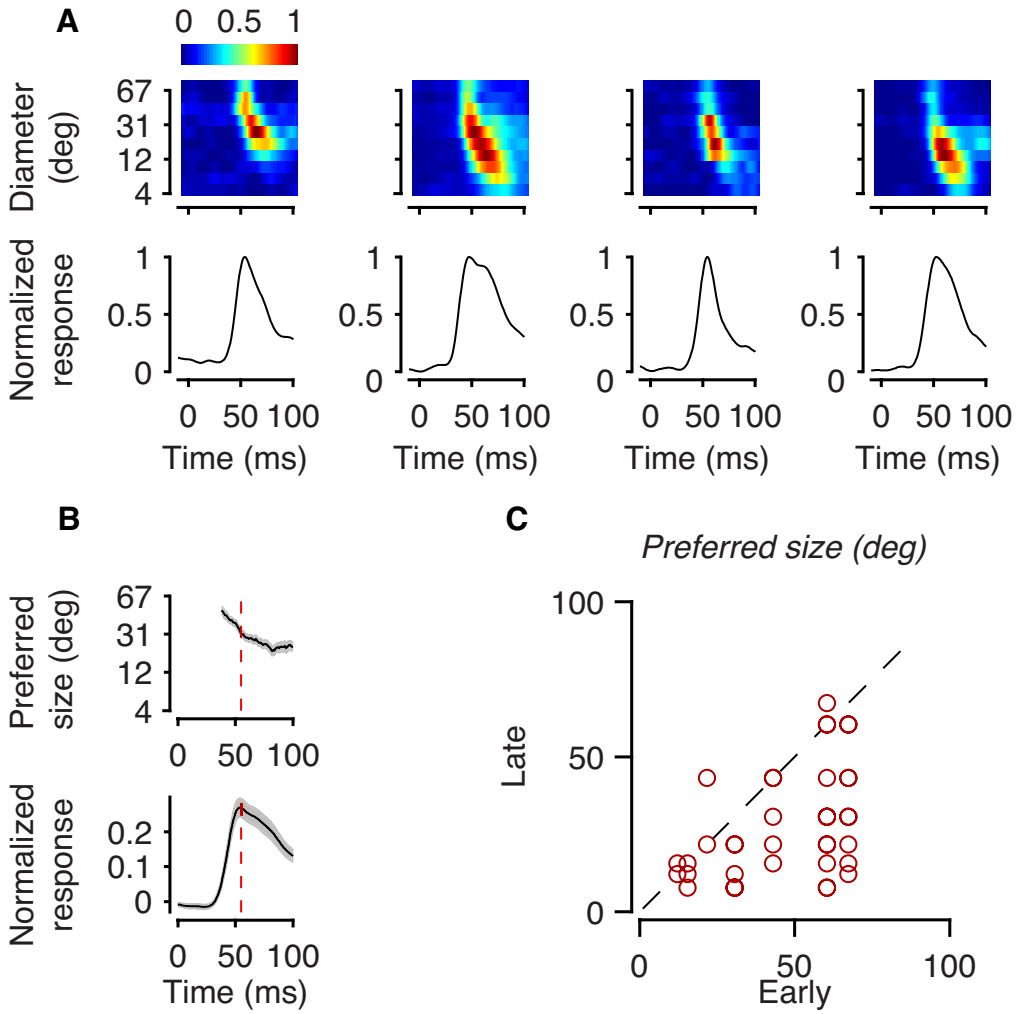

Figure 42. The time course of responses to the stimulus size. A: Top row: Responses to all stimuli across time for four example multiunits. Bottom row: Temporal development of average firing rates in response to all stimuli for the same example multiunits. B: Dissociation between dynamics of firing rates and dynamics of size preference in the entire population of recorded multiunits. Top: development of preferred size. Bottom: development of average firing rates. Responses are normalized to the peak response across stimulus conditions. C: Preferred stimulus size at response onset ("early") and 40 ms later ("late") for each neuron recorded during wakefulness.

3.1.4 Role of PV+ interneurons in spatial integration

Finally, we assessed the role of PV+ interneurons on spatial integration. We conditionally expressed the light-sensitive cation channel channelrhodopsin 2 (ChR2) by injecting adeno-associated viral vectors (AAV) into V1 of PV-Cre

transgenic mice (see Figure 33 in Methods). We performed size tuning experiments, where in half of the trials we photostimulated PV+ interneurons. Since the recorded multiunit responses mostly reflected pyramidal cell activity, we typically observed a reduction in firing rate during light stimulation (Figure 43A). In addition, we found that PV+ interneuron activation markedly affected the two key features of spatial integration: the size of RF center widened, and suppression strength decreased (Figure 43B). These effects were consistent across the population of recorded multiunits (Figure 43C-F). On average, driving PV+ neurons decreased firing rates (24.7 $\pm$ 3.6 to 20.0 $\pm$ 2.7 spikes/s, paired t-test, n = 28, $p < 0.002$). More importantly, RF center size widened from 16.2 $\pm$ 1.8 to 23.3 $\pm$ 3.3 (paired t-test, $p < 0.004$) and suppression strength decreased from SI = 0.71 $\pm$ 0.04 to SI = 0.55 $\pm$ 0.07 (paired t-test, $p < 0.001$). Consistent with this decrease of suppression strength, the ratio of responses during photostimulation vs. control condition was smaller at optimal than at maximal stimulus size (0.79 $\pm$ 0.04 vs. 1.22 $\pm$ 0.22, paired t-test, $p < 0.05$). We found the effects of PV+ interneuron activation to be very similar to the effects of reducing stimulus contrast (compare Figure 40C-E to Figure 43B-D). These observations indicate that PV+ interneurons in mouse V1 might contribute to surround suppression by reducing overall stimulus drive.

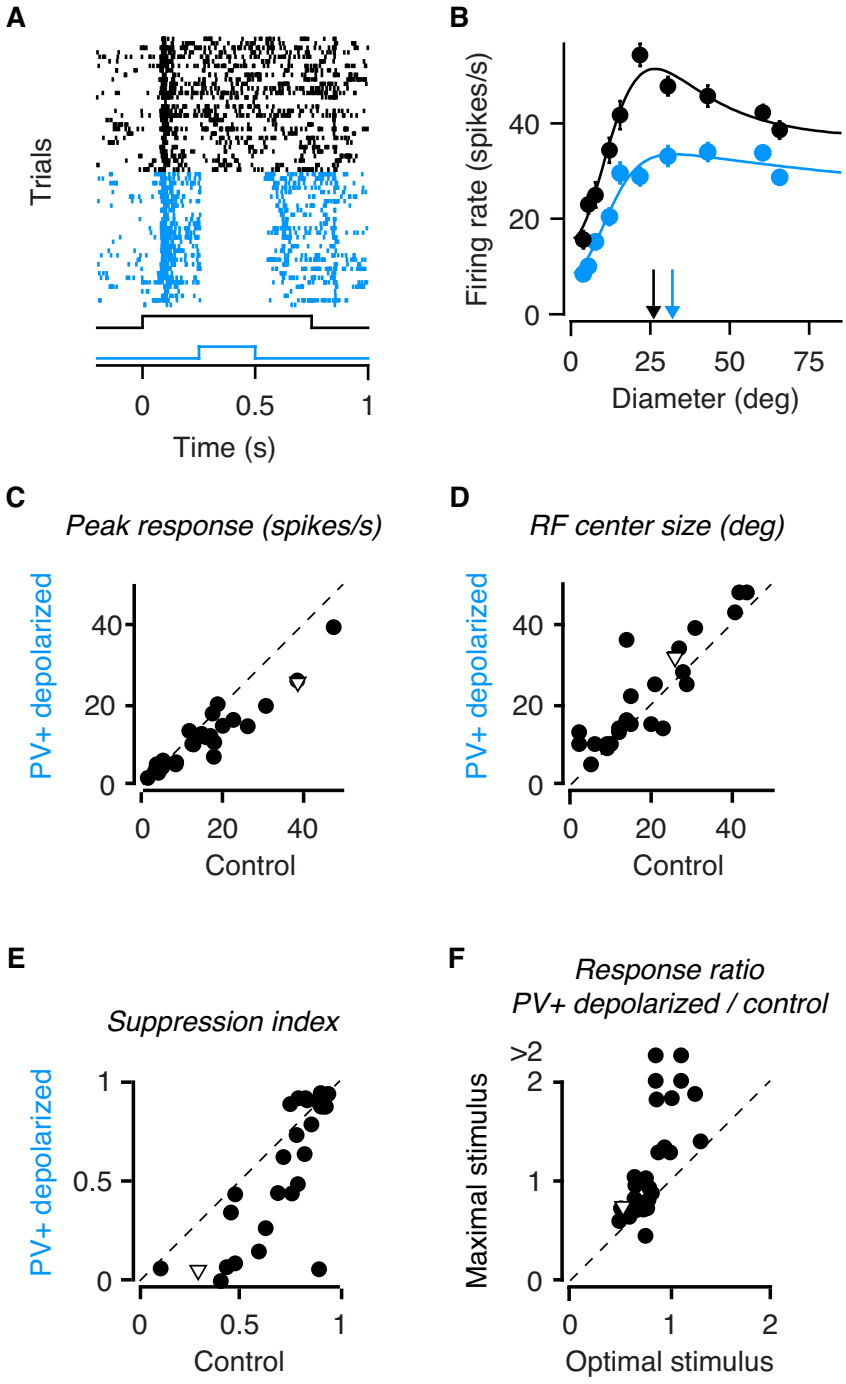

Figure 43. PV+ interneurons influence spatial integration. A: Raster plots of responses to a grating of 15.5 deg without (black) and with (blue) optogenetic depolarization of PV+ interneurons. Black trace: visual stimulus. Blue trace: photostimulation. B: Size tuning curves, same conventions as in (A). Arrows depict RF center size. Same example multiunit as in (A). C: Changes in peak firing rates with optogenetic depolarization of PV+ interneurons. D: Same, for RF center size. E: Same, for suppression strength. F: Ratio of responses with

and without photostimulation to optimal and to largest stimulus. (C-F) Triangle depicts example multiunit from (A-B).

3.2 Results part II: Attention-like signatures of locomotion in the early visual system of the mouse

3.2.1 Locomotion-related response modulations

To measure locomotion-related response modulations in individual neurons, we placed head-fixed mice on an air-cushioned Styrofoam ball and recorded extracellular single-unit activity from upper layers of V1 during locomotion and stationary periods. We found an enhancement of responses around locomotion onset during spontaneous and visually driven activity (Figure 44A,B). During spontaneous activity, i.e. during the presentation of an isoluminant gray screen, the firing rate of individual neurons increased around locomotion onset (Figure 44A). This increase was consistent in the recorded population (22.3% $\pm$ 4.4; mean standard error; $p < 0.001$, N = 176 neurons; Figure 44B, top). Similarly, firing rates also increased around locomotion onsets during stimulus-driven activity (28.8% $\pm$ 2.3; $p < 0.001$, N = 232 neurons; Figure 44B, bottom). Overall, this increase was stronger during visually driven compared to spontaneous activity ($p = 0.015$, ANOVA) and present in more neurons (23.3% vs. 11.9%, $p = 0.003$, chi-square test). We found that locomotion did not alter selectivity for stimulus orientation (Figure 44C-F). Comparing orientation-tuning curves in the presence or absence of locomotion, we found individual neurons that increased their activity in a roughly multiplicative way (Figure 44C). Despite considerable variability across neurons, the population average also showed a gain modulation during locomotion (Figure 44D), with an increase in the peak

response of 34.1% $\pm$ 11.6 (Figure 44E, p = 0.011, N = 31) but no change in selectivity (Figure 44F, p = 0.21).

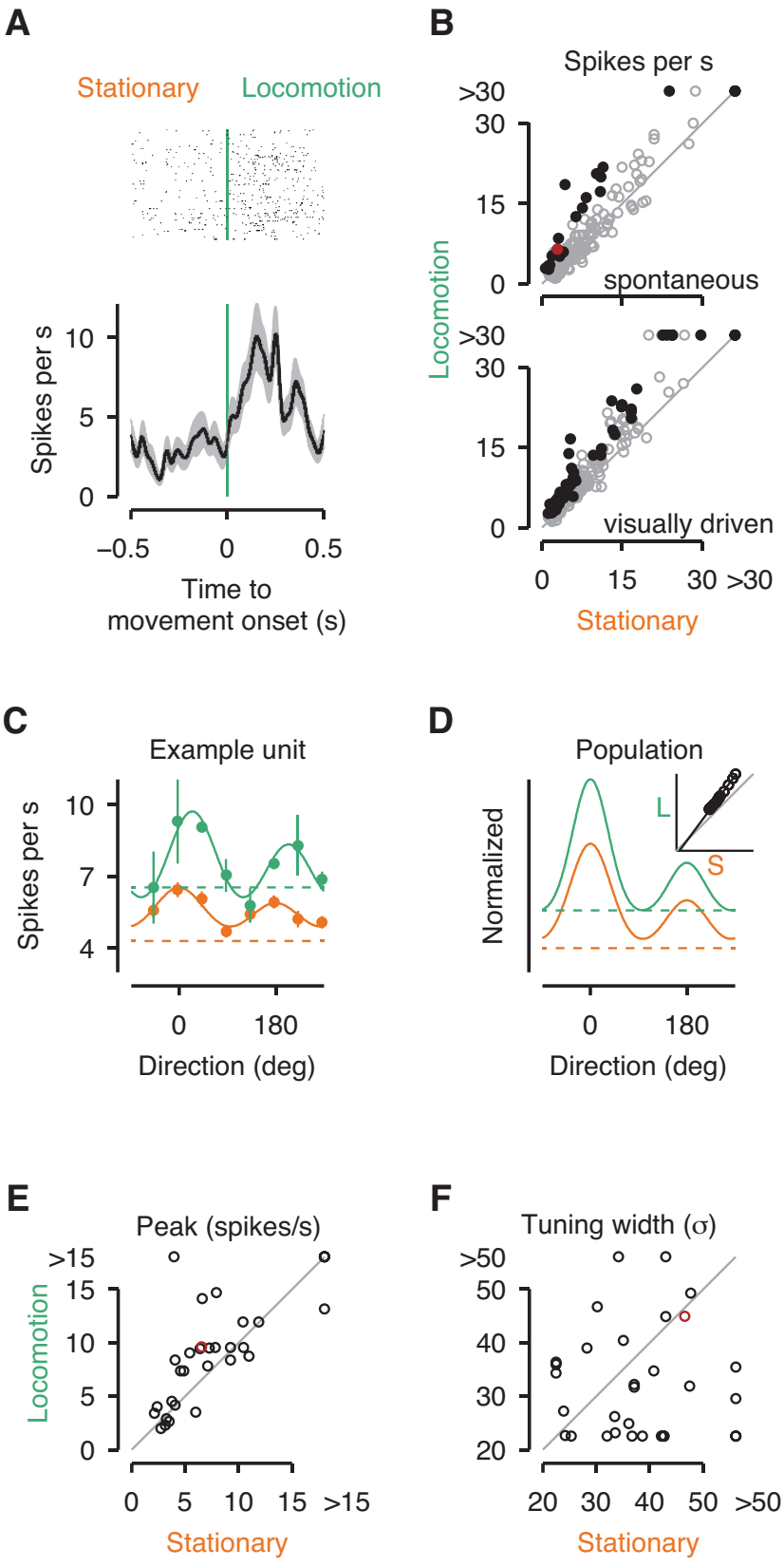
A
Stationary
Locomotion
Spikes per s
10
5
0
−0.5
0
0.5
Time to
movement onset (s)
B
Spikes per s
>30
30
15
0
Locomotion
spontaneous
visually driven
0
15
30
>30
Stationary
C
Example unit
Spikes per s
10
7
4
0
180
Direction (deg)
D
Population
Normalized
L
S
0
180
Direction (deg)
E
Peak (spikes/s)
Locomotion
>15
15
10
5
0
0
5
10
15
>15
Stationary
F
Tuning width (σ)
>50
50
40
30
20
20
30
40
50
>50
Stationary

Figure 44. Locomotion enhances firing rates of neurons in mouse V1. A: Spike rasters (top) and spike density function (bottom) of an example neuron in V1 aligned with locomotion onset during spontaneous activity. N = 116 onsets. B: Firing rates of neurons in 500 ms windows before and after locomotion onset during spontaneous (top, N = 176) and visually driven activity (bottom, N = 232). C: Orientation tuning of an example neuron, during locomotion (green) and stationary (orange) trials. Solid line is fitted Sum-of-Gaussians model; dashed line is response to mean-luminance gray screen. D: Same, for the average fits aligned to preferred direction across the population (N = 31). Inset shows population-tuning curve evaluated in 10 deg steps for locomotion vs. stationary conditions, black line is obtained by robust regression (y = -0.55 + 1.35 * x). E: Peak response during locomotion versus stationary periods. F: Same, for tuning width. Example cells are marked in red, filled symbols are neurons with individually significant modulations; error bars represent standard error of the mean.

3.2.2 Locomotion effects on V1 interneuronal correlations

Considering that cortical state is typically characterized by the magnitude of common fluctuations in population spiking activity (Harris & Thiele 2011), we next asked whether locomotion, apart from enhancing activity of single neurons, also reduces interneuronal correlations. We focused on spontaneous activity (Figure 45). We first segmented all locomotion and stationary periods into 100 ms bins, for which we determined the spike counts of all recorded pairs (Figure 45A). We then concatenated all locomotion or stationary periods, and computed the Pearson's correlation coefficient on the spike counts of each pair of neurons (r_{sc}). Consider, for example, the distribution of spike counts of an example pair of neurons shown in Figure 45B. This pair had a weak positive correlation, which, indeed, was lower during locomotion (r_{sc} = 0.05) compared to stationary periods (r_{sc} = 0.15). Likewise, in the population of recorded pairs mean r_{sc} decreased from 0.07 ± 0.003 during stationary periods to 0.03 ± 0.003 during locomotion ($p < 0.001$, Figure 45C). Importantly, this decrease in r_{sc} could not be explained by an increase in neuronal variability during

locomotion, as the Fano factor was lower during locomotion (1.20 ± 0.04) compared to stationary periods (1.32 ± 0.04, $p < 0.001$). The de-correlation and reduction of the Fano factor are remarkable, considering that locomotion on- and offsets induce common changes in the population activity (e.g., Figure 44B), and that mouse V1 neurons can be tuned for running speed (Saleem et al 2013), which both induce firing rate variability during the locomotion state. Previous studies in visual cortex have documented that interneuronal correlations are higher for pairs with similar tuning properties (Ch'ng & Reid 2010, Cohen & Newsome 2008, Denman & Contreras 2013, Ecker et al 2010, Gu et al 2011, Gutnisky & Dragoi 2008, Ko et al 2011, Kohn & Smith 2005, Smith & Kohn 2008, Zohary et al 1994) but it is unknown whether locomotion changes this relationship. To address this issue, we quantified for each recorded pair the similarity of orientation tuning by computing the Pearson correlation coefficient of average responses across all stimulus orientations (signal correlation, r_{signal}). In the population of recorded pairs, we examined the relationship between r_{signal} and r_{sc} by fitting linear models (analysis of covariance, ANCOVA, Figure 45D). Consistent with previous studies, we found that spike count correlations generally increased with tuning similarity ($p < 0.001$), and, consistent with our previous analysis, locomotion decreased the overall level of spike count correlations ($p < 0.001$, ANCOVA). Locomotion also had a modest effect on the strength of the relationship between r_{signal} and r_{sc} ($p = 0.03$, ANCOVA). We summarize the locomotion-induced changes in r_{sc} by separating pairs on the basis of their tuning similarity (Figure 45E).

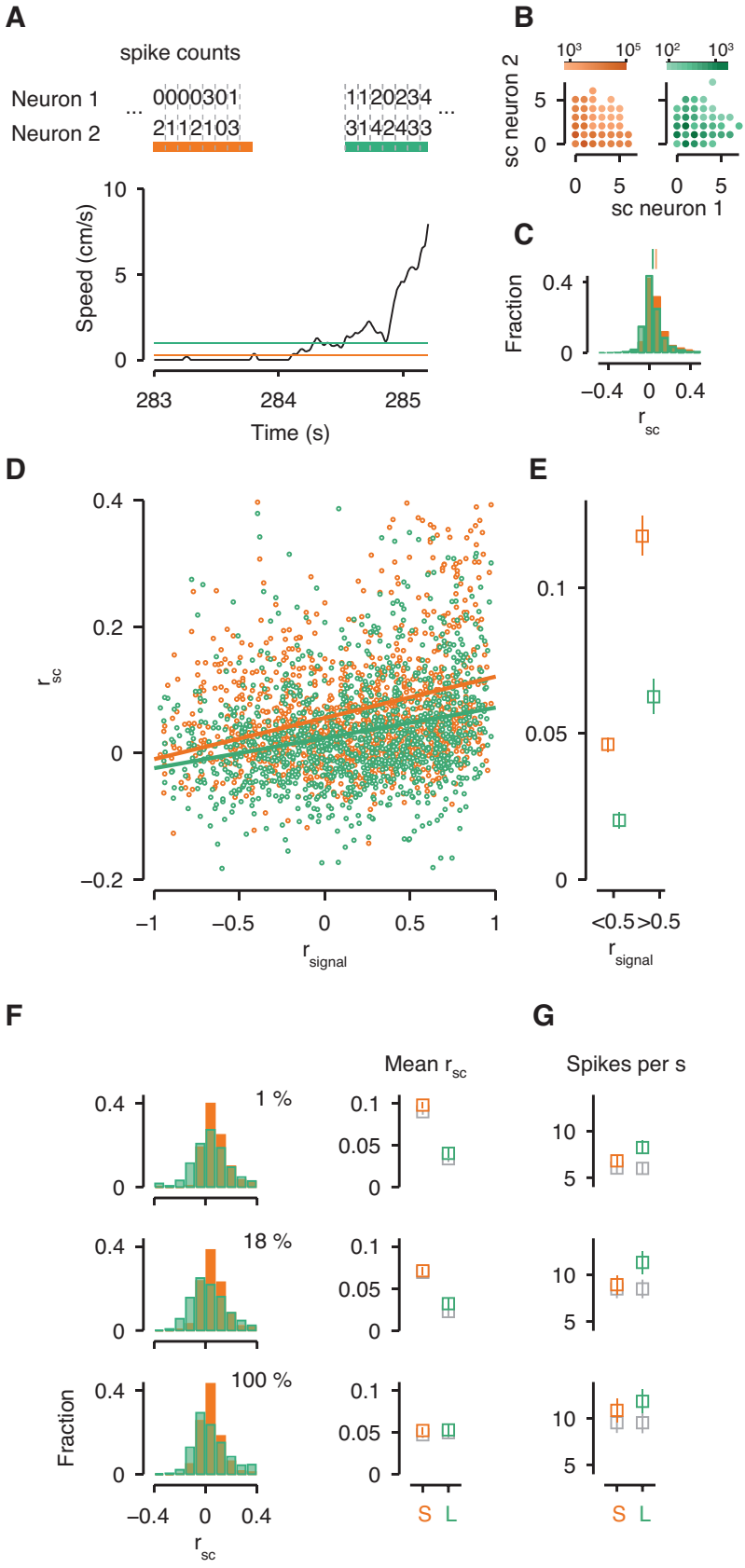
A
spike counts
Neuron 1
Neuron 2
0000301
2112103
1120234
3142433
Speed (cm/s)
Time (s)
B
sc neuron 2
sc neuron 1
C
Fraction
D
E
F
1 %
18 %
100 %
Mean r_sc
G
Spikes per s
S
L

Figure 45. Locomotion reduces interneuronal correlations. A: Example speed trace with segmentation of locomotion and stationary periods into spike-count bins. Horizontal lines indicate stationary (orange) and locomotion (green) thresholds. B: Distribution of spike counts during spontaneous activity for the pair shown in (a) across locomotion and stationary periods. C: Distribution of average spike count correlations in the population of recorded pairs (N = 1338 pairs) during spontaneous activity. D: Relation between tuning similarity (signal correlation) and spike count correlations for locomotion and stationary periods during spontaneous activity. Solid lines represent regression fits. E: Average spike count correlations for pairs with high signal correlations (>0.5) and the remaining population (<0.5). F: Left: Distributions of spike count correlations during locomotion and stationary periods for different levels of stimulus contrast. Right: Means of the distributions (N = 586/584/616 pairs). G: Average firing rates during locomotion and stationary periods. Green: locomotion; orange: stationary; gray: data after mean matching of firing rates.

3.2.3 Effect of stimulus contrast on locomotion-based decorrelation of population responses

Previous studies in anesthetized monkeys and cats have also provided evidence for a decrease of network correlations with increasing stimulus contrast (Kohn & Smith 2005, Nauhaus et al 2009), raising the possibility that the de-correlation of population responses by locomotion could have an impact only during spontaneous activity or low-contrast visual stimulation. To assess any effect of stimulus contrast on locomotion-based decorrelation of population responses, we computed pairwise correlations during locomotion and stationary periods while presenting gratings of varying contrast. Note that these correlations inevitably contain components due to stimulus signals, since locomotion and stationary periods occurred at random times relative to stimulus-induced activity. We found, indeed, a contrast-dependence of interneuronal correlations only for the stationary, but not for the locomotion condition (Figure 45F,G). Pairwise correlations during locomotion were low across all contrast levels and only during stationary

periods decreased from 0.09 at 1% contrast to 0.05 at 100% contrast ($p < 0.001$, ANOVA interaction term). In fact, during full contrast (100%) stimuli, pairwise correlations were not different between stationary and locomotion conditions ($p = 0.67$, post-hoc comparison). The similarly low magnitude of correlations during full contrast stimulation suggests that, during stationary periods, the salient visual stimulus might act as an exogenous cue driving the visual cortex into an activated state. Importantly, the differences in correlations between locomotion and stationary periods cannot not be explained by differences in firing rate (Figure 45F,G): equalizing mean firing rates for each neuron across locomotion conditions by randomly deleting excess spikes did not change the pattern of results: pairwise correlations were generally lower for locomotion compared to stationary periods ($p < 0.001$, ANOVA) and exhibited a contrast dependence only during stationary periods ($p < 0.001$, ANOVA interaction term).

3.2.4 Laminar profile of V1 locomotion effects

As most previous studies of locomotion-related modulations have concentrated on superficial layers in area V1 (Bennett, 2013; Keller, 2012; Niell, 2010), we next asked whether locomotion effects have a distinct laminar pattern. To simultaneously sample neurons from all V1 layers, we used linear multi-contact probes and applied current source density (CSD) analysis to the visually evoked LFP response for localization of electrode contacts within the cortical column (Figure 46A). We determined the base of layer 4 by the polarity inversion of the CSD and used this as a reference to assign electrode contacts to putative supragranular, granular, and infragranular layers. When we examined firing rates around locomotion onset, we found, consistent with the data shown in Figure 44 and with previous studies, locomotion-based response enhancements of spontaneous activity in supragranular and granular layers (Figure 46B, top, middle). In

addition to these enhancements, locomotion onset also reduced activity in a number of neurons (Figure 46B, bottom), which seemed to be located preferentially in the upper portion of infragranular layers. To quantify this observed laminar difference in the population, we analyzed the ratio of responses before and after locomotion onset relative to layer 4. We found that neurons in the upper part of the infragranular layers decreased rather than increased their responses after locomotion onset, during both spontaneous (Figure 46C, $p = 0.004$, Kruskal-Wallis, interaction term) and visually-driven activity (Figure 46D, $p < 0.001$, Kruskal-Wallis, interaction term). This relative abundance of neurons with decreasing responses in the upper part of the infragranular layers seems to counteract locomotion-based response enhancements that are common to all layers, such that there was little response modulation by locomotion in the population average. The small size of locomotion-based response enhancements in the upper part of the infragranular population average should therefore not be interpreted as a lack of response modulations, but rather as an increase in diversity.

This small average locomotion-based response modulation of infragranular neurons cannot be explained by low overall firing rates which might in turn lead to small modulations, because firing rates in infragranular layers exceeded those in the supragranular layers (spontaneous activity: 7.6 spikes/s $\pm$ 0.4 vs. 5.0 spikes/s $\pm$ 0.5, $p = 0.003$; visually driven activity: 8.1 spike/s $\pm$ 0.4 vs. 5.9 spikes/s $\pm$ 0.4, $p = 0.004$, post-hoc analyses); nor can it be explained by a small sample size as our recorded population was largest in the infragranular layers.

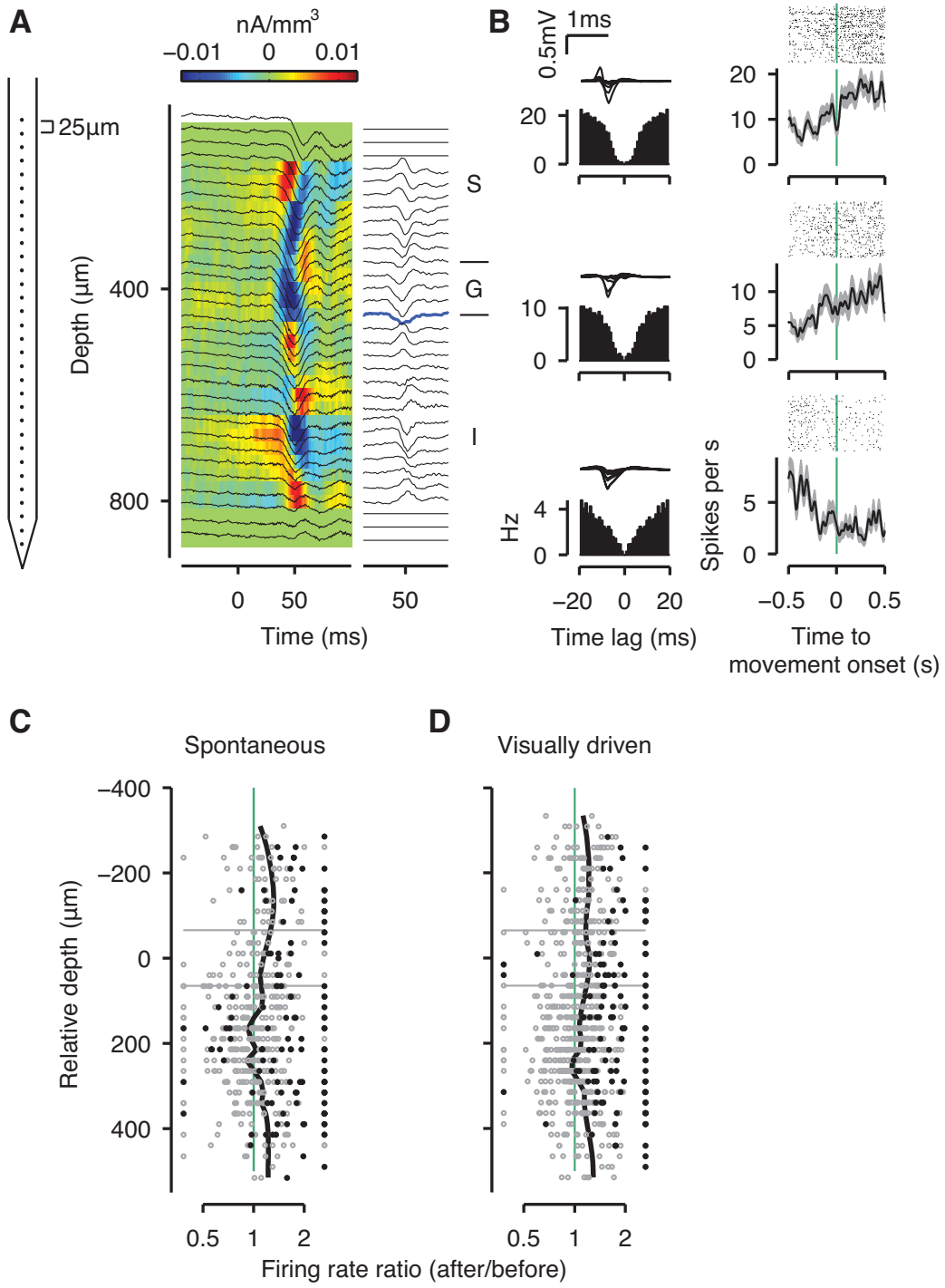

Figure 46. Locomotion-triggered response modulations are diverse in infragranular layers. A: Left: schematic drawing of a linear 32-channel probe. Middle: CSD image (color) and superimposed LFP traces (black). Right: CSD traces. Thick blue line marks the polarity inversion of the CSD used to determine the base of putative layer 4. S: supragranular, G: granular, I: infragranular. B: Left: Spike waveforms and autocorrelograms of representative neurons for each putative laminar location. Right: Spike

rasters and spike density functions of example neurons aligned with locomotion onset during spontaneous activity. N = 64 onsets. C: Ratios of spontaneous activity 500 ms after vs. before locomotion onset (abscissa) as a function of depth relative to putative layer 4 (ordinate). Solid black line represents the running average; gray lines mark the extent of putative layer 4. Data points beyond the range of the abscissa represent values smaller than 0.5 and larger than 2. Black data points are neurons with individually significant modulations. D: Same, for visually driven activity.

3.2.5 Locomotion effects upstream of primary visual cortex

Having documented prominent locomotion-based response modulations in the granular layer of mouse V1, we next investigated whether locomotion modulates processing stages upstream of area V1. We first recorded from the mouse dLGN (Figure 47A) and found, contrary to common belief, that locomotion does increase firing rates already at the level of the thalamus. Consider, for example, the dLGN cell shown in Figure 47B, which transiently increases its firing around locomotion onset. Such an increase was consistent across cells recorded in dLGN (Figure 47C, $p = 0.0013$, $N = 93$ neurons, Wilcoxon signed rank), but smaller in magnitude and more variable (median $11.5\% \pm 98.4$ m.a.d.) compared to the increase in V1 (median $25.9\% \pm 25.4$ m.a.d.). In addition to transient increases in neural activity around locomotion onsets, we also found that grating stimuli elicited higher firing rates during locomotion vs. stationary trials (Figure 47D,E). This effect was consistent across the dLGN population, where average firing rates (F0) increased by $16.1\% \pm 26.2$ (median $\pm$ m.a.d.; $p = 0.002$, $N = 73$, Wilcoxon signed rank test; Figure 47E). Interestingly, the timing of the additional spikes was not tightly related to the temporal frequency of the stimulus, as the F1 response component did not differ between locomotion and stationary conditions ($p = 0.95$, Wilcoxon signed-rank test). Together, this led to an increase of the median F0/F1 ratio during locomotion (Figure 47F, $p < 0.001$,

Wilcoxon signed-rank test), indicating that firing rate enhancements were not necessarily temporally specific. Replicating previous results (Niell & Stryker 2010), we also noticed that dLGN neurons decreased burst spiking during locomotion (2.0% $\pm$ 0.2 vs. 0.7% $\pm$ 0.09, $p < 0.001$, N=73 neurons; Figure 47G). Since we found locomotion effects on firing rates in both dLGN and V1, we asked if the decorrelation of V1 populations by locomotion was also already present in the thalamus. We computed spike count correlations for pairs of cells in dLGN during spontaneous activity (Figure 47H) and found slightly higher correlations during locomotion compared to stationary periods (rsc = 0.02 $\pm$ 0.003 vs. 0.01 $\pm$ 0.003, $p < 0.001$; similar for mean-matched pairs). This suggests that the decrease in interneuronal correlations observed in V1 does not originate from de-correlated feed-forward thalamic input, but rather emerges in cortex.

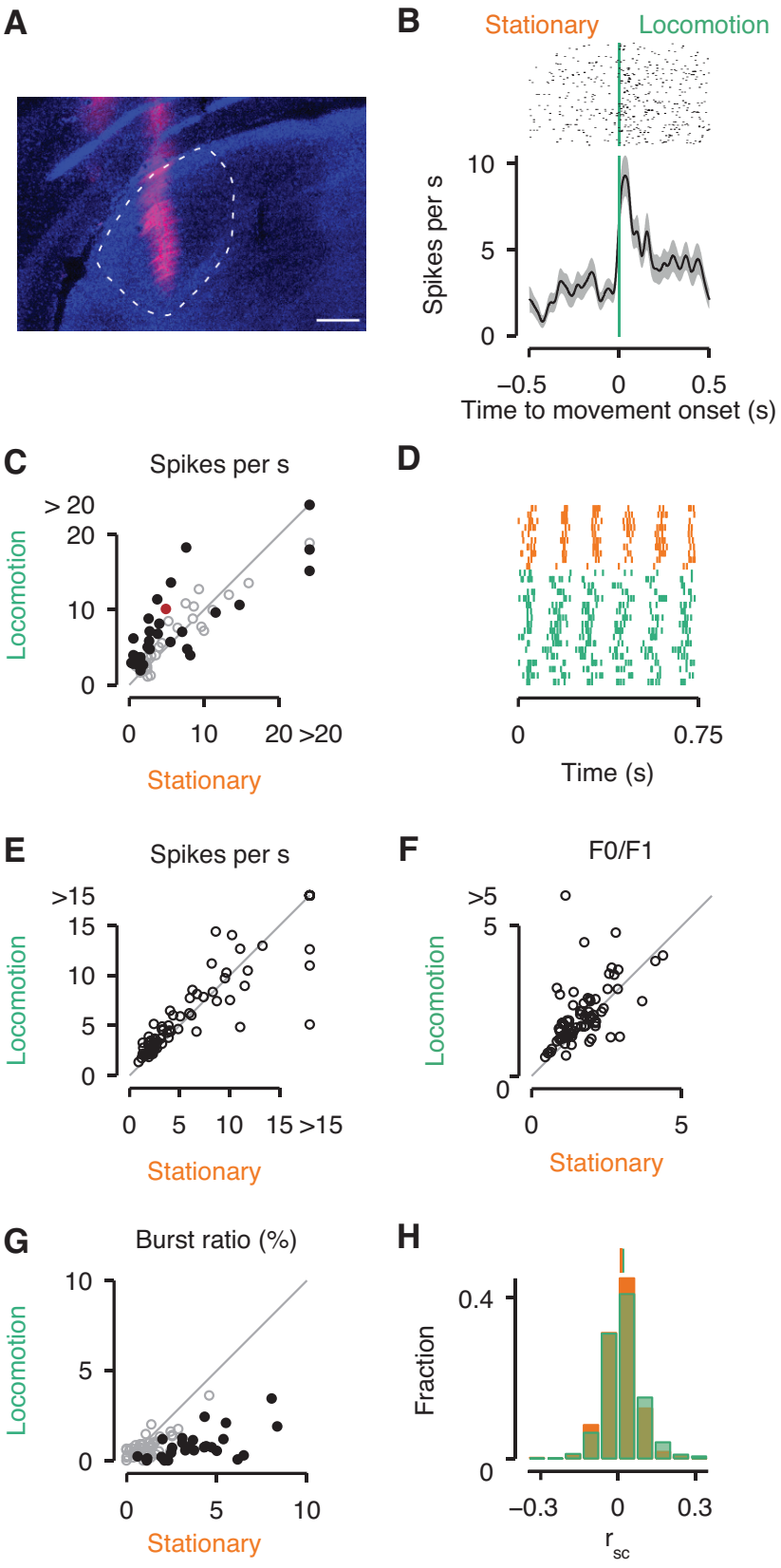
A
B
Stationary
Locomotion
Spikes per s
10
5
0
–0.5
0
0.5
Time to movement onset (s)
C
Spikes per s
Locomotion
> 20
20
10
0
0
10
20 >20
Stationary
D
0
0.75
Time (s)
E
Spikes per s
Locomotion
>15
15
10
5
0
0
5
10
15 >15
Stationary
F
F0/F1
Locomotion
>5
5
0
0
5
Stationary
G
Burst ratio (%)
Locomotion
10
5
0
0
5
10
Stationary
H
Fraction
0.4
0
–0.3
0
0.3
r sc

Figure 47. Effects of locomotion in dLGN. A: Coronal section of dLGN, marked by white outline. Blue, DAPI; red, DiD. Scale bar 200 μm. B: Spike rasters (top) and spike density function (bottom) of responses aligned to locomotion onset of an example dLGN neuron. N = 130 onsets. C: Firing rates in the 0.5s after versus before locomotion onset (N = 93 neurons). D: Spike raster of an example unit during presentation of a drifting grating, separately for trials with locomotion (green) and without (orange). N = 28 trials. E: Average firing rates in response to full-contrast gratings during locomotion (green) and stationary (orange) trials (N = 73 neurons). F: Same, for the ratio of F0/F1 response components. G: Same, for burst ratio. H: Distribution of spike count correlations in the population of simultaneously recorded pairs (N = 628) during spontaneous activity for locomotion (green) and stationary periods (orange).

3.2.6 Locomotion and pupil size

Given that a prominent behavioral marker of attentive states is pupil size we finally asked whether effects of locomotion could also be observed at the level of the eye (Figure 48). Attention research in humans has long relied on pupil dilation under constant illumination to non-invasively infer the attentiveness of an observer (Bradshaw 1967). Using camera based eye tracking under infrared illumination, we measured pupil position and size during the presentation of a blank screen and correlated these variables to changes in locomotion.

Under mouse head-fixation the overall eye saccade frequency was low (0.94 Hz $\pm$ 0.29); yet, saccades were more frequent during locomotion (1.54 Hz $\pm$ 0.29) compared to stationary periods (0.34 Hz $\pm$ 0.23, $p < 0.001$; Figure 48A-D). Much more striking was the close tracking of running speed by pupil size (Figure 48E). To quantify this observation, we related the average speed in each locomotion and stationary period to average pupil size (Figure 48F, Pearson's = 0.56, $p < 0.001$ for the locomotion periods). Although the distribution of pupil size in this recording session was generally broad, we found that average pupil size was larger (39.7%, $p < 0.001$, two-sample t-test)

during locomotion compared to stationary periods. This effect was consistent across experiments: during locomotion compared to stationary periods average pupil size was ~45.0% ± 9.1 larger (Figure 48G, $p < 0.001$). We also consistently observed dilations when the pupil data were aligned to locomotion onsets (Figure 48H), both for individual onsets (gray traces) as well as for the average pupil response in different experiments (black traces). Neither pupil dilation nor eye movements could account for the transient locomotion-related effects observed in dLGN and V1 (Figure 49). Instead, pupil dilation seems to serve, as known from attention studies, as a reliable marker for behavioral state.

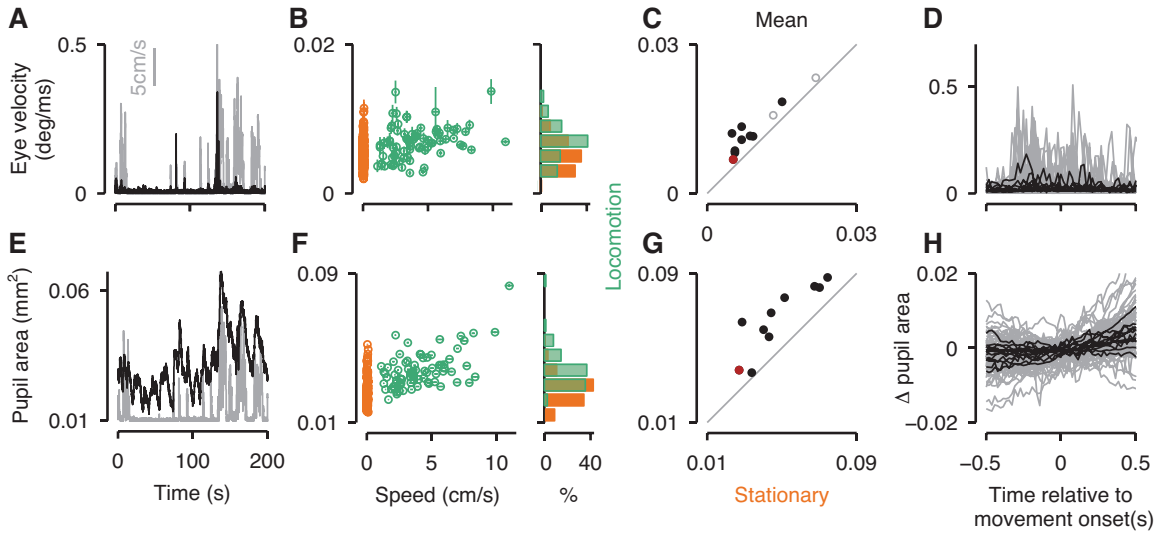

Figure 48. Effects of locomotion on eye velocity and pupil size. A: Example time course of eye velocity (black) and locomotion speed (gray). B: Average eye velocity for locomotion (green) and stationary (orange) periods as a function of average locomotion speed per period. Right side: distributions of eye velocity. N = 160 periods. C: Mean of the eye velocity distributions during locomotion versus stationary periods, N = 13 recording sessions. D: Locomotion onset-triggered eye velocity. Gray lines represent individual onsets, black lines averages of sessions. Error bars represent s.e.m. E: Example time course of pupil size (black) and locomotion speed (gray). F: Average pupil size for locomotion (green) and stationary periods as a function of average locomotion speed per period. Right side: marginal distributions of pupil size. N = 160 periods. G: Means of the pupil size distributions during locomotion versus stationary periods, N = 13 recording sessions. H:

Locomotion onset-triggered pupil size. Gray lines represent individual onsets, black lines averages of recording sessions.

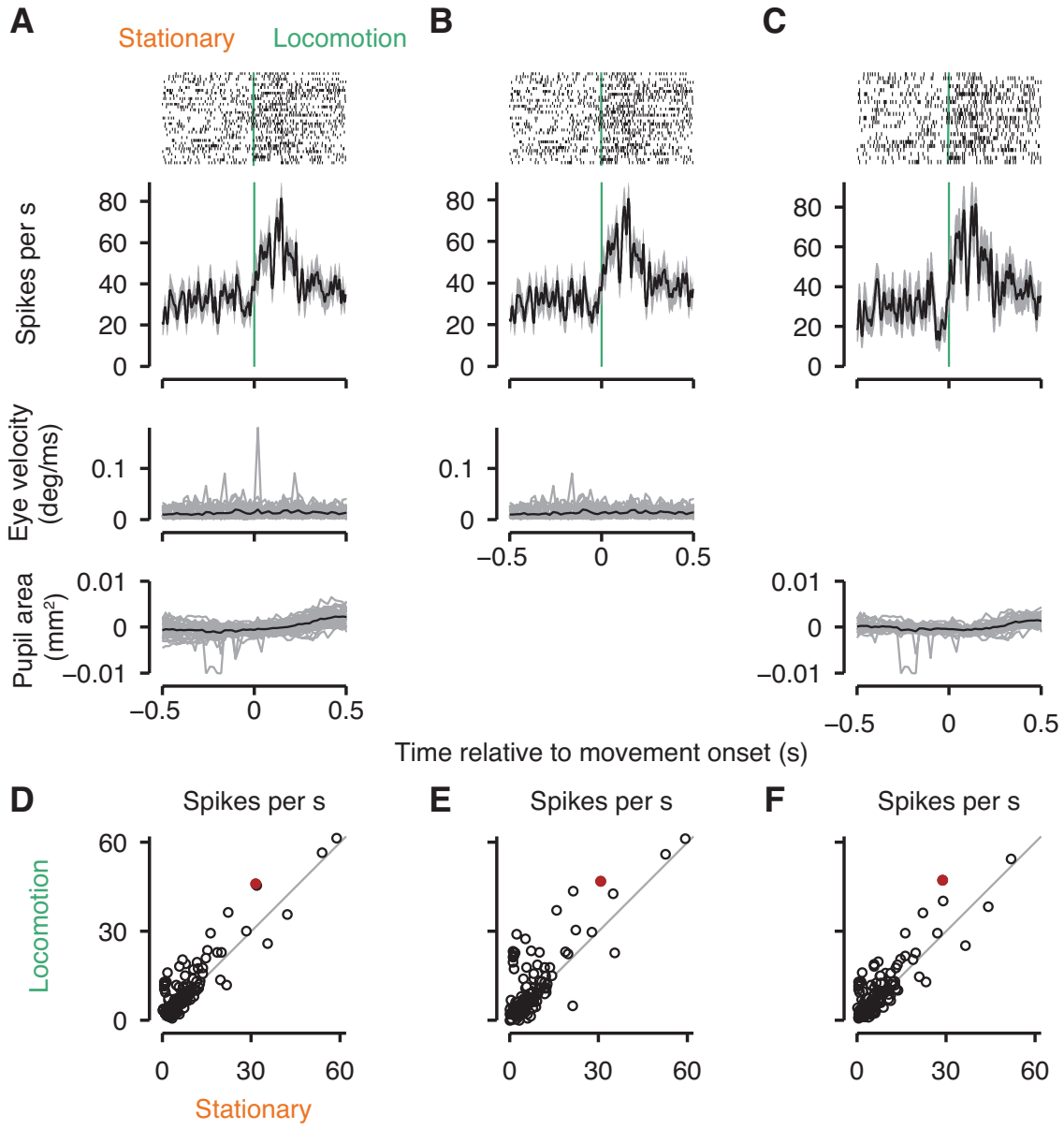

Figure 49. Neural responses at locomotion onset without saccades or dilated pupils. A: Locomotion-triggered response of example neuron (top), eye velocity (middle) and pupil area (bottom). All trials. B: Same, except onsets with saccades were removed. C: Same, except onsets with the 30% strongest pupil dilations were removed. D: Responses of all neurons before and after locomotion onset (N = 188). E: Same, except onsets with saccades were removed. F: Same, except onsets with 30% strongest pupil dilations were removed. Error bars represent s.e.m.

4 Discussion

The aim of this thesis is to investigate effects of stimulus context and behavioral context on information processing in the early visual system of the mouse. A lot of contemporary neuroscience research focuses on the mechanisms by which cortical neurons obtain their well-known response properties. There is a common agreement that multiple mechanisms can play a role, but we do not yet understand their relative contributions.

Stimulus context can modulate visual responses to visual stimuli often by suppressing them. Furthermore, neural responses are not only modulated by stimulus context but also by behavioral context. In primates, one such powerful modulatory influence is selective attention (e.g. (Roberts et al 2007)); in rodents, a potentially related phenomenon is state-dependent processing (e.g. (Harris & Thiele 2011)). How does an attentive or active brain state modulate neuronal responses in sensory cortex and influence perceptual judgments?

In this work, we show how visual responses are changed by internal context as surround suppression and external context as a brain state. As a brain state here we focus not only on how anesthesia and awake states influence visual processing, but also divide the awake state into stationary and locomotion. To investigate these issues, we used in-vivo extracellular electrophysiological recordings and circuit disruption method (optogenetics) in mice.

4.1 Discussion of part I: "Surround suppression in mouse primary visual cortex: laminar dependence and effects of anesthesia"

First we investigated the laminar profile of spatial integration and the role of PV+ interneurons in mouse V1. Analogous to what is seen in higher-order mammals, we have demonstrated that the majority of V1 neurons show surround suppression, which is most pronounced in superficial cortical layers. Signatures of spatial integration strongly depend on brain state: under isoflurane/urethane anesthesia, the laminar specificity of spatial integration is decreased, the strength of surround suppression is reduced, RF size is increased, and responses are slower and more sluggish. These effects of brain state on spatial integration can be parsimoniously explained by assuming that anesthesia affects contrast normalization in visual cortex. Finally, we report that optogenetic depolarization of PV+ interneurons affects surround suppression by increasing RF size and decreasing suppression strength, similar to an overall reduction of contrast.

As for anesthetized recordings, our characterization of spatial integration is consistent with a previous report on center-surround interactions in mouse V1. Under anesthesia, we found RF center sizes (median = 32.4 deg diameter) and surround sizes (median = 98.7 deg) comparable to those earlier reported (medians of 28.85 deg and 92.5 deg) and no dependence of suppression strength on laminar location (Van den Bergh et al 2010). This independence of suppression strength and laminar location stands in sharp contrast to results obtained in higher-order mammals, where suppression is typically strongest in superficial layers (Levitt & Lund 2002, Sceniak et al 2001, Shushruth et al 2009).

Our results obtained during wakefulness, however, are profoundly different

and, despite larger RFs in mice, similar to those in higher-order mammals. We found that in V1 of awake mice, spatial integration is layer dependent: RF center size is smallest and surround suppression is strongest in superficial layers.

Recent work in supragranular layers of mouse visual cortex has identified a specific intracortical circuit for spatial integration, in which SOM+ interneurons play a major role (Adesnik et al 2012). SOM+ interneurons include Martinotti cells, which have ascending axon collaterals into layer 1 and make synaptic contact to the distal tuft dendrites of pyramidal cells across neighboring columns (Silberberg & Markram 2007, Wang et al 2004). In layers 2/3, SOM+ interneurons are preferentially recruited by horizontal cortical axons and, in contrast to pyramidal cells, do not show surround suppression (Adesnik et al 2012). Rather, SOM+ neurons increase firing rates with stimulation of the RF surround, allowing them to downregulate the firing rate of their pyramidal targets with increasing stimulus size. Indeed, optogenetic hyperpolarization of SOM+ interneurons specifically reduces the strength of surround suppression (Adesnik et al 2012). This circuit likely contributes to the relatively strong surround suppression that we observe in superficial layers.

Our data indicate that PV+ interneurons also contribute to spatial integration in mouse V1, but rather indirectly by affecting overall stimulus drive. PV+ neurons mainly correspond to soma-targeting fast-spiking inhibitory interneurons (reviewed in (Markram et al 2004) and have been shown to be involved in cortical feedforward inhibition (e.g., (Swadlow 2003, Yoshimura & Callaway 2005)). We have demonstrated that, in contrast to SOM+, PV+ interneurons need to be depolarized to reduce surround suppression. Increasing PV+ activity likely reduces stimulus drive by controlling the overall responsiveness in the network. Indeed, our observed effects of PV+

interneuron activation on spatial integration are similar to those obtained when stimulus contrast is lowered (see also (Nienborg et al 2013)). Consistent with a general modulation of stimulus drive, PV+ interneurons have recently been implicated in gain control (Atallah et al 2012, Ma et al 2010, Wilson et al 2012).

Whether these interneurons contribute in the same way to spatial integration in primates remains to be tested. In monkeys, orientation-tuned surround suppression in area V1, together with the absence of pronounced orientation tuning in earlier processing stages, have been taken as evidence for intracortical and feedback circuits involved in spatial integration (Angelucci & Bressloff 2006). In mice, orientation tuned responses have recently been documented for the lateral geniculate nucleus (Cruz-Martin et al 2014, Marshel et al 2012, Piscopo et al 2013). This observation could point toward a potential species difference in the relative contribution of feedforward, lateral, and feedback circuits contributing to surround suppression.

Caution should be taken when directly comparing RF sizes and suppression strength between this study in mouse V1 and previous studies in cats and monkeys because of methodological differences. Previous studies on spatial integration in higher-order mammals typically recorded from single cells and optimized stimulus parameters, such as position, orientation, spatial, and temporal frequency, for the isolated neuron. This is different from our approach, in which we recorded simultaneously from multiple sites, focused on multiunit activity, and adjusted stimulus parameters to match the average preferences. It is well documented that stimulus orientation, spatial frequency, and position can affect measures of spatial integration (e.g., (Osaki et al 2011, Shushruth et al 2012, Tailby et al 2007)). Hence, a less than perfect match between stimulus properties and neuronal preferences likely could have contributed to the variability of the effects we observed. Yet, our

results obtained in anesthetized mice closely match those obtained by Van den Bergh et al. (2010), who recorded from single units and tailored stimuli to neuronal preferences, indicating that our procedure likely did not introduce systematic biases.

We also document that anesthesia composed of isoflurane and urethane strongly influences neural response properties in visual cortex. Isoflurane has typically been avoided in the study of the visual system because of adverse side effects, such as alterations of the time course of synaptic transmission (Ries & Puil 1999), reduction of overall responsiveness (Villeneuve & Casanova 2003), and decreased contrast sensitivity (Solomon et al 1999). Nevertheless, isoflurane is frequently used for acute studies of the mouse visual system (e.g., (Bonin et al 2011, Runyan et al 2010, Smith & Hausser 2010)) because it allows precise control over depth of anesthesia despite the small size of the mouse. Another popular anesthetic for acute neurophysiology in rodents is urethane (e.g., (Niell & Stryker 2008, Van den Bergh et al 2010, Wang et al 2013)), which seems to reduce overall neuronal excitability (Girman et al 1999, Sceniak & Maciver 2006) without changing synaptic transmission and without affecting tuning properties (Sceniak & Maciver 2006). Considering these findings, one might ascribe the effects of brain state on surround suppression primarily to isoflurane. However, in control experiments using urethane as the sole anesthetic, we still found attenuated suppressive effects and lower contrast sensitivity compared with recordings during wakefulness (albeit less pronounced). We conclude that the full extent of surround suppression cannot be revealed under isoflurane or urethane anesthesia (see also (Adesnik et al 2012, Haider et al 2013)).

Our finding that brain state strongly modulates tuning for stimulus size is consistent with a recent intracellular recording study in mouse V1 (Haider et al 2013). Here, the authors showed that during anesthesia with

chlorprothixene and either isoflurane or urethane, responses were persistent in time and broad in space compared with those obtained under wakefulness. Their recordings of synaptic conductances revealed that a dominance of inhibition during wakefulness is responsible for the temporal and spatial restriction of responses.

We hypothesized that the differences in spatial integration between the awake and anesthetized brain arise because reduced inhibition during anesthesia alters mechanisms of contrast normalization. Contrast normalization has been successfully used to model surround suppression (Carandini & Heeger 2012). In primate and cat V1, spatial and temporal properties of center-surround interactions depend on stimulus contrast (Kapadia et al 1999, Sadakane et al 2006, Sceniak et al 1999, Schwabe et al 2010, Webb et al 2005). In the present study, we have shown that stimulus contrast similarly influences surround suppression in mouse V1, where lower stimulus contrast leads to larger RF center sizes and weaker suppression strength (see also (Ayaz et al 2013, Nienborg et al 2013)). Since anesthesia also substantially reduced contrast sensitivity, the decrease in suppression strength and the slow time course of responses under anesthesia could be attributed to anesthesia affecting contrast normalization: a full contrast stimulus presented during anesthesia might evoke comparable responses to a reduced contrast stimulus seen by an awake mouse.

We conclude that mouse V1 is a valuable model to study the circuit-level mechanisms of spatial integration in visual cortex. As for intracortical inhibitory neurons alone, a picture emerges in which at least two cell types, SOM+ and PV+ inhibitory interneurons, shape spatial integration in distinct ways. The application of genetic tools promises to further disentangle the relative impact of feedforward, intracortical, and feedback connections.

4.2 Discussion of part II: Attention-like signatures of locomotion in the early visual system of the mouse

We tested the impact of locomotion on responses of neural populations in area V1 and pre-cortical processing stages, and present three main findings: First, apart from enhancing single unit activity, locomotion decreases interneuronal correlations in the population response of area V1. Second, far from being limited to cortical neurons, locomotion-based response enhancements occurred in the dLGN of the thalamus; the de-correlation of population responses by locomotion, in contrast, appears to be restricted to cortex. Third, as the speed of locomotion increases, the pupil dilates. These findings document previously unknown and far-reaching effects of locomotion across all processing stages of the early visual system.

Desynchronization of population responses during active brain states has long been known from studies of state-dependent processing in rodents. State-dependent reductions in common fluctuations have most often been measured in local field potentials. Such reductions are typically observed in rodents during active behaviors such as running (Niell & Stryker 2010, Polack et al 2013) and are also present in our own data (not shown). Decreases in common fluctuations can also be measured directly within the spiking activity of the population (Harris et al 2011). Indeed, our result that locomotion reduces interneuronal correlations is generally consistent with previous work in urethane anesthetized rats, showing a reduction of spike count correlations during periods of activated cortical state (Renart et al 2010) or during basal forebrain stimulation (Goard & Dan 2009). Our finding is also consistent with a previous study using dual whole-cell recordings in the somatosensory system which reported less correlated fluctuations in the membrane potential of neighboring pyramidal neurons during active

whisking compared to quiet wakefulness (Poulet & Petersen 2008).

Our results argue for a re-assessment of the previously reported contrast-dependence of network correlations (Kohn & Smith 2005, Nauhaus et al 2009). We propose that the previously observed contrast-dependence is most prominent during anesthetized or inactive brain states, where higher contrast stimuli could act as an exogenous cue driving the visual cortex into an activated state. If, however, the brain is in an active state already, such as during task performance or locomotion, the impact of stimulus contrast should be much reduced. Apart from our own observations, this proposal receives support from recent studies finding negligible effects of stimulus contrast on interneuronal correlations in attending primates (Berens et al 2012, Ecker et al 2014, Ecker et al 2010).

The de-correlation of population responses during locomotion observed in our study cannot be accounted for by differences in firing rates between locomotion and stationary periods, as mean-matching the firing rates had little effect on pairwise correlations. Importantly, the observed reduction in interneuronal correlations was not due to increased variability in the neuronal responses with locomotion. Indeed, consistent with a previously reported decrease in trial-by-trial variability during locomotion (Bennett et al 2013), we found the Fano factors to be lower during locomotion compared to stationary periods. It is unlikely that this reduction of the Fano factor is due to differences in eye movements, as higher eye velocity, i.e. more saccades, were observed during locomotion, which should increase rather than decrease variability of neuronal responses.

While there is general agreement that locomotion enhances visually evoked responses in upper-layer V1, its effects on the magnitude of spontaneous activity are more contentious. Some studies find locomotion-related increases in spontaneous spiking activity (Andermann et al 2013, Ayaz et al

2013, Keller et al 2012, Saleem et al 2013), others find no effect in broad-spiking (Niell & Stryker 2010) or pyramidal neurons (Polack et al 2013), and even others find decreases (Bennett et al 2013). Our study helps to clarify this issue by providing clear evidence for locomotion-related increase during spontaneous activity. We argue that one reason for the discrepancy between studies may be sampling of different populations and differences in analysis methods. Even for upper-layer V1, we find rather heterogeneous effects, with locomotion modulating neurons positively, negatively, or not at all. With small sample sizes, detection of consistent modulations might therefore easily fail. Furthermore, locomotion-based modulations might best be revealed through locomotion-triggered analyses, which most of the previous studies have not performed. Notwithstanding the controversy about locomotion-effects on spontaneous activity, we show that during spontaneous activity the impact of locomotion on interneuronal spike count correlations is strongest. We therefore conclude that locomotion can exert profound influences on spiking activity even during spontaneous activity.

Most previous studies of locomotion-based response modulations have focused on superficial layers (Bennett et al 2013, Keller et al 2012, Niell & Stryker 2010, Polack et al 2013). This turns out to be an excellent choice, as our laminar recordings show that superficial layers are indeed the sites with the most consistent and strongest overall locomotion-related enhancements. Extragranular layers, in general, are the targets of feedback connections (Douglas & Martin 2004, Felleman & Van Essen 1991, Rockland & Pandya 1979). In addition to the superficial layers, we also find modulations of firing rates by locomotion in the putative granular layer. Together with our finding of locomotion-based firing rate enhancements in dLGN neurons, this argues for a contribution of feedforward connectivity to effects of locomotion in visual cortex. These results also offer an interpretation of the locomotion-

related depolarization of membrane potential observed in L4 (Polack et al 2013), which might reflect, at least partly, an enhanced output of dLGN neurons. Finally, a recent two-photon calcium imaging study pointed out neurons with strong suppression at running onset in deep layers (Andermann et al 2013). This observation is consistent with our finding that locomotion-based response modulations are diverse, and often of negative sign in putative infragranular layers, and the approximate cortical depth of suppressed cells between the two studies seems similar. Whether and how suppression of neuronal responses in deep layers by locomotion might mediate locomotion-related response enhancements within the cortical column currently is unclear. Still, the prevalence of suppressed cells in infragranular layers resonates well with the finding that decrease of L6 activity exert gain increase in upper layers (Olsen et al 2012).

In pioneering work (Niell & Stryker 2010), Niell & Stryker have reported that response enhancements by locomotion along the visual pathway are restricted to cortical neurons. Here, we argue against this notion by providing clear evidence that locomotion can enhance neural activity even in mouse dLGN. Since the locomotion-based influences we observed in dLGN are smaller and more variable than those in area V1, it is not surprising that they so far have gone unnoticed. Yet, they are reliably revealed even in single dLGN neurons by examining the locomotion-triggered average response, an analysis that had not been reported for this population. Otherwise, our data agree well with Niell & Stryker's result (Niell & Stryker 2010) that burst mode firing of dLGN neurons is reduced by locomotion and with related findings during inattentive or quiescent states (Bezdudnaya et al 2006, Harris & Thiele 2011). Moreover, like Niell & Stryker, we also find no significant difference in the response component entrained by the temporal frequency of the stimulus, indicating that response enhancements by locomotion in dLGN

are not temporally specific. Whether the response modulations in dLGN by locomotion first arise in the dLGN, reflect L6 cortico-thalamic feedback (Sillito et al 2006) or influences from other subcortical pathways (Saalmann & Kastner 2009) is currently an open question.

The striking relationship between locomotion and pupil size has so far gone unnoticed despite the well-known relationship between pupil dilation and alertness or arousal in humans (Bradshaw 1967, Yoss et al 1970). Pupil dilation under steady illumination is one component of the orienting response, which serves to prepare body and senses for responding to critical changes in the environment (Sokolov 1963). What could be the functional role of pupil dilation for visual processing? One suggestion is that pupil dilation could increase visual sensitivity (Lynn 1966, Wang et al 2012). While larger pupil sizes are generally associated with better performance, direct experimental evidence for this proposal is sparse (Nieuwenhuis et al 2010, Wang et al 2012). In the mouse eye, pupil dilation can lead to a more than 20-fold increase in retinal brightness (Pennesi et al 1998). Given the presence of powerful gain control mechanisms starting from the earliest stages of visual processing (Carandini & Heeger 2012), it is unclear how much of this brightness enhancement translates into potential increase in sensitivity.

Two recent reviews (Harris & Thiele 2011, Maimon 2011) have raised the provocative hypothesis that state-dependent processing studied in rodents may involve processes similar to attention, as studied in primates. Our study provides a direct test of this hypothesis and offers novel support, as all observed effects of locomotion indeed parallel key signatures of attention in primates. First, although experimental evidence for a specific laminar pattern of attention effects in area V1 is sparse, it has been reported that firing rate enhancements by attention in monkey V1 can be among the strongest in superficial layers (Mehta et al 2000). Second, de-correlation of population

responses is a hallmark of attention: visual attention has been shown to reduce trial-to-trial variability of individual neurons and decrease interneuronal correlations (Cohen & Maunsell 2009, Cohen & Newsome 2008, Mitchell et al 2007). Moreover, de-correlation, rather than changes in firing rates, seems to be the major cause for improvements of visual performance under attention (Cohen & Maunsell 2009). In mice, locomotion improves behavioral sensitivity in a contrast detection task (Bennett et al 2013), but whether this performance boost is mediated mainly via enhancements of firing rates, de-correlation of population responses or yet other factors is currently unknown. Third, effects of visual attention have also been observed on the level of the LGN (McAlonan et al 2008, O'Connor et al 2002, Schneider 2011, Schneider & Kastner 2009). Most of this attention work has relied on functional magnetic resonance imaging (fMRI) in humans, where it has been reported that both spatial (O'Connor et al 2002, Schneider & Kastner 2009) and feature-based attention (Schneider 2011) can enhance responses. These findings are supported by one single unit study, which found attention-related increases in neural responses of both magnocellular and parvocellular neurons in monkey dLGN (McAlonan et al 2008). Taken together, our results provide novel evidence for shared processes between locomotion in rodents and attention in primates.

Despite these similarities between effects of locomotion and attention, there is a fundamental difference in scale. One defining feature of attention is its selectivity, i.e. modulations by attention are restricted to the attended spatial location (Moran & Desimone 1985, Treue & Maunsell 1996), feature (McAdams & Maunsell 1999, Treue & Martinez-Trujillo 1999), or object (Roelfsema et al 1998). To achieve such selectivity, attention studies typically take great care to compare conditions that are identical in terms of sensory stimulation, task difficulty, and arousal, and therefore only differ in the focus

of attention. In studies of locomotion, however, the comparison between conditions rests on the presence vs. absence of behavior, which can entail additional uncontrolled factors, such as motivational state or level of arousal. Notwithstanding this fundamental difference in selectivity, the similarity between attention and locomotion effects is encouraging and opens the possibility to investigate, in the rodent model, shared processes on the level of the microcircuit.

Few neuropharmacological experiments have directly studied the role of neuromodulators in mediating attentional effects (Herrero et al 2008, Thiele 2013). As for locomotion, recent work has suggested that maintaining the tonic depolarization associated with locomotion critically relies on norepinephrine (Polack et al 2013). The importance of norepinephrine has also been highlighted in barrel cortex, where blockade of noradrenergic pathways induced 'quiescent-like' cortical dynamics during wakefulness (Constantinople & Bruno 2011). The major source of norepinephrine in the brain is the locus coeruleus (LC), which has been found to increase activity during treadmill walking in cats (Rasmussen et al 1986) and even be causally related to locomotion in the mouse (Carter et al 2010). While our results do not provide direct evidence for an involvement of norepinephrine, the signatures of locomotion observed in our study are consistent with noradrenergic effects. First, converging findings from anatomy (Szabadi 2013), electrophysiology (Aston-Jones & Cohen 2005), pharmacology (Phillips et al 2000) and human imaging (Murphy et al 2014, Sterpenich et al 2006) suggest that the action of norepinephrine is linked to pupil dilation under constant illumination. Second, electrical stimulation of the rat LC (Holdefer & Jacobs 1994) and pharmacological application of norepinephrine agonists in the cat LGN (Funke et al 1993) reduce thalamic burst mode firing. Third, norepinephrine might contribute to cortical de-synchronization, which

in turn might be related to the de-correlation of the population response we observed (Harris & Thiele 2011). Finally, in rats, the outer layers of the visual cortex are more densely innervated by noradrenergic fibers than the inner ones (Morrison et al 1978), consistent with the laminar profile of modulations we observed.

Taken together, our results provide evidence that visual responses at cortical and subcortical level are highly sensitive to both stimulus context, as assessed by surround suppression (part 1), and behavioral context, as assessed by differences in processing during anesthesia and wakefulness (part 1), as well as within in the awake state (part 2). Both types of contextual modulations share similarities in their laminar profiles: influences of both stimulus and behavioral context are strongest in upper layers, where horizontal connectivity is most abundant and feedback connections terminate. But there are also differences: while spatial integration gets progressively broader across layers, locomotion-related suppressive effects are most prevalent and strongest in the upper part of infragranular layers, potentially corresponding to L5. Regarding state-dependent processing, there is an ongoing debate whether there are several distinct states or whether they form a continuum of gradually changing brain processing. Here, we show in accordance with several modern investigations (Niell & Stryker 2010, Wester & McBain 2014, Zagha & McCormick 2014), that even within the waking states exist several processing modes, which we delineate via locomotor activity. We see some similarities between anesthetized (compared to awake) and stationary (compared to locomotion) states in mouse: firing rate is decreased and orientation tuning is scaled down without changes in width. The decrease in gain can be partly explained by changes in the balance of neuromodulators (Polack et al 2013) or changes in variability

of the membrane potential (Bennett et al 2013). Besides these resemblances, there is also a difference: during anesthetized state we observed changes in contrast sensitivity, while during locomotion we observed changes in contrast gain. Interestingly, surround suppression is decreased not only with anesthesia, but also with running.

In summary, this thesis demonstrates that both stimulus and behavioral context can have profound influences on neural information processing, even along the earliest stages of the visual system.

5 Conclusions

1. The laminar profile of spatial integration in mouse V1 is similar to that of higher order mammals: center size is smallest and surround suppression is strongest in superficial layers;
2. The strength of surround suppression increases over time;
3. Activation of PV+ interneurons influences size tuning in mouse V1, and the effects are similar to an overall reduction of stimulus drive: RF center increases and suppression strength decreases;
4. Spatial integration is profoundly influenced by anesthetic state: under isoflurane/urethane anesthesia, the laminar specificity of spatial integration is decreased, the strength of surround suppression is reduced, RF size is increased, and responses are slower and more sluggish;
5. Locomotion-based response enhancements occur already at the level of the LGN;
6. Pupil size increases with locomotion speed;

6 References

1. Adesnik H, Bruns W, Taniguchi H, Huang ZJ, Scanziani M. 2012. A neural circuit for spatial summation in visual cortex. *Nature* 490: 226-31
2. Adesnik H, Scanziani M. 2010. Lateral competition for cortical space by layer-specific horizontal circuits. *Nature* 464: 1155-60
3. Albrecht DG, Geisler WS, Frazor RA, Crane AM. 2002. Visual Cortex Neurons of Monkeys and Cats: Temporal Dynamics of the Contrast Response Function. *J Neurophysiol* 88: 888-913
4. Albrecht DG, Hamilton DB. 1982. Striate cortex of monkey and cat: contrast response function. *J Neurophysiol* 48: 217-37
5. Alitto HJ, Usrey WM. 2008. Origin and Dynamics of Extraclassical Suppression in the Lateral Geniculate Nucleus of the Macaque Monkey. *Neuron* 57: 135-46
6. Allman J, Miezin F, McGuinness E. 1985. Stimulus specific responses from beyond the classical receptive field: neurophysiological mechanisms for local-global comparisons in visual neurons. *Annu Rev Neurosci* 8: 407-30
7. Altholtz LY, Fowler KA, Badura LL, Kovacs MS. 2006. Comparison of the stress response in rats to repeated isoflurane or CO2:O2 anesthesia used for restraint during serial blood collection via the jugular vein. *J Am Assoc Lab Anim Sci* 45: 17-22
8. Andermann ML, Gilfoy NB, Goldey GJ, Sachdev RNS, Wölfel M, et al. 2013. Chronic Cellular Imaging of Entire Cortical Columns in Awake Mice Using Microprisms. *Neuron*

9. Andermann ML, Kerlin AM, Roumis DK, Glickfeld LL, Reid RC. 2011. Functional Specialization of Mouse Higher Visual Cortical Areas. *Neuron* 72: 1025--39
10. Angelucci A, Bressloff PC. 2006. Contribution of feedforward, lateral and feedback connections to the classical receptive field center and extra-classical receptive field surround of primate V1 neurons. *Prog Brain Res* 154: 93-120
11. Angelucci A, Levitt JB, Walton EJS, Hupe J-M, Bullier J, Lund JS. 2002. Circuits for local and global signal integration in primary visual cortex. *J Neurosci* 22: 8633-46
12. Antonini A, Fagiolini M, Stryker MP. 1999. Anatomical Correlates of Functional Plasticity in Mouse Visual Cortex. *J Neurosci* 19: 4388-406
13. Arcelli P, Frassoni C, Regondi MC, De Biasi S, Spreafico R. 1997. GABAergic neurons in mammalian thalamus: a marker of thalamic complexity? *Brain Research Bulletin* 42: 27-37
14. Ascoli GA, Alonso-Nanclares L, Anderson SA, Barrionuevo G, Benavides-Piccione R, et al. 2008. Petilla terminology: nomenclature of features of GABAergic interneurons of the cerebral cortex. *Nat Rev Neurosci* 9: 557-68
15. Aston-Jones G, Cohen JD. 2005. An integrative theory of locus coeruleus norepinephrine function: adaptive gain and optimal performance. *Annu Rev Neurosci* 28: 403-50
16. Atallah BV, Bruns W, Carandini M, Scanziani M. 2012. Parvalbumin-Expressing Interneurons Linearly Transform Cortical Responses to Visual Stimuli. *Neuron* 73: 159--70
17. Atencio CA, Schreiner CE. 2008. Spectrotemporal Processing Differences between Auditory Cortical Fast-Spiking and Regular-Spiking Neurons. *The Journal of Neuroscience* 28: 3897-910

18. Ayaz A, Saleem AB, Schölvinck ML, Carandini M. 2013. Locomotion Controls Spatial Integration in Mouse Visual Cortex. *Curr Biol* 23: 890-94
19. Baden T, Berens P, Bethge M, Euler T. 2013a. Spikes in mammalian bipolar cells support temporal layering of the inner retina. *Curr Biol* 23: 48-52
20. Baden T, Schubert T, Chang L, Wei T, Zaichuk M, et al. 2013b. A tale of two retinal domains: near-optimal sampling of achromatic contrasts in natural scenes through asymmetric photoreceptor distribution. *Neuron* 80: 1206-17
21. Bair W, Cavanaugh JR, Movshon JA. 2003. Time course and time-distance relationships for surround suppression in macaque V1 neurons. *J Neurosci* 23: 7690-701
22. Banks MI, Pearce RA. 1999. Dual actions of volatile anesthetics on GABA(A) IPSCs: dissociation of blocking and prolonging effects. *Anesthesiology* 90: 120-34
23. Bartho P, Hirase H, Monconduit L, Zugaro M, Harris KD, Buzsaki G. 2004. Characterization of Neocortical Principal Cells and Interneurons by Network Interactions and Extracellular Features. *J Neurophysiol* 92: 600-08
24. Bennett C, Arroyo S, Hestrin S. 2013. Subthreshold Mechanisms Underlying State-Dependent Modulation of Visual Responses. *Neuron* 80: 350--57
25. Berens P, Ecker AS, Cotton RJ, Ma WJ, Bethge M, Tolias AS. 2012. A Fast and Simple Population Code for Orientation in Primate V1. *The Journal of Neuroscience* 32: 10618--26

26. Bezdudnaya T, Cano M, Bereshpolova Y, Stoelzel CR, Alonso JM, Swadlow HA. 2006. Thalamic burst mode and inattention in the awake LGNd. *Neuron* 49: 421-32
27. Blakemore C, Tobin EA. 1972. Lateral inhibition between orientation detectors in the cat's visual cortex. *Exp Brain Res* 15: 439-40
28. Blatow M, Rozov A, Katona I, Hormuzdi SG, Mayer AH, et al. 2003. A novel network of multipolar bursting interneurons generates theta frequency oscillations in neocortex. *Neuron* 38: 805-17
29. Bode-Greuel KM, Singer W, Aldenhoff JB. 1987. A current source density analysis of field potentials evoked in slices of visual cortex. *Exp Brain Res* 69: 213-19
30. Bonin V, Histed MH, Yurgenson S, Reid RC. 2011. Local Diversity and Fine-Scale Organization of Receptive Fields in Mouse Visual Cortex. *The Journal of Neuroscience* 31: 18506--21
31. Bradley MM, Miccoli L, A EM, J LP. 2008. The pupil as a measure of emotional arousal and autonomic activation. *Psychophysiology* 45: 602-07
32. Bradshaw J. 1967. Pupil size as a measure of arousal during information processing. *Nature* 216: 515-16
33. Briggs F. 2010. Organizing principles of cortical layer 6. *Front Neural Circuits* 4: 3
34. Burkhalter A. 2008. Many specialists for suppressing cortical excitation. *Frontiers in Neuroscience* 2: 155-67
35. Busse L, Ayaz A, Dhruv NT, Katzner S, Saleem AB, et al. 2011. The Detection of Visual Contrast in the Behaving Mouse. *The Journal of Neuroscience* 31: 11351--61

36. Butt SJ, Fuccillo M, Nery S, Noctor S, Kriegstein A, et al. 2005. The temporal and spatial origins of cortical interneurons predict their physiological subtype. *Neuron* 48: 591-604
37. Carandini M, Heeger DJ. 2012. Normalization as a canonical neural computation. *Nat Rev Neurosci* 13: 51--62
38. Cardin JA, Carlen M, Meletis K, Knoblich U, Zhang F, et al. 2009. Driving fast-spiking cells induces gamma rhythm and controls sensory responses. *Nature* 459: 663-67
39. Carter ME, Yizhar O, Chikahisa S, Nguyen H, Adamantidis A, et al. 2010. Tuning arousal with optogenetic modulation of locus coeruleus neurons. *Nat Neurosci* 13: 1526-33
40. Cavanaugh JR, Bair W, Movshon JA. 2002. Nature and interaction of signals from the receptive field center and surround in macaque V1 neurons. *J Neurophysiol* 88: 2530-46
41. Ch'ng YH, Reid RC. 2010. Cellular imaging of visual cortex reveals the spatial and functional organization of spontaneous activity. *Front Integr Neurosci* 4
42. Clement EA, Richard A, Twaites M, Ailon J. 2008. Cyclic and Sleep-Like Spontaneous Alternations of Brain State Under Urethane Anaesthesia. *PLoS One* 3: e2004
43. Cohen MR, Maunsell JHR. 2009. Attention improves performance primarily by reducing interneuronal correlations. *Nat Neurosci* 12: 1594-600
44. Cohen MR, Newsome WT. 2008. Context-Dependent Changes in Functional Circuitry in Visual Area MT. *Neuron* 60: 162-73
45. Coleman JP, Law K, Bear MF. 2009. Anatomical origins of ocular dominance in mouse primary visual cortex. *Neuroscience* 161: 561-71

46. Connors BW, Gutnick MJ. 1990. Intrinsic firing patterns of diverse neocortical neurons. *TINS* 13: 99-104
47. Constantinople CM, Bruno RM. 2011. Effects and mechanisms of wakefulness on local cortical networks. *Neuron* 69: 1061-8
48. Corneil BD, Munoz DP. 2014. Overt Responses during Covert Orienting. *Neuron* 82: 1230-43
49. Cruikshank SJ, Urabe H, Nurmikko AV, Connors BW. 2010. Pathway-Specific Feedforward Circuits between Thalamus and Neocortex Revealed by Selective Optical Stimulation of Axons. 65: 230-45
50. Cruz-Martin A, El-Danaf RN, Osakada F, Sriram B, Dhande OS, et al. 2014. A dedicated circuit links direction-selective retinal ganglion cells to the primary visual cortex. *Nature* 507: 358-61
51. da Silveira RA, Roska B. 2011. Cell types, circuits, computation. *Curr Opin Neurobiol* 21: 664-71
52. DeAngelis GC, Freeman RD, Ohzawa I. 1994. Length and width tuning of neurons in the cat's primary visual cortex. *Journal of Neurophysiology* 71: 347--74
53. DeFelipe J. 1999. Chandelier cells and epilepsy. *Brain* 122: 1807-22
54. Defelipe J, López-Cruz PL, Benavides-Piccione R, Bielza C, Larrañaga P, et al. 2013. New insights into the classification and nomenclature of cortical GABAergic interneurons. *Nat Rev Neurosci* 14: 202-16
55. Denman DJ, Contreras D. 2013. The Structure of Pairwise Correlation in Mouse Primary Visual Cortex Reveals Functional Organization in the Absence of an Orientation Map. *Cereb Cortex* 24: 2707-0720
56. Devonshire IM, Grandy TH, Dommett EJ, Greenfield SA. 2010. Effects of urethane anaesthesia on sensory processing in the rat barrel cortex revealed by combined optical imaging and electrophysiology. *Eur J Neurosci* 32: 786-97

57. Dombeck DA, Khabbaz AN, Collman F, Adelman TL, Tank DW. 2007. Imaging Large-Scale Neural Activity with Cellular Resolution in Awake, Mobile Mice. *Neuron* 56: 43-57
58. Douglas RJ, Martin KAC. 2004. Neuronal circuits of the neocortex. *Annual Review of Neuroscience* 27: 419-51
59. Ecker AS, Berens P, Cotton RJ, Subramaniyan M, Denfield GH, et al. 2014. State dependence of noise correlations in macaque primary visual cortex. *Neuron* 82: 235-48
60. Ecker AS, Berens P, Keliris GA, Bethge M, Logothetis NK, Tolias AS. 2010. Decorrelated Neuronal Firing in Cortical Microcircuits. *Science* 327: 584-87
61. Einevoll GT, Franke F, Hagen E, Pouzat C, Harris KD. 2012. Towards reliable spike-train recordings from thousands of neurons with multielectrodes. *Curr Opin Neurobiol* 22: 11-7
62. Felleman DJ, Van Essen DC. 1991. Distributed hierarchical processing in the primate cerebral cortex. *Cereb Cortex* 1: 1-47
63. Ferezou I, Haiss F, Gentet LJ, Aronoff R, Weber B, Petersen CCH. 2007. Spatiotemporal Dynamics of Cortical Sensorimotor Integration in Behaving Mice. *Neuron* 56: 907-23
64. Ferron J-F, Kroeger D, Chever O, Amzica F. 2009. Cortical Inhibition during Burst Suppression Induced with Isoflurane Anesthesia. *The Journal of Neuroscience* 29: 9850-60
65. Field KJ, Lang CM. 1988. Hazards of urethane (ethyl carbamate): a review of the literature. *Lab Anim* 22: 255-62
66. Flecknell PA. 1996. *Laboratory Animal Anesthesia*. London: Academic Press.
67. Franklin KBJ, Paxinos G. 2008. *The mouse brain in stereotaxic coordinates*. Elsevier.

68. Friedlander MJ. 1982. Structure of physiologically classified neurones in the kitten dorsal lateral geniculate nucleus. *Nature* 300: 180-83
69. Frost DO, Caviness J, V S. 1980. Radial organization of thalamic projections to the neocortex in the mouse. *J Comp Neurol* 194: 369-93
70. Funke K, Pape HC, Eysel UT. 1993. Noradrenergic modulation of retinogeniculate transmission in the cat. *J Physiol* 463
71. Gabriel S, Gabriel HJ, Grützmann R, Berlin K, Davidowa H. 1996. Effects of cholecystokinin on Y, X, and W cells in the dorsal lateral geniculate nucleus of rats. *Exp Brain Res* 109: 43-55
72. Garcia PS, Kolesky SE, Jenkins A. 2010. General Anesthetic Actions on GABA-A Receptors. *Current Neuropharmacology* 8: 2-9
73. Ghanayem BI. 2007. Inhibition of urethane-induced carcinogenicity in cyp2e1-/- in comparison to cyp2e1+/+ mice. *Toxicol Sci* 95: 331-39
74. Gilbert CD, Das A, Ito M, Kapadia M, Westheimer G. 1996. Spatial integration and cortical dynamics. *Proc Natl Acad Sci U S A* 93: 615-22
75. Gilbert CD, Wiesel TN. 1990. The influence of contextual stimuli on the orientation selectivity of cells in primary visual cortex of the cat. *Vision Research* 30: 1689--701
76. Girman SV, Sauvé Y, Lund RD. 1999. Receptive field properties of single neurons in rat primary visual cortex. *J Neurophysiol* 82: 301-11
77. Girshick AR, Landy MS, Simoncelli EP. 2011. Cardinal rules: visual orientation perception reflects knowledge of environmental statistics. *Nat Neurosci* 14: 926-32
78. Glickfeld LL, Andermann ML, Bonin V, Reid RC. 2013. Cortico-cortical projections in mouse visual cortex are functionally target specific. *Nat Neurosci* 16: 219-26
79. Goard M, Dan Y. 2009. Basal forebrain activation enhances cortical coding of natural scenes. *Nat Neurosci* 12: 1444-49

80. Goldinger SD, Papesh MH. 2012. Pupil Dilation Reflects the Creation and Retrieval of Memories. *Current Directions in Psychological Science* 21: 90-95
81. Gonchar Y, Wang Q, Burkhalter A. 2007a. Multiple distinct subtypes of GABAergic neurons in mouse visual cortex identified by triple immunostaining. *Frontiers in neuroanatomy* 1: 3
82. Gonchar Y, Wang Q, Burkhalter A. 2007b. Multiple distinct subtypes of GABAergic neurons in mouse visual cortex identified by triple immunostaining. *Front Neuroanat* 1: 3
83. Gordon JA, Stryker MP. 1996. Experience-dependent plasticity of binocular responses in the primary visual cortex of the mouse. *The Journal of Neuroscience* 16: 3274-86
84. Grubb MS, Thompson ID. 2003. Quantitative characterization of visual response properties in the mouse dorsal lateral geniculate nucleus. *J Neurophysiol* 90: 3594-607
85. Grubb MS, Thompson ID. 2004. Visual response properties in the dorsal lateral geniculate nucleus of mice lacking the beta2 subunit of the nicotinic acetylcholine receptor. *J neurosci* 24: 8459-69
86. Grubb MS, Thompson ID. 2005. Visual response properties of burst and tonic firing in the mouse dorsal lateral geniculate nucleus. *J Neurophysiol* 93: 3224-47
87. Gu Y, Liu S, Fetsch CR, Yang Y, Fok S, et al. 2011. Perceptual Learning Reduces Interneuronal Correlations in Macaque Visual Cortex. *Neuron* 71: 750--61
88. Gur M, Kagan I, Snodderly DM. 2005. Orientation and Direction Selectivity of Neurons in V1 of Alert Monkeys: Functional Relationships and Laminar Distributions. *Cereb Cortex* 15: 1207-21

89. Gutnisky DA, Dragoi V. 2008. Adaptive coding of visual information in neural populations. *Nature* 452: 220-24
90. Haider B, Häusser M, Carandini M. 2013. Inhibition dominates sensory responses in the awake cortex. *Nature* 493: 97-100
91. Halnes G, Augustinaite S, Heggelund P, Einevoll GT, Migliore M. 2011. A Multi-Compartment Model for Interneurons in the Dorsal Lateral Geniculate Nucleus. *PLoS Comput Biol* 7: 1-12
92. Hara K, Harris RA. 2002. The Anesthetic Mechanism of Urethane: The Effects on Neurotransmitter-Gated Ion Channels. *Anesthetic Pharmacology* 94: 313-18
93. Harris KD, Bartho P, Chadderton P, Curto C, de la Rocha J, et al. 2011. How do neurons work together? Lessons from auditory cortex. *Hearing Research* 271: 37-53
94. Harris KD, Thiele A. 2011. Cortical state and attention. *Nat Rev Neurosci*
95. Hattox AM, Nelson SB. 2007. Layer V Neurons in Mouse Cortex Projecting to Different Targets Have Distinct Physiological Properties. *J Neurophysiol* 98: 3330-40
96. Haverkamp S, Wässle H, Duebel J, Kuner T, Augustine GJ, et al. 2005. The primordial, blue-cone color system of the mouse retina. *J Neurosci* 25: 5438-45
97. Hawken MJ, Shapley R, Grosof DH. 1996. Temporal frequency selectivity in macaque visual cortex. *Vis Neurosci* 133: 477-92
98. Hazan L, Zugaro M, Buzsaki G. 2006. Klusters, NeuroScope, NDManager: A free software suite for neurophysiological data processing and visualization. *Journal of Neuroscience Methods* 155: 207-16

99. Helm J, Akgul G, Wollmuth LP. 2013. Subgroups of parvalbumin-expressing interneurons in layers 2/3 of the visual cortex. *J Neurophysiol* 109: 1600-13
100. Helmsteadter M, Briggman KL, Turaga SC, Jain V, Seung HS, Denk W. 2013. Connectomic reconstruction of the inner plexiform layer in the mouse retina. *Nature* 500: 168-74
101. Henze DA, Borhegyi Z, Csicsvari J, Mamiya A, Harris KD, Buzsaki G. 2000. Intracellular Features Predicted by Extracellular Recordings in the Hippocampus In Vivo. *J Neurophysiol* 84: 390-400
102. Herrero JL, Roberts MJ, Delicato LS, Gieselmann MA, Dayan P, Thiele A. 2008. Acetylcholine contributes through muscarinic receptors to attentional modulation in V1. *Nature* 454: 1110-14
103. Hirsch JA, Martinez LM. 2006. Circuits that build visual cortical receptive fields. *Trends Neurosci* 29: 30-39
104. Hoeks B, Levelt WJ. 1993. Pupillary dilation as a measure of attention: A quantitative system analysis. *Behavior Research Methods, Instruments, & Computers* 25: 16-26
105. Holdefer RN, Jacobs BL. 1994. Phasic stimulation of the locus coeruleus: effects on activity in the lateral geniculate nucleus. *Exp Brain Res* 100: 444-52
106. Huang X, Albright TD, Stoner GR. 2008. Stimulus Dependency and Mechanisms of Surround Modulation in Cortical Area MT. *J Neurosci* 28: 13889-906
107. Hubel DH, Wiesel TN. 1961. Integrative action in the cat's lateral geniculate body. *The Journal of Physiology Online* 155: 385-98
108. Hubel DH, Wiesel TN. 1962. Receptive fields, binocular interaction and functional architecture in the cat's visual cortex. *Journal of Physiology* 160: 106-54

109. Huberman AD, Niell CM. 2011. What can mice tell us about how vision works? *Trends Neurosci* 34: 464-73
110. Huberman AD, Wei W, Elstrott J, Stafford BK, Feller MB, Barres BA. 2009. Genetic Identification of an On-Off Direction-Selective Retinal Ganglion Cell Subtype Reveals a Layer-Specific Subcortical Map of Posterior Motion. *Neuron* 62: 327-34
111. Hudetz AG, Vizuete JA, Pillay S. 2011. Differential effects of isoflurane on high-frequency and low-frequency γ oscillations in the cerebral cortex and hippocampus in freely moving rats. *Anesthesiology* 114: 588-95
112. Jaubert-Miazza L, Green E, Lo F-S, Bui K, Mills J, Guido W. 2005. Structural and functional composition of the developing retinogeniculate pathway in the mouse. *Vis Neurosci* 22
113. Jeon C-J, Strettoi E, Masland RH. 1998. The major cell populations of the mouse retina. *The Journal of Neuroscience* 18: 8936–46
114. Jin J, Wang Y, Swadlow HA, Alonso JM. 2011. Population receptive fields of ON and OFF thalamic inputs to an orientation column in visual cortex. *Nat Neurosci* 14: 232--38
115. Jones HE, Andolina IM, Oakely NM, Murphy PC, Sillito AM. 2000. Spatial summation in lateral geniculate nucleus and visual cortex. *Exp Brain Res* 135: 279-84
116. Jones HE, Grieve KL, Wang W, Sillito AM. 2001. Surround suppression in primate V1. *J Neurophysiol* 86: 2011-28
117. Jurgens CWD, Bell KA, McQuiston RA, Guido W. 2012. Optogenetic Stimulation of the Corticothalamic Pathway Affects Relay Cells and GABAergic Neurons Differently in the Mouse Visual Thalamus. *PLoS One* 7: e45717

118. Jurkus P, Ruksenas O, Heggelund P. 2013. Temporally advanced dynamic change of receptive field of lateral geniculate neurons during brief visual stimulation: Effects of brainstem peribrachial stimulation. *Neuroscience* 242: 85-96
119. Kapadia MK, Westheimer G, Gilbert CD. 1999. Dynamics of spatial summation in primary visual cortex of alert monkeys. *Proc Natl Acad Sci U S A* 96: 12073-8
120. Karube F, Kubota Y, Kawaguchi Y. 2004. Axon Branching and Synaptic Bouton Phenotypes in GABAergic Nonpyramidal Cell Subtypes. *The Journal of Neuroscience* 24: 2853-65
121. Katzner S, Busse L, Carandini M. 2011. GABA$_A$ Inhibition Controls Response Gain in Visual Cortex. *J Neurosci* 31: 5931-41
122. Katzner S, Weigelt S. 2013. Visual cortical networks: of mice and men. *Curr Opin Neurobiol* 23: 202-6
123. Kawaguchi Y. 1993. Physiological, morphological, and histochemical characterization of three classes of interneurons in rat neostriatum. *J Neurosci* 13: 4908-23
124. Kawaguchi Y, Kondo S. 2002. Parvalbumin, somatostatin and cholecystokinin as chemical markers for specific GABAergic interneuron types in the rat frontal cortex. *Journal of Neurocytology* 31: 277-87
125. Kawaguchi Y, Kubota Y. 1997. GABAergic cell subtypes and their synaptic connections in rat frontal cortex. *Cereb Cortex* 7: 476-86
126. Kay JN, De la Huerta I, Zhang Y, Yamagata M, Chu MW, et al. 2011. Retinal Ganglion Cells with Distinct Directional Preferences Differ in Molecular Identity, Structure, and Central Projections. *The Journal of Neuroscience* 31: 7753-62

127. Keller GB, Bonhoeffer T, Hübener M. 2012. Sensorimotor mismatch signals in primary visual cortex of the behaving mouse. *Neuron* 74: 809-15
128. Kim I-J, Zhang Y, Meister M, Sanes JR. 2010. Laminar restriction of retinal ganglion cell dendrites and axons: subtype-specific developmental patterns revealed with transgenic markers. *J neurosci* 30: 1452-62
129. Kim I-J, Zhang Y, Yamagata M, Meister M, Sanes JR. 2008. Molecular identification of a retinal cell type that responds to upward motion. *Nature* 452: 478-82
130. Knierim JJ, van Essen DC. 1992. Neuronal responses to static texture patterns in area V1 of the alert macaque monkey. *J Neurophysiol* 67: 961-80
131. Ko H, Hofer SB, Pichler B, Buchanan KA, Sjostrom PJ, Mrsic-Flogel TD. 2011. Functional specificity of local synaptic connections in neocortical networks. *Nature* 473: 87--91
132. Kohn A, Smith MA. 2005. Stimulus dependence of neuronal correlation in primary visual cortex of the macaque. *J Neurosci* 25: 3661-73
133. Krahe TE, El-Danaf RN, Dilger EK, Henderson SC, Guido W. 2011. Morphologically Distinct Classes of Relay Cells Exhibit Regional Preferences in the Dorsal Lateral Geniculate Nucleus of the Mouse. *The Journal of Neuroscience* 31: 17437--48
134. Kravitz DJ, Saleem KS, Baker CI, Mishkin M. 2011. A new neural framework for visuospatial processing. *Nat Rev Neurosci* 12: 217-30
135. Krimer LS, Zaitsev AV, Czanner G, Kroner S, Gonzalez-Burgos G, et al. 2005. Cluster analysis-based physiological classification and morphological properties of inhibitory neurons in layers 2-3 of monkey dorsolateral prefrontal cortex. *J Neurophysiol* 94: 3009-22

136. Kroeger D, Amzica F. 2007. Hypersensitivity of the Anesthesia-Induced Comatose Brain. *The Journal of Neuroscience* 27: 10597-607
137. Lee S, Hjerling-Leffler J, Zagha E, Fishell G, Rudy B. 2010. The largest group of superficial neocortical GABAergic interneurons expresses ionotropic serotonin receptors. *The Journal of neuroscience : the official journal of the Society for Neuroscience* 30: 16796-808
138. Lee S-H, Kwan AC, Zhang S, Phoumthipphavong V, Flannery JG, et al. 2012. Activation of specific interneurons improves V1 feature selectivity and visual perception. *Nature* 488: 379-83
139. Levitt JB, Lund JS. 2002. The spatial extent over which neurons in macaque striate cortex pool visual signals. *Vis Neurosci* 19: 439-52
140. Li LY, Xiong XR, Ibrahim LA, Yuan W, Tao HW, Zhang LI. 2014. Differential Receptive Field Properties of Parvalbumin and Somatostatin Inhibitory Neurons in Mouse Auditory Cortex. *Cereb Cortex*
141. Li Y-T, Ibrahim LA, Liu B-H, Zhang LI, Tao HW. 2013. Linear transformation of thalamocortical input by intracortical excitation. *Nat Neurosci* 16: 1324-30
142. Li Y-t, Ma W-p, Li L-y, Ibrahim LA, Wang S-z, Tao HW. 2012. Broadening of Inhibitory Tuning Underlies Contrast-Dependent Sharpening of Orientation Selectivity in Mouse Visual Cortex. *The Journal of Neuroscience* 32: 16466--77
143. Liu B-h, Li P, Sun YJ, Li Y-t, Zhang LI, Tao HW. 2009. Intervening inhibition underlies simple-cell receptive field structure in visual cortex. *Nat Neurosci* 13: 89-96
144. Liu X-B, Jones EG. 1999. Predominance of corticothalamic synaptic inputs to thalamic reticular nucleus neurons in the rat. *The Journal of Comparative Neurology* 414: 67-79

145. Lynn R. 1966. *Attention, Arousal and the Orientation Reaction*. Oxford: Pergamon Press.
146. Ma W-p, Liu B-h, Li Y-t, Josh Huang Z, Zhang LI, Tao HW. 2010. Visual Representations by Cortical Somatostatin Inhibitory Neurons--Selective But with Weak and Delayed Responses. *Journal of Neuroscience* 30: 14371--79
147. Maier A, Aura CJ, Leopold DA. 2011. Infragranular Sources of Sustained Local Field Potential Responses in Macaque Primary Visual Cortex. *Journal of Neuroscience* 31: 1971--80
148. Maimon G. 2011. Modulation of visual physiology by behavioral state in monkeys, mice, and flies. *Curr Opin Neurobiol* 21: 559-64
149. Mao R, Schummers J, Knoblich U, Lacey C, Van Wart A, et al. 2012. Influence of a Subtype of Inhibitory Interneuron on Stimulus-Specific Responses in Visual Cortex. *Cereb Cortex* 22: 493-508
150. Markram H, Toledo-Rodriguez M, Wang Y, Gupta A, Silberberg G, Wu C. 2004. Interneurons of the neocortical inhibitory system. *Nat Rev Neurosci* 5: 793-807
151. Marshel JH, Garrett ME, Nauhaus I, Callaway EM. 2011. Functional Specialization of Seven Mouse Visual Cortical Areas. *Neuron* 72: 1040--54
152. Marshel JH, Kaye AP, Nauhaus I, Callaway EM. 2012. Anterior-posterior direction opponency in the superficial mouse lateral geniculate nucleus. *Neuron* 76: 713-20
153. Martin DC, Adams RJ, Aronstam RS. 1990. The Influence of Isoflurane on the Synaptic Activity of 5-Hydroxytryptamine. *Neurochemical Research* 15: 969-73
154. Martin P, Grünert U. 1992. Spatial density and immunoreactivity of bipolar cells in the macaque monkey retina. *J Comp Neurol* 323: 269-87

155. Masland RH. 2012. The neuronal organization of the retina. *Neuron* 76
156. Masland RH, Martin PR. 2007. The unsolved mystery of vision. *Curr Biol* 17: R577-R82
157. McAdams CJ, Maunsell JH. 1999. Effects of attention on orientation-tuning functions of single neurons in macaque cortical area V4. *J Neurosci* 19: 431-41
158. McAlonan K, Cavanaugh J, Wurtz RH. 2008. Guarding the gateway to cortex with attention in visual thalamus. *Nature* 456: 391-94
159. McCormick DA, Connors BW, Lighthall JW, Prince DA. 1985. Comparative electrophysiology of pyramidal and sparsely spiny stellate neurons of the neocortex. *J Neurophysiol* 54: 782-806
160. Mehta AD, Ulbert I, Schroeder CE. 2000. Intermodal selective attention in monkeys. I: distribution and timing of effects across visual areas. *Cereb Cortex* 10: 343-58
161. Metin C, Godement P, Imbert M. 1988. The primary visual cortex in the mouse: Receptive field properties and functional organization. *Exp Brain Res* 69: 594-612
162. Mitchell JF, Sundberg KA, Reynolds JH. 2007. Differential Attention-Dependent Response Modulation across Cell Classes in Macaque Visual Area V4. *Neuron* 55: 131-41
163. Mitzdorf U. 1985. Current source-density method and application in cat cerebral cortex: investigation of evoked potentials and EEG phenomena. *Physiological Reviews* 65: 37-100
164. Moran J, Desimone R. 1985. Selective attention gates visual processing in the extrastriate cortex. *Science* 229: 782-84
165. Morrison JH, Grzanna R, Molliver ME, Coyle JT. 1978. The distribution and orientation of noradrenergic fibers in neocortex of the rat: An

immunofluorescence study. *Journal of Comparative Neurology* 181: 17-39

166. Murphy PR, O'Connell RG, O'Sullivan M, Robertson IH, Balsters JH. 2014. Pupil diameter covaries with BOLD activity in human locus coeruleus. *Human Brain Mapping* 35: 4140-54
167. Murray KD, Rubin CM, Jones EG, Chalupa LM. 2008. Molecular correlates of laminar differences in the macaque dorsal lateral geniculate nucleus. *J Neurosci* 28: 12010-22
168. Nauhaus I, Busse L, Carandini M, Ringach DL. 2009. Stimulus contrast modulates functional connectivity in visual cortex. *Nat Neurosci* 12: 70-76
169. Nelson JI, Frost BJ. 1978. Orientation-selective inhibition from beyond the classic visual receptive field. *Brain Research* 139: 359--65
170. Niell CM. 2011. Exploring the Next Frontier of Mouse Vision. *Neuron* 72: 889-92
171. Niell CM. 2013. Vision: more than expected in the early visual system. *Curr Biol* 23: R681-4
172. Niell CM, Stryker MP. 2008. Highly Selective Receptive Fields in Mouse Visual Cortex. *J Neurosci* 28: 7520-36
173. Niell CM, Stryker MP. 2010. Modulation of Visual Responses by Behavioral State in Mouse Visual Cortex. 65: 472-79
174. Nienborg H, Hasenstaub A, Nauhaus I, Taniguchi H, Huang ZJ, Callaway EM. 2013. Contrast dependence and differential contributions from somatostatin- and parvalbumin-expressing neurons to spatial integration in mouse v1. *J Neurosci* 33: 11145-54
175. Nieuwenhuis S, De Geus EJ, Aston-Jones G. 2010. The anatomical and functional relationship between the P3 and autonomic components of the orienting response. *Psychophysiology* 48: 162-85

176. Nirenberg S, Meister M. 1997. The light response of retinal ganglion cells is truncated by a displaced amacrine circuit. *Neuron* 18: 637-50
177. Noudoost B. 2010. Top-down control of visual attention. *Curr Opin Neurobiol* 20: 183-90
178. O'Connor DH, Fukui MM, Pinsk MA, Kastner S. 2002. Attention modulates responses in the human lateral geniculate nucleus. *Nat Neurosci* 5: 1203-09
179. Ohki K, Chung S, Ch'ng YH, Kara P, Reid RC. 2005. Functional imaging with cellular resolution reveals precise micro-architecture in visual cortex. *Nature* 433: 597-603
180. Olivas ND, Quintanar-Zilinskas V, Nenadic Z, Xu X. 2012. Laminar circuit organization and response modulation in mouse visual cortex. *Frontiers in neural circuits* 6: 1-21
181. Olsen SR, Bortone DS, Adesnik H, Scanziani M. 2012. Gain control by layer six in cortical circuits of vision. *Nature* 483: 47--52
182. Osaki H, Naito T, Sadakane O, Okamoto M, Sato H. 2011. Surround suppression by high spatial frequency stimuli in the cat primary visual cortex. *Eur J Neurosci* 33: 923-32
183. Otazu GH, Tai L-H, Yang Y, Zador AM. 2009. Engaging in an auditory task suppresses responses in auditory cortex. *Nat Neurosci* 12: 646-54
184. Patz S, Grabert J, Gorba T, Wirth MJ, Wahle P. 2004. Parvalbumin Expression in Visual Cortical Interneurons Depends on Neuronal Activity and TrkB Ligands during an Early Period of Postnatal Development *Cereb Cortex* 14: 342-51
185. Pearce RA. 1996. Volatile anaesthetic enhancement of paired-pulse depression investigated in the rat hippocampus in vitro. *J Physiol* 492: 823-40

186. Pennesi ME, Lyubarsky AL, Pugh ENJ. 1998. Extreme responsiveness of the pupil of the dark-adapted mouse to steady retinal illumination. *Investigative ophtalmology and visual science* 39: 2148-56
187. Peterson MR, Li B, Freeman RD. 2004. The derivation of direction selectivity in the striate cortex. *The Journal of Neuroscience* 24: 3583-91
188. Pfeiffenberger C, Cutforth T, Woods G, Yamada J, Renteria RC, et al. 2005. Ephrin-As and neural activity are required for eyespecific patterning during retinogeniculate mapping. *Nat Neurosci* 8: 1022-27
189. Phillips MA, Szabadi E, Bradshaw CM. 2000. Comparison of the effects of clonidine and yohimbine on spontaneous pupillary fluctuations in healthy human volunteers. *PsychopharMACOLOGY (Berl)* 150: 85-89
190. Piscopo DM, El-Danaf RN, Huberman AD, Niell CM. 2013. Diverse visual features encoded in mouse lateral geniculate nucleus. *J Neurosci* 33: 4642-56
191. Polack P-O, Friedman J, Golshani P. 2013. Cellular mechanisms of brain state-dependent gain modulation in visual cortex. *Nat Neurosci* 16: 1331-9
192. Porciatti V, Pizzorusso T, Maffei L. 1999. The visual physiology of the wild type mouse determined with pattern VEPs. *Vision Res* 39: 3071-81
193. Porter JT, Johnson CK, Agmon A. 2001. Diverse Types of Interneurons Generate Thalamus-Evoked Feedforward Inhibition in the Mouse Barrel Cortex. *The Journal of Neuroscience* 21: 2699-710
194. Poulet JFA, Petersen CCH. 2008. Internal brain state regulates membrane potential synchrony in barrel cortex of behaving mice. *Nature* 454: 881-85
195. Prusky GT, Douglas RM. 2004. Characterization of mouse cortical spatial vision. *Vision Res* 44: 3411-18

196. Quiroga RQ, Nadasdy Z, Ben-Shaul Y. 2004. Unsupervised spike detection and sorting with wavelets and superparamagnetic clustering. *Neural Comput* 16: 1661-87
197. Rafols JA, Valverde F. 1973. The structure of the dorsal lateral geniculate nucleus in the mouse. A Golgi and electron microscopic study. *J Comp Neurol* 150: 303-32
198. Ranft A, Kurz J, Deuringer M, Haseneder R, Dodt HU, et al. 2004. Isoflurane modulates glutamatergic and GABAergic neurotransmission in the amygdala. *Eur J Neurosci* 20: 1276-80
199. Rasmussen K, Morilak DA, Jacobs BL. 1986. Single unit activity of locus coeruleus neurons in the freely moving cat. I. During naturalistic behaviors and in response to simple and complex stimuli. *Brain Res* 371: 324-34
200. Reese BE. 1988. 'Hidden lamination' in the dorsal lateral geniculate nucleus: the functional organization of this thalamic region in the rat. *Brain Res* 472: 119-37
201. Renart A, de la Rocha J, Bartho P, Hollender L, Parga N, et al. 2010. The Asynchronous State in Cortical Circuits. *Science* 327: 587-90
202. Reynaud A, Masson GS, Chavane F. 2012. Dynamics of Local Input Normalization Result from Balanced Short- and Long-Range Intracortical Interactions in Area V1. *The Journal of Neuroscience* 32: 12558--69
203. Ries CR, Puil E. 1999. Ionic mechanism of isoflurane's actions on thalamocortical neurons. *J Neurophysiol* 81: 1802-9
204. Ringach DL, Hawken MJ, Shapley R. 2003. Dynamics of Orientation Tuning in Macaque V1: The Role of Global and Tuned Suppression. *J Neurophysiol* 90: 342-52

205. Rivlin-Etzion M, Zhou K, Wei W, Elstrott J, Nguyen PL, et al. 2011. Transgenic mice reveal unexpected diversity of on-off direction-selective retinal ganglion cell subtypes and brain structures involved in motion processing. *J Neurosci* 31: 8760-69
206. Roberts M, Delicato LS, Herrero J, Gieselmann MA, Thiele A. 2007. Attention alters spatial integration in macaque V1 in an eccentricity-dependent manner. *Nat Neurosci* 10: 1483-91
207. Rockland KS, Pandya DN. 1979. Laminar origins and terminations of cortical connections of the occipital lobe in the rhesus monkey. *Brain Res* 179
208. Roelfsema PR, Lamme VA, Spekreijse H. 1998. Object-based attention in the primary visual cortex of the macaque monkey. *Nature* 395: 376-81
209. Romand S, Wang Y, Toledo-Rodriguez M, Markram H. 2011. Morphological development of thick-tufted layer V pyramidal cells in the rat somatosensory cortex. *Frontiers in Neuroanatomy* 5: 1-27
210. Roth MM, Helmchen F, Kampa BM. 2012. Distinct functional properties of primary and posteromedial visual area of mouse neocortex. *J Neurosci* 32: 9716-26
211. Ruksenas O, Bulatov A, Heggelund P. 2007. Dynamics of spatial resolution of single units in the lateral geniculate nucleus of cat during brief visual stimulation. *J Neurophysiol* 97: 1445-56
212. Runyan CA, Schummers J, Van Wart A, Kuhlman SJ, Wilson NR, et al. 2010. Response Features of Parvalbumin-Expressing Interneurons Suggest Precise Roles for Subtypes of Inhibition in Visual Cortex. *Neuron* 67: 847--57
213. Saalmann YB, Kastner S. 2009. Gain control in the visual thalamus during perception and cognition. *Curr Opin Neurobiol* 19: 408-14

214. Saalmann YB, Kastner S. 2011. Cognitive and perceptual functions of the visual thalamus. *Neuron* 71: 209-23
215. Sachdev RNS, Krause MR, Mazer JA. 2012. Surround suppression and sparse coding in visual and barrel cortices. *Front Neural Circuits* 6: 43
216. Sadakane O, Ozeki H, Naito T, Akasaki T, Kasamatsu T, Sato H. 2006. Contrast-dependent, contextual response modulation in primary visual cortex and lateral geniculate nucleus of the cat. *Eur J Neurosci* 23: 1633-42
217. Sagdullaev BT, McCall MA. 2005. Stimulus size and intensity alter fundamental receptive-field properties of mouse retinal ganglion cells in vivo. *Vis Neurosci* 22: 649-59
218. Sakatani T, Isa T. 2007. Quantitative analysis of spontaneous saccade-like rapid eye movements in C57BL/6 mice. *Neurosci Res* 58: 324-31
219. Saleem AB, Ayaz A, Jeffery KJ, Harris KD, Carandini M. 2013. Integration of visual motion and locomotion in mouse visual cortex. *Nat Neurosci* 16: 1864-9
220. Sceniak MP, Hawken MJ, Shapley R. 2001. Visual Spatial Characterization of Macaque V1 Neurons. *Journal of Neurophysiology* 85: 1873-87
221. Sceniak MP, Maciver MB. 2006. Cellular actions of urethane on rat visual cortical neurons in vitro. *J Neurophysiol* 95: 3865-74
222. Sceniak MP, Ringach DL, Hawken MJ, Shapley R. 1999. Contrast's effect on spatial summation by macaque V1 neurons. *Nat Neurosci* 2: 733-39
223. Schneider KA. 2011. Subcortical mechanisms of feature-based attention. *J Neurosci* 31: 8643-53
224. Schneider KA, Kastner S. 2009. Effects of sustained spatial attention in the human lateral geniculate nucleus and superior colliculus. *J Neurosci* 29

225. Scholl B, Tan AYY, Corey J, Priebe NJ. 2013. Emergence of orientation selectivity in the Mammalian visual pathway. *J Neurosci* 33: 10616-24
226. Schwabe L, Ichida JM, Shushruth S, Mangapathy P, Angelucci A. 2010. Contrast-dependence of surround suppression in Macaque V1: experimental testing of a recurrent network model. *Neuroimage* 52: 777-92
227. Sherman SM. 2001 Feb. Tonic and burst firing: dual modes of thalamocortical relay. *Trends Neurosci* 24: 122-26
228. Sherman SM. 2004. Interneurons and triadic circuitry of the thalamus. *Trends in Neurosciences* 27: 670-75
229. Sherman SM, Guillery RW. 2006. *Exploring the Thalamus and Its Role in Cortical Function*. pp. 484. MIT Press.
230. Shushruth S, Ichida JM, Levitt JB, Angelucci A. 2009. Comparison of spatial summation properties of neurons in macaque V1 and V2. *J Neurophysiol* 102: 2069-83
231. Shushruth S, Mangapathy P, Ichida JM, Bressloff PC, Schwabe L, Angelucci A. 2012. Strong Recurrent Networks Compute the Orientation Tuning of Surround Modulation in the Primate Primary Visual Cortex. *The Journal of Neuroscience* 32: 308--21
232. Silberberg G, Markram H. 2007. Disynaptic inhibition between neocortical pyramidal cells mediated by Martinotti cells. *Neuron* 53: 735-46
233. Sillito AM, Cudeiro J, Jones HE. 2006. Always returning: feedback and sensory processing in visual cortex and thalamus. *Trends Neurosci* 29: 307-16
234. Sinclair JR, Jacobs AL, Nirenberg S. 2004. Selective Ablation of a Class of Amacrine Cells Alters Spatial Processing in the Retina. *The Journal of Neuroscience* 24: 1459-67

235. Sirotin YB, Das A. 2010. Zooming in on mouse vision. *Nat Neurosci* 13: 1045-46
236. Smith MA, Kohn A. 2008. Spatial and Temporal Scales of Neuronal Correlation in Primary Visual Cortex. *J Neurosci* 28: 12591-603
237. Smith SL, Hausser M. 2010. Parallel processing of visual space by neighboring neurons in mouse visual cortex. *Nat Neurosci* 13: 1144--49
238. Sokolov EN. 1963. *Perception and the conditioned reflex*. New York: Macmillan.
239. Solomon JA. 2002. Noise reveals visual mechanisms of detection and discrimination. *J Vis* 2: 105-20
240. Solomon SG, White AJ, Martin PR. 1999. Temporal contrast sensitivity in the lateral geniculate nucleus of a New World monkey, the marmoset Callithrix jacchus. *J Physiol* 517 (Pt 3): 907-17
241. Somers DC, Todorov EV, Siapas AG, Toth LJ, Kim DS, Sur M. 1998. A local circuit approach to understanding integration of long-range inputs in primary visual cortex. *Cereb Cortex* 8: 204-17
242. Stahl JS, van Alphen AM, De Zeeuw CI. 2000. A comparison of video and magnetic search coil recordings of mouse eye movements. *Journal of Neuroscience Methods* 99: 101-10
243. Steriade M, Jones EG, McCormick DA. 1997. *Thalamus. Organization and function.* New York: Elsevier.
244. Sterpenich V, D'Argembeau A, Desseilles M, Balteau E, Albouy G, et al. 2006. The locus ceruleus is involved in the successful retrieval of emotional memories in humans. *J Neurosci* 26: 7416-23
245. Stone C, Pinto LH. 1993. Response properties of ganglion cells in the isolated mouse retina. *Vis Neurosci* 10: 31-39

246. Strettoi E, Masland RH. 1995. The organization of the inner nuclear layer of the rabbit retina. *The Journal of Neuroscience* 15: 875-88
247. Swadlow HA. 2003. Fast-spike interneurons and feedforward inhibition in awake sensory neocortex. *Cereb Cortex* 13: 25-32
248. Swaroop A, Douglas K, Forrest D. 2010. Transcriptional regulation of photoreceptor development and homeostasis in the mammalian retina. *Nat Rev Neurosci* 11: 563-76
249. Szabadi E. 2013. Functional neuroanatomy of the central noradrenergic system. *Journal of psychopharmacology* 27: 659-93
250. Szczesny G, Veihelmann A, Massberg S, Nolte D, Messmer K. 2004. Long-term anaesthesia using inhalatory isoflurane in different strains of mice-the haemodynamic effects. *Lab Anim* 38: 64-69
251. Szuts TA, Fadeyev V, Kachiguine S, Sher A, Grivich MV, et al. 2011. A wireless multi-channel neural amplifier for freely moving animals. *Nat Neurosci* 14: 263--69
252. Tailby C, Solomon SG, Dhruv NT, Majaj NJ, Sokol SH, Lennie P. 2007. A New Code for Contrast in the Primate Visual Pathway. *J Neurosci* 27: 3904-09
253. Thiele A. 2013. Muscarinic signaling in the brain. *Annu Rev Neurosci* 36: 271-94
254. Thomson AM, Bannister PA. 2003. Interlaminar Connections in the Neocortex. *Cereb Cortex* 13: 5-14
255. Thomson AM, West DC, Wang Y, Bannister PA. 2002. Synaptic connections and small circuits involving excitatory and inhibitory neurons in layers 2–5 of adult rat and cat neocortex: triple intracellular recordings and biocytin labelling in vitro. *Cereb Cortex* 12: 936-53

256. Tohmi M, Takahashi K, Kubota Y, Hishida R, Shibuki K. 2009. Transcranial flavoprotein fluorescence imaging of mouse cortical activity and plasticity. *Journal of Neurochemistry* 109: 3--9
257. Treue S, Martinez-Trujillo JC. 1999. Feature-based attention influences motion processing gain in macaque visual cortex. *Nature* 399: 575-79
258. Treue S, Maunsell JHR. 1996. Attentional modulation of visual motion processing in cortical areas MT and MST. *Nature* 382: 539-41
259. Usrey MW, Reid RC. 2000. Visual physiology of the lateral geniculate nucleus in two species of New World monkey: Saimiri sciureus and Aotus trivirgatis. *Journal of Physiology* 523: 755-69
260. Usrey WM, Reid RC. 1999. Synchronous activity in the visual system. *Annu Rev Physiol* 61: 435-56
261. Van den Bergh G, Zhang B, Arckens L, Chino YM. 2010. Receptive-field properties of V1 and V2 neurons in mice and macaque monkeys. *The Journal of Comparative Neurology* 518: 2051-70
262. Van Essen DC. 2004. Surface-based approaches to spatial localization and registration in primate cerebral cortex. *NeuroImage* 23: 97-107
263. Van Hooser SD, Heimel JAF, Chung S, Nelson SB, Toth LJ. 2005. Orientation Selectivity without Orientation Maps in Visual Cortex of a Highly Visual Mammal. *Journal of Neuroscience* 25: 19--28
264. Van Horn SC, Erisir A, Sherman SM. 2000. Relative Distribution of Synapses in the A-Laminae of the Lateral Geniculate Nucleus of the Cat. *The Journal of Comparative Neurology* 416: 416-520
265. Villeneuve MY, Casanova C. 2003. On the use of isoflurane versus halothane in the study of visual response properties of single cells in the primary visual cortex. *J Neurosci Methods* 129: 19-31

266. Völgyi B, Chheda S, Bloomfield SA. 2009. Tracer coupling patterns of the ganglion cell subtypes in the mouse retina. *J Comp Neurol* 512: 664-87
267. Vreysen S, Zhang B, Chino YM, Arckens L, Van den Bergh G. 2012. Dynamics of spatial frequency tuning in mouse visual cortex. *J Neurophysiol* 107: 2937-49
268. Wallace DJ, Greenberg DS, Sawinski J, Rulla S, Notaro G, Kerr JND. 2013. Visual response properties of burst and tonic firing in the mouse dorsal lateral geniculate nucleus. *Nature* 498: 65-69
269. Wang K, Zhu H, Chen C-Y, LI P, Jin C-H, et al. 2013. Effects of ketamine and urethane on stimulation-induced c-fos expression in neurons of cat visual cortex. *Zoological research* 34: 582-88
270. Wang Q, Burkhalter A. 2007. Area map of mouse visual cortex. *The Journal of Comparative Neurology* 502: 339-57
271. Wang Q, Gao E, Burkhalter A. 2011a. Gateways of Ventral and Dorsal Streams in Mouse Visual Cortex. *Journal of Neuroscience* 31: 1905--18
272. Wang Q, Sporns O, Burkhalter A. 2012. Network Analysis of Corticocortical Connections Reveals Ventral and Dorsal Processing Streams in Mouse Visual Cortex. *The Journal of Neuroscience* 32: 4386--99
273. Wang X, Vaingankar V, Sanchez CS, Sommer FT, Hirsch JA. 2011b. Thalamic interneurons and relay cells use complementary synaptic mechanisms for visual processing. *Nat Neurosci* 14: 224--31
274. Wang Y, Toledo-Rodriguez M, Gupta A, Wu C, Silberberg G, et al. 2004. Anatomical, physiological and molecular properties of Martinotti cells in the somatosensory cortex of the juvenile rat. *J Physiol* 561: 65-90

275. Wang YV, Weick M, Demb JB. 2011c. Spectral and Temporal Sensitivity of Cone-Mediated Responses in Mouse Retinal Ganglion Cells. *The Journal of Neuroscience* 31: 7670-81
276. Wang Z, McCormick DA. 1993. Control of firing mode of corticotectal and corticopontine layer V burst-generating neurons by norepinephrine, acetylcholine, and 1S,3R-ACPD. *J neurosci* 13: 2199-216
277. Wässle H. 2004. Parallel processing in the mammalian retina. *Nat Rev Neurosci* 5: 1-11
278. Webb BS, Dhruv NT, Solomon SG, Tailby C, Lennie P. 2005. Early and late mechanisms of surround suppression in striate cortex of macaque. *J Neurosci* 25: 11666-75
279. Webb BS, Tinsley CJ, Barraclough NE, Easton A, Parker A, Derrington AM. 2002. Feedback from V1 and inhibition from beyond the classical receptive field modulates the responses of neurons in the primate lateral geniculate nucleus. *Visual Neuroscience* 19: 583-92
280. Weng S, Sun W, He S. 2005. Identification of ON-OFF direction-selective ganglion cells in the mouse retina. *J Physiol* 562: 915-23
281. Wester JC, McBain CJ. 2014. Behavioral state-dependent modulation of distinct interneuron subtypes and consequences for circuit function. *Curr Opin Neurobiol* 29: 118-25
282. Westphalen RI, Hemmings HC. 2003. Selective depression by general anesthetics of glutamate versus GABA release from isolated
283. cortical nerve terminals. *J Pharmacol Exp Ther* 304: 1188-96
284. White EL, Hersch SM. 1982. A quantitative study of thalamocortical and other synapses involving the apical dendrites of corticothalamic projection cells in mouse SmI cortex. *Journal of Neurocytology* 11: 137-57

285. Whittington RA, Virag L. 2006. Isoflurane Decreases Extracellular Serotonin in the Mouse Hippocampus. *Anesth Analg* 103: 92-98
286. Wilson JR. 1986. Synaptic connections of relay and local circuit neurons in the monkey's dorsal lateral geniculate nucleus. *Neuroscience Letters* 66: 79-84
287. Wilson NR, Runyan CA, Wang FL, Sur M. 2012. Division and subtraction by distinct cortical inhibitory networks in vivo. *Nature* 488: 343--48
288. Winfield DA, Hiorns RW, Powell TP. 1980. A quantitative electron-microscopical study of the postnatal development of the lateral geniculate nucleus in normal kittens and in kittens with eyelid suture. *Proc R Soc Lond B Biol Sci* 210: 211-34
289. Xing D, Ringach DL, Hawken MJ, Shapley RM. 2011. Untuned Suppression Makes a Major Contribution to the Enhancement of Orientation Selectivity in Macaque V1. *The Journal of Neuroscience* 31: 15972--82
290. Xu X, Collins CE, Kaskan PM, Khaytin I, Kaas JH, Casagrande VA. 2004. Optical imaging of visually evoked responses in prosimian primates reveals conserved features of the middle temporal visual area. *Proc Natl Acad Sci U S A* 101: 2566-71
291. Yoshimura Y, Callaway EM. 2005. Fine-scale specificity of cortical networks depends on inhibitory cell type and connectivity. *Nat Neurosci* 8: 1552-9
292. Yoss RE, Moyer NJ, Hollenhorst RW. 1970. Pupil size and spontaneous pupillary waves associated with alertness, drowsiness, and sleep. *Neurology* 20: 545-54
293. Zagha E, McCormick DA. 2014. Neural control of brain state *Curr Opin Neurobiol* 29: 178-86

294. Zhang T, Heuer HW, Britten KH. 2004. Parietal Area VIP Neuronal Responses to Heading Stimuli Are Encoded in Head-Centered Coordinates. *Neuron* 42: 993-1001
295. Zhang Z-W, Deschenes M. 1997. Intracortical Axonal Projections of Lamina VI Cells of the Primary Somatosensory Cortex in the Rat: A Single-Cell Labeling Study. *The Journal of Neuroscience* 17: 6365-79
296. Ziburkus J, Lo F-S, Guido W. 2003. Nature of inhibitory postsynaptic activity in developing relay cells of the lateral geniculate nucleus. *J Neurophysiol* 90: 1063-70
297. Zohary E, Shadlen MN, Newsome WT. 1994. Correlated neuronal discharge rate and its implications for psychophysical performance. *Nature* 370: 140-43

Interactive references:

http://jaxmice.jax.org/strain/008069.html cited 23.05.2014
https://sites.google.com/a/nyu.edu/expo/home cited 10.02.2014

7 Publications

Journal articles:

1. Erisken S, **Vaiceliunaite A**, Jurjut O, Fiorini M, Katzner S and Busse L. Effects of locomotion extend throughout the mouse early visual system. Current Biology. 2014 Dec;15;24(24):2899-907.
2. **Vaiceliunaite A**, Erisken S, Franzen F, Katzner S, Busse L. Spatial integration in mouse primary visual cortex. J Neurophysiol. 2013 Aug;110(4):964-72.

Journal articles, not included in this thesis:

1. Egle Danieliene, Egle Gabryte, Romualdas Danielius, Mikas Vengris, **Agne Vaiceliunaite**, Vaidotas Morkunas, Osvaldas Ruksenas. Corneal stromal ablation with femtosecond ultraviolet pulses in rabbits. J Cataract Refract Surg. 2013 Feb;39(2):258-67.
2. Vengris M, Gabryte E, Aleknavicius A, Barkauskas M, Ruksenas O, **Vaiceliunaite A**, Danielius R. Corneal shaping and ablation of transparent media by femtosecond pulses in deep ultraviolet range. J Cataract Refract Surg. 2010 Sep;36(9):1579-87.

Conference presentations:

1. **Vaiceliunaite, A**., Erisken, S., Jurjut, O., Katzner, S. and Busse, L. (2014). The influence of cortical feedback on visual information processing in mouse dorsolateral geniculate nucleus. Neuroscience 2014, SfN's 44th annual meeting, Washington, DC, USA. Poster.
2. Erisken S, **Vaiceliunaite A**, Jurjut O, Fiorini M, Katzner S and Busse L. (2014). Effects of locomotion on pre-cortical and cortical neural

populations in the mouse visual system. Neuroscience 2014, SfN's 44th annual meeting, Washington, DC, USA. Oral presentation.

3. Fiorini, M., **Vaiceliunaite, A**., Erisken, S., Jurjut, O., Katzner, S. and Busse, L. (2014). A critical role of NMDA receptors in parvalbumin interneurons for visual information processing in mouse V1. Neuroscience 2014, SfN's 44th annual meeting, Washington, DC, USA. Poster.
4. O. Jurjut O, Erisken S, **Vaiceliunaite A**, Busse L, Katzner S. (2014). Learning improves robustness of spiking activity in mouse primary visual cortex. Neuroscience 2014, SfN's 44th annual meeting, Washington, DC, USA. Poster.
5. **Vaiceliunaite, A**., Erisken, S., Fiorini, M., Jurjut, O., Katzner, S. and Busse, L. (2014). Influence of cortico-thalamic feedback on visual information processing in mouse dorsolateral geniculate nucleus. Bernstein Conference on Computational Neuroscience (BCCN), Göttingen, Germany. Poster.
6. Fiorini, M., **Vaiceliunaite, A**., Erisken, S., Jurjut, O., Katzner, S. and Busse, L. (2014). A critical role of NMDA receptors in parvalbumin interneurons for visual information processing in mouse V1. Bernstein Conference on Computational Neuroscience (BCCN), Göttingen, Germany. Poster.
7. **Vaiceliunaite, A**., Erisken, S., Fiorini, M., Jurjut, O., Katzner, S. and Busse, L. (2014). The influence of cortical feedback on size tuning in mouse lateral geniculate nucleus. FENS Forum of Neuroscience, Milan, Italy. Poster.
8. Fiorini, M., **Vaiceliunaite, A**., Merseburg, A., Isbrandt, D. and Busse, L. (2014). Effects of HCN channel deficiency in forebrain neurons on stimulus selectivity and oscillatory activity in mouse primary visual

cortex. FENS Forum of Neuroscience, Milan, Italy. Poster.

9. **Vaiceliunaite, A**., Erisken, S., Katzner, S. and Busse, L. (2013). The influence of cortical feedback on size tuning in mouse lateral geniculate nucleus. FENS-IBRO-HERTIE winter school 2013, University center Obergurgl, Austria. Oral presentation.
10. **A. Vaiceliunaite**, S. Erisken, A. Wal, S. Katzner, L.Busse. (2013). The influence of cortical feedback on size tuning in mouse lateral geniculate nucleus. The 5th annual conference of Lithuanian Neuroscience Association, Vilnius, Lithuania. Poster.
11. Erisken, S., **Vaiceliunaite, A**., Katzner, S. and Busse, L. (2013). Effects of locomotion on response properties and functional connectivity in mouse primary visual cortex. Bernstein Conference on Computational Neuroscience (BCCN), Tübingen, Germany. Poster.
12. Erisken, S., **Vaiceliunaite, A**., Katzner, S. and Busse, L. (2013). Effects of locomotion on network activity in mouse primary visual cortex. European Visual Cortex Meeting (EVCP), Sv. Kriz Zacretje, Croatia. *Poster*.
13. Erisken, S., **Vaiceliunaite, A**., Franzen, F., Wal, A., Katzner, S. and Busse, L. (2013). Effects of locomotion on network activity in mouse primary visual cortex. The 10th Göttingen meeting of the German Neuroscience Society. Poster.
14. **A. Vaiceliunaite**, S. Erisken, A. Wal, S. Katzner, L.Busse. (2013). The influence of cortical feedback on size tuning in mouse lateral geniculate nucleus. The 4th German Neurophysiology PhD Meeting, Tübingen, Germany. Poster.
15. **Vaiceliunaite A**, Erisken S, Franzen F, Katzner S, Busse L. (2013). Spatial integration in mouse visual system. Cold Spring Harbor

Laboratory meeting: Vision: A Platform for Linking Circuits, Perception & Behavior. Lloyd Harbor, New York, USA. Oral presentation.

16. **A. Vaiceliunaite**, S. Erisken, F. Franzen, O. Ruksenas, S. Katzner, L. Busse. (2012). Surround suppression in mouse primary visual cortex: laminar dependence and effects of anesthesia. Neuroscience 2012, SfN's 42nd annual meeting, New Orleans, USA. Poster.
17. S. Erisken, **A. Vaiceliunaite**, F. Franzen, Z. Khastkhodaei, S. Katzner, L. Busse. Effects of locomotion on response properties and functional connectivity in mouse V1. Neuroscience 2012, SfN's 42nd annual meeting, New Orleans, USA. Poster.
18. **A. Vaiceliunaite**, S. Erisken, F. Franzen, O. Ruksenas, S. Katzner, L. Busse. (2012). Surround suppression in mouse primary visual cortex: laminar dependence and effects of anesthesia. Second Joint CIN-NIPS Symposium, Tübingen, Germany. Poster.
19. **A. Vaiceliunaite**, Z. Khastkhodaei, S. Erisken, F. Franzen, O. Ruksenas, S. Katzner, L. Busse (2012). Surround suppression in mouse primary visual cortex: laminar dependence and effects of anesthesia. 3rd Networks Symposium, Berlin, Germany. Poster.
20. **A. Vaiceliunaite**, Z. Khastkhodaei, S. Erisken, F. Franzen, O. Ruksenas, S. Katzner, L. Busse. (2012). Surround suppression in mouse primary visual cortex: laminar dependence and effects of anesthesia. The 8th FENS forum of Neuroscience", Barcelona, Spain. Poster.
21. Egle Danieliene, Romualdas Danielius, Egle Gabryte, Osvaldas Ruksenas, **Agne Vaiceliunaite**, Mikas Vengris. (2010). Corneal stromal ablation by femtosecond UV pulses: in vivo study. World Ophthalmology Congress 2010 ICC, Berlin, Germany. Oral presentation.

22. M. Vengris, E. Gabryte, O. Ruksenas, **A.Vaiceliunaite**, E. Danieliene, R. Danielius. (2010). Femtosecond solid-state laser for refractive eye surgery. International Conference on Laser Applications in Life Sciences. Oulu, Finland. Oral presentation.
23. E. Gabrytė, M. Vengris, R. Danielius, O. Rukšėnas, **A.Vaičeliūnaitė** (2010). Efficient ablation of ex vivo cornea using the fifth harmonic of femtosecond Yb:KGW laser. Biomedical engineering: Proceedings of International conference. Kaunas: Technologija, p. 176-178. Oral presentation.
24. O. Ruksenas, M. Vengris, E. Gabryte, **A. Vaiceliunaite**, E. Danieliene, R. Danielius. (2009). Rabbit eye as a model system for corneal ablation using femtosecond UV pulses. LASA winter meeting. Animal models of disease. Birmingham, United Kingdom. Poster.
25. **A. Vaičeliūnaitė**, O. Rukšėnas. (2009). The research of rat's visual system. First scientific conference of Lithuanian association of neurosciences. Vilnius, p. 22. Oral presentation.
26. E. Gabrytė, M. Vengris, R. Danielius, O. Rukšėnas, **A. Vaičeliūnaitė** (2009). Efficient ablation of ex vivo cornea using the fifth harmonic of femtosecond Yb:KGW laser // Biomedical engineering: Proceedings of International conference. Kaunas: Technologija, p. 176-178. Oral presentation.

Acknowledgements

Foremost, I would like to express my sincere gratitude to my supervisors Prof. dr. Osvaldas Rukšėnas and dr. Laura Busse. I would never have been able to finish my dissertation without their guidance. My stay in dr. Laura Busse lab was partly supported by ERASMUS and DAAD scholarships and I am grateful for this. Also, this thesis wouldn't be finished without great help of my "Matlab guru" Sinem Erisken. My special thanks for support and being patient to my beloved parents, sister and Carsten. Also I am grateful for the help of the super labs of dr. Laura Busse and dr. Steffen Katzner (to every single member!). I am very happy that all these years I had a huge support of my friends in Lithuania. Moreover, I am thankful to a beautiful Tübingen and friends in Germany for not letting me go crazy. Also thanks to Department of Neurobiology and Biophysics (especially for Ramunė and Aidas). And last but not least, I would like to say big "thank you" to my board members and opponents.

Contributions of author

Agnė Vaičeliūnaitė participated in building experimental setup and designing experiments. Contributions of Agnė in the first and in the second parts of this thesis were slightly different.

Contribution in the first part:

Agnė Vaičeliūnaitė did all surgeries, virus injections, experiments, perfusions, histological procedures and stimuli design. Agnė Vaičeliūnaitė and Laura Busse made data analysis and manuscript writing.

Contribution in the second part:

Agnė Vaičeliūnaitė, Sinem Erisken, Ovidiu Jurjut, Matilde Fiorini and Redas Dulinskas did experiments and surgeries in V1. Agnė Vaičeliūnaitė did all

surgical procedures, perfusions and histology for LGN experiments. Agnė Vaičeliūnaitė and Sinem Erisken performed experiments in LGN. Sinem Erisken and Laura Busse did analysis and manuscript writing. Agnė Vaičeliūnaitė, Steffen Katzner, Ovidiu Jurjut and Matilde Fiorini did manuscript editing.